ISTANBUL TECHNICAL UNIVERSITY ★ ENERGY INSTITUTE

**THE EFFECT OF BORAX ADDITION TO
POLY(METHYL METHACRYLATE)**

M.Sc. THESIS

Yusuf YİĞİT

Energy Science and Technology Division

Energy Science and Technology Programme

JANUARY 2020

ISTANBUL TECHNICAL UNIVERSITY ★ENERGY INSTITUTE

THE EFFECT OF BORAX ADDITION TO POLY(METHYL METHACRYLATE)

M.Sc. THESIS

Yusuf YİĞİT
(301181035)

Energy Science and Technology Division

Energy Science and Technology Programme

Thesis Advisor: Prof. Dr. Nilgün BAYDOĞAN

JANUARY 2020

İSTANBUL TEKNİK ÜNİVERSİTESİ ★ENERJİ ENSTİTÜSÜ

**BORAKS TAKVİYESİNİN
POLİ(METİL METAKRİLAT) ÜZERİNDEKİ ETKİSİ**

YÜKSEK LİSANS TEZİ

**Yusuf YİĞİT
(301181035)**

Enerji Bilim ve Teknoloji Anabilim Dalı

Enerji Bilim ve Teknoloji Programı

Tez Danışmanı: Prof. Dr. Nilgün BAYDOĞAN

OCAK 2020

Yusuf YİĞİT M.Sc. student of ITU Institute of Energy student ID 301181035 successfully defended the thesis entitled "THE EFFECT OF BORAX ADDITION TO POLY(METHYL METHACRYLATE)", which he prepared after fulfilling the requirements specified in the associated legislations, before the jury whose signatures are below.

Thesis Advisor :   **Prof. Dr. Nilgün BAYDOĞAN**   ....
Istanbul Technical University

Jury Members :   **Prof. Dr. Nilgün Karatepe YAVUZ**   ....
Istanbul Technical University

                Prof. Dr. Afife Binnaz HAZAR   ....
Yıldız Technical University

Date of Submission : 15 November 2019
Date of Defense   : 07 January 2020

To my family,

FOREWORD

January 2020   Yusuf YİĞİT
                                                                                                  Mechanical Engineer

TABLE OF CONTENS

ABBREVIATIONS

ATRP	**:**	Atom Transfer Radical Polymerization
BSE	**:**	Backscattered Electron
Bu$_4$NBr	**:**	Tetrabutylammonium bromide
DP	**:**	Degree of Polymerization
EBIB	**:**	Ethyl α-bromoisobutyrate as initiator
EDX	**:**	Energy Dispersive X-Ray Analysis
EMR	**:**	Electromagnetic Radiation
FTIR	**:**	Fourier Transform Infrared
HPDE	**:**	High-Density Polyethylene
eV	**:**	Electron volt
L.C.F	**:**	Linear Chemical Formula
LDPE	**:**	Low Density Polyethylene
MMA	**:**	Methyl Methacrylate
NMP	**:**	Nitroxide Mediated Polymerization
MWIR	**:**	Midway IR
PDI	**:**	Polydispersity Index
PMDETA	**:**	Pentamethyldiethylenetriamine
PMMA	**:**	Poly(methyl methacrylate)
PPMS	**:**	Physical Property Measurement System
RAFT	**:**	Reversible Addition-Fragmentation Chain Transfer
SE	**:**	Secondary Electron
SEM	**:**	Scanning Electron Microscope
Tg	**:**	Glass Transition Temperature
Tw	**:**	Terawatt
UV	**:**	Ultraviolet
VIS	**:**	Visible
VSM	**:**	Vibrating-Sample Magnetometer
TGA	**:**	Thermogravimetric Analysis
XRD	**:**	X-ray Diffraction
XPS	**:**	X-ray photoelectron spectroscopy
wt.	**:**	Weight

SYMBOLS

A	**:**	Amplitude
B	**:**	Magnetic flux density
Cu	**:**	Copper
CuBr	**:**	Copper Bromide
cP	**:**	Centipoise
ε_r	**:**	Relative Dielectric Constant
F	**:**	Frequency
g	**:**	Gram
H	**:**	Magnetic field strength
Hz	**:**	Hertz
i	*:*	Number of Polymer Molecules
k_{active}	**:**	Activation of Atom Transfer Radical Polymerization
$k_{dactive}$	**:**	Deactivation of Atom Transfer Radical Polymerization
kg	**:**	Kilogram
M	**:**	Magnetization
Mi	**:**	Molecular Weight of a Chain
Mn	**:**	Number Average Molecular Weight
Mv	**:**	Viscosity Average Molecular Weight
Mw	**:**	Weight Average Molecular Weight
Mz	**:**	Z-Average Molecular Weight
Ni	*:*	Number of Chains of molecular weight.
Oe	**:**	Oersted
R	**:**	Radicals
T	**:**	Tesla
η	**:**	Intrinsic viscosity
η_{inh}	**:**	Inherent viscosity
η_{rel}	**:**	Relative viscosity
η_{sp}	**:**	Specific viscosity
θ	**:**	Contact Angle
λ	**:**	Wavelength

μd	*:* Permeability of diamagnetic material.
μf	**:** Permeability of ferromagnetic materials
μo	**:** Permeability of vacuum
μp	*:* Permeability of paramagnetic materials
χ	**:** Dielectric Constant
χr	**:** Relative dielectric constant

LIST OF TABLES

xix

TABLE OF FIGURES

THE EFFECT OF BORAX ADDITION TO POLY(METHYL METHACRYLATE)

SUMMARY

Poly(methyl methacrylate) PMMA is a thermoplastic having outstanding optical properties, transparent and bright appearance, rigid and robust dimensional properties, being hard, scratch-resistant and resistance to ultraviolet radiation. The Atom Transfer Radical Polymerization (ATRP) method is one of the types of polymerization that allows the polymerization of monomers in a controlled manner. Therefore, the ATRP method allows obtaining the PMMA with higher molecular weight and lower Polydispersity index. Base PMMA by ATRP was reinforced borax ($Na_2[B_4O_5(OH)_4].8H_2O$) at 5 and 10 (wt.%) amount to improve the mechanical properties of polymer composite.

The effect of the borax reinforcement on the average molecular weight was investigated in PMMA synthesized by the ATRP method. For this purpose, solutions derived from the synthesized polymers and toluene (solvent for PMMA) were prepared at 25°C to determine the average molecular weight of base PMMA and PMMA/Borax composite. Relative viscosity, specific viscosity, inherent viscosity, and the intrinsic viscosity of the solution were calculated and the average molecular weights of polymers were determined by using the Mark-Houwink Sakurada Equation. It was determined that base PMMA had an average molecular weight of 270.000 g/mol. Besides, this value of PMMA/Borax composite with 5 (wt.%) borax amount was determined as 275.000 g/mol. The average molecular weight of PMMA/Borax composite containing 10 (wt.%) borax was determined as 670.000 g/mol.

Shore D Hardness test was applied to base PMMA and PMMA/Borax composite samples. As a result of the hardness tests, 75 Shore D hardness was determined for base PMMA sample. 88 Shore D hardness was specified for PMMA with 5 (wt.%) Borax. Besides, 86 Shore D hardness was detected were determined for PMMA/Borax composite (with 10 wt.%). Therefore, the borax addition to PMMA has enhanced the hardness value of PMMA with ~5 (wt.%) borax reinforcement. The reinforcement with borax has decreased slightly the hardness value at ~10 (wt.%) borax.

The effect of borax addition in PMMA has affected the magnetic properties of PMMA. It was determined that base PMMA indicates diamagnetic properties when it exposed to an external magnetic field. On the other hand, PMMA/Borax composite samples magnetized slightly in the same direction as the applied external magnetic field.

The effects of borax addition on the optical properties of PMMA were investigated. Transmittance percentages of PMMA / Borax composite samples in the visible range (380-700 nm) were measured as 1%. The borax addition in PMMA decreased the optical transmittance of the polymer composite as borax addition made PMMA more opaque.

The effects of borax addition in PMMA on the wettability were investigated. As the contact angle was a way to measure the wettability of the sample surface the contact angle of the sample surface was detected for all samples. This angle in base PMMA

was detected as 95°. In PMMA with 5 (wt.%) borax for base PMMA was detected as 81°. Besides, this angle in PMMA with 10 (wt.%) borax was 71°. As a result of these measurements, the borax addition in PMMA caused to increase in the wettability of PMMA.

The effect of borax addition on thermal stability was investigated in PMMA by thermal gravimetric analysis. When the borax amount increased in PMMA the thermal stability of polymer composite decreased due to the high moisture content of borax. The weight loss of base PMMA was measured %5 at 208°C, whereas this amount of weight loss was measured at 192°C in PMMA with 10 (wt.%) borax.

In order to detect the functional groups formed in the base and composite samples, infrared rays with a wavelength of 4000-400 cm^{-1} were applied to the polymers. In FTIR spectroscopies of these polymers were observed the following peaks: the peaks formed at 2994 cm^{-1} and 2952 cm^{-1} belong to C-H stretching, 1772 cm^{-1} C = 0 stretching, 1484 cm^{-1} and 1435 cm^{-1} C-H bending or scissoring, 1271 cm^{-1} and 1240 cm^{-1} C-0 stretching, 1190 cm^{-1} C-O-C bending, 1144 cm^{-1} C-H_2 bending and finally, the peak formed at 1063 cm^{-1} belongs to the C-0 stretching.

X-ray diffraction (XRD) patterns were examined for the detection of crystal structures in polymers. There were three broad humps in PMMA without borax due to the amorphous structure of PMMA. These humps were in the range of ~ 10–25°, 25-35°, 35-45°. Three peaks on these humps were determined at PMMA/Borax composite samples. Besides, the rise of borax amount resulted in the increase of diffraction peaks. The positions of these peaks were 18 °, 20 °, 25 ° and it was determined to belong to borax.

BORAKS TAKVİYESİNİN POLİ(METİL METAKRİLAT) ÜZERİNDEKİ ETKİSİ

ÖZET

Son yıllarda artan enerji talebine karşın konvansiyonel enerji (odun, kömür, petrol) rezervlerinin gitgide azalması ve bu enerji kaynaklarının kullanılması sırasında açığa çıkan gazların ya da katı partiküllerin çevreye ve insan sağlığına olumsuz etkisinden dolayı çevreye daha duyarlı güneş pilleri gibi alternatif kaynaklara (yenilenebilir enerji) yönelim olmuştur.

Güneş hücrelerinde, güneş ışınlarının (fotonlar) taşıdığı iç enerji fotoelektrik reaksiyonlardan yararlanılarak doğrudan elektrik enerjisine dönüştürülür. Güneş hücrelerinin, şehirden uzak bölgelerde veya şehir içindeki konutların yeterli genişlikteki çatılarda kullanımının, daha etkin bir şekilde sağlanması çalışmaları, devam etmektedir. Bu çalışmalar güneş pilleri üretimi sırasında kullanılan güneş hücrelerini taşıyan daha hafif, yüzey çizilmelerine karşı daha dayanıklı, kendi kendini temizleme özellikleri daha da gelişmiş ve ekonomik alternatif güneş hücresi taşıyıcıları konusundaki araştırmaları da yaygınlaştırmıştır. Bu tez çalışmasında, hem doğal kaynakları verimli kullanmak, hem de güneş pillerinde kullanılan taşıyıcıların ağırlıklarını azaltmak amaçlanmıştır. Ağırlığı azaltılan güneş hücresi taşıyıcıların, imalattan kuruluma kadar geçen süreçlerde, enerji tasarrufu, kurulum kolaylığı gibi çeşitli ek avantajlar sağlaması beklenmektedir.

Poli(metil metakrilat) (PMMA) olağanüstü optik özelliklere sahip, saydam ve parlak görüntülü, rijit ve sağlam boyutsal özellikler taşıyan, sert ve çizilmeye karşı dayanaklı, morötesi bölgedeki güneş ışınlarına ve hava etkisiyle aşınmaya karşı mükemmel direnç gösteren termoplastik türüdür. PMMA metil grubuna ait bir polimer olduğundan dolayı birçok farklı polimerizasyon tekniğiyle üretilebilmektedir. Atom Transfer Radikal Polimerizasyonu (ATRP) metodu bu polimerizasyon tekniklerinden birisidir. Bu polimerizasyon tekniğinde, monomerlerin kontrollü bir şekilde polimerleşmesini sağlanmaktadır. Bu sayede daha yüksek moleküler ağırlıkta ve daha düşük polidispersite indeksine sahip polimerler sentezlenebilmektedir. Bu çalışmada base PMMA, ATRP yöntemiyle sentezlenmiş olup, katalizör olarak literatürde CuBr, ligand olarak PMDETA (N,N,N′,N″,N″-Pentamethyldiethylenetriamine), solvent olarak Tetrabutylammonium bromide (Bu_4NBr), başlatıcı olarak Ethyl α-bromoisobutyrate (EBIB) ve monomer olarak ise Methyl Methacrylate (MMA) kullanılmıştır.

ATRP metodu ile sentezlenmiş PMMA'ya, sentez sırasında yüzey sertliğinin ve ıslanabilirlik özelliğinin artırılması amacıyla boraks eklenmiştir. Bu amaçla, ağırlıkça % 5 ve 10 olmak üzere, polimere iki farklı miktarda boraks ($Na_2[B_4O_5(OH)_4]·8H_2O$) takviyesi yapılmıştır. ATRP metoduyla sentezlenen boraks takviyesiz ve boraks takviyeli PMMA'nın ortalama moleküler ağırlığı incelenmiştir. Sentezlenen bu polimerlerin ortalama moleküler ağırlığını ölçmek için, çözücü olarak tolüen kullanılarak, polimer ve çözücüden oluşan solüsyonlar oluşturulmuştur. Bu solüsyonlara ait bağıl viskozite, spesifik viskozite, içsel (intrinsic-gerçek) viskozite ve

logaritmik viskozite sayısı (inherent viscosity) değerleri hesaplanarak, Mark-Houwink Sakurada denkleminde kullanılmıştır. Sentezlenen bu polimerlere ait ortalama moleküler ağırlık değerleri hesaplanmıştır. Bu hesaplamalar neticesinde, katkısız PMMA'nın ortalama moleküler ağırlığı 270.000 g/mol, ağırlıkça %5 boraks katkılı PMMA'da bu değer 275.000 g/mol, ağırlıkça %10 boraks katkılı PMMA'da, ortalama moleküler ağırlık değeri 670.000 g/mol elde edilmiştir. Viskozite ortalama molekül ağırlık deneyi sonuçları, ATRP yönteminin ortalama moleküler ağırlığa olumlu etkisini açıkça göstermiştir. Boraks katkısının ortalama moleküler ağırlığa etkisi ise ağırlıkça %5 katkı oranı için sabit iken, ağırlıkça % 10 boraks katkısında ise PMMA kompozitin ortalama moleküler ağırlığı önemli ölçüde arttığı tespit edilmiştir.

Sentez yöntemi olarak seçilen ATRP yöntemi ve takviye malzemesi olan boraksın PMMA'nın sertlik değeri üzerindeki etkisi, Shore D sertlik skalasında ölçülmüştür. Bu ölçümler neticesinde, katkısız PMMA'nın sertlik değeri 75 olarak ölçülürken, ağırlıkça %5 boraks takviyeli PMMA'nın sertlik değeri 88, ağırlıkça %10 boraks takviyeli PMMA'nın ise 86 olarak ölçülmüştür. Elde edilen bu sonuçlar neticesinde, sentez yöntemi olan ATRP'nin ve takviye maddesi olarak seçilen boraksın PMMA'nın sertlik değeri üzerindeki pozitif etkisi tespit edilmiştir. Ancak boraks takviye oranının bir miktardan sonra sertliği olumsuz yönde etkilediği görülmüştür. Sertlik açısından ideal takviye miktarının, yapının homojenliği de göz önüne alınarak, ağırlıkça % 5-10 arasında olduğu tespit edilmiştir.

Boraks katkısının manyetik özelliklere etkisi incelenmiştir. Boraks katkısı ile birlikte PMMA'nın dış manyetik alana maruz kaldığında paramanyetik özellik göstermeye başladığı tespit edilmiştir. Elde edilen bu yapının manyetizasyonunu daha da artırmak için çeşitli ek takviyelere ihtiyaç duyulduğu sonucuna varılmıştır.

ATRP ve boraks katkısının PMMA'nın optik özellikleri üzerindeki etkileri araştırılmıştır. ATRP yöntemi ile sentezlenen, PMMA'nın (2 mm kalınlık) görünür bölgede maksimum ~ % 60 geçirgenlik tespit edilmiştir. Boraks katkısının bu polimerin optik özelliğini neredeyse yok ettiği (görünür bölgede %1'lik geçirgenlik oranı) ve PMMA'yı opak bir malzemeye dönüştürdüğü tespit edilmiştir.

ATRP yöntemi ile sentezlenen boraks takviyeli ve takviyesiz PMMA'nın ıslanabilirlik özelliği üzerindeki etkileri karşılaştırmalı olarak incelenmiştir. Bunun sonuncunda, ATRP yöntemi ile sentezlenen PMMA'nın, temas açısı değerini artırdığı (95°), dolayısıyla yüzeyin daha az ıslanmasına sebebiyet verdiği tespit edilmiştir. Boraks katkısının, polimer kompozit yüzeyin ıslanabilirlik özelliğini artırdığı belirlenmiştir. Bu açı değeri, ağırlıkça % 5. boraks katkılı PMMA'da 81°, ağırlıkça %10 boraks katkılı PMMA'da ise 71° olarak ölçülmüştür. Bir başka deyişle, boraks takviyesi ile birlikte PMMA kompozitinin kendi kendini temizleme özelliği artmıştır. Bu durum özellikle güneş pillerinin yüzeyine kum, toprak, toz gibi yabancı materyallerin yapışmasını azaltıp oldukça avantaj sağlayacaktır.

Sentez yöntemi olan ATRP ile boraks takviyesinin, PMMA'nın termal kararlılığı üzerindeki etkisi termogravimetrik analiz yöntemiyle incelenmiştir. Boraks takviyesiz PMMA yapıda, %5 ağırlık kaybı 208°C'de meydana gelmiştir. Bu oranda ağırlık kaybı ağırlıkça % 5 boraks katkılı PMMA'da, 202°C'de ve ağırlıkça % 10 boraks katkılı PMMA'da 198°C'de tespit edilmiştir. Elde edilen sonuçlar neticesinde, boraks takviyesinin içerdiği yoğun nem nedeniyle PMMA'nın termal kararlılığını azalttığı tespit edilmiştir.

Bu çalışmada sentezlenen boraks katkılı ve boraks katkısız PMMA'larda oluşan bağları tespit etmek için, polimere ve kompozitlerine 4000-400 cm^{-1} dalga boyuna sahip kızılötesi ışınlar uygulanmıştır. Polimer ve kompozitlerinde aynı pikler tespit edilmiştir. Fourier dönüşümlü kızılötesi spektroskopisi (FTIR) analizine göre tespit edilen pikler: 2994 cm^{-1} ve 2952 cm^{-1}'deki pikler C-H gerilme, 1772 cm^{-1} 'deki pik C = O gerilme, 1484 cm^{-1} ve 1435 cm^{-1}'deki pikler C-H bükülme veya makaslanma, 1271 cm^{-1} ve 1240 cm^{-1}'deki pikler C-O gerilme, 1190 cm^{-1} 'deki pikler C-O-C bükülme, 1144 cm^{-1} C-H$_2$ bükülme ve son olarak, 1063 cm^{-1}'de oluşan pik ise, C-O gerilmesine aittir.

Polimerlerin yapısında oluşan kristal yapıların tespiti için, X ışını kırınımı (XRD) desenleri incelenmiş olup, boraks takviyesiz PMMA'da amorf yapıdan kaynaklı kambur şeklinde eğriler oluştuğu tespit edilmiştir. X-ışını analizlerinde belirlenen bu kamburlar üç adet olup, bunlar ~10°–25°, 25-35°, 35-45° aralıklarında yer almaktadır. Boraks takviyeli PMMA örneklerinde ise bu kamburlar üzerinde pikler oluştuğu tespit edilmiştir. Bu piklerin konumu, 18°, 20° ve 25° oluşmuş olup, boraksa ait olduğu belirlenmiştir.

Sonuç olarak, ATRP metodu ile sentezlenen PMMA'nın yüzey sertliği, borax takviyesiyle modifiye edilerek, artırılmıştır. Böylece, güneş pillerinin maruz kalabileceği kum fırtınaları vb. mekanik hasara karşı, polimer kompozitin direncini arttırmıştır. Ayrıca, boraks katkılandırması yapının ıslanabilirliğini arttırmış olup, bu sayede yapı kendini daha çabuk temizleyebilir hale gelmiştir.

1. INTRODUCTION

The reserves of conventional energy sources such as coal, oil, natural gas are decreasing day by day due to the increasing demand for energy. In addition, due to the negative effects of gases or solid particles resulting from the combustion of these resources on nature and human health, the demand for energy sources more sensitive to the environment and human health is increasing day by day such as solar energy, wind energy and geothermal energy.

Solar photovoltaic systems convert sunlight into electricity. The solar photovoltaic energy consumption has increased to 510 TWh in 2018 while the energy produced from solar photovoltaic in 2017 was 407 TWh worldwide. The increase in the use of these systems also causes an increase in the materials used in the production stage. Therefore, this change in energy consumption needs to be supported by the production of materials used in energy systems [1-4].

The lightweight of the produced materials in photovoltaic systems provide energy efficiency as it will reduce fuel consumption from the end of the production stage to the assembly stage. Besides, since the photovoltaic system is mostly used on roofs, it provides ease of installation, and in any failure will provide ease of dismantling.

The photovoltaic systems used in roofs should be able to combat natural phenomena such as snow they will be exposed to these natural phenomena more. Photovoltaics are also used in rural areas away from settlements.

Soil or sand hurricanes caused by winds can erode the surface in time. The material used in these systems is expected to be resistant to this effect. Besides, more water retention of the structure will cause a self-cleaning effect on the system. This will be very advantageous when the surface is subjected to coverings such as dust, soil or sand and where intervention is difficult.

Poly(methyl methacrylate) (PMMA) is a thermoplastic having outstanding optical properties (%93 transmittance in the visible range) with low density (1,18 g/cm^3), transparent and bright appearance, rigid and robust dimensional properties, being hard

scratch-resistant and resistance to ultraviolet radiation [5-6]. These properties of PMMA have greatly expanded its use. To give an example, it is used commonly in the health applications, optical applications, greenhouses, interior and exterior lighting of the automotive sector.

When the structural properties of PMMA are evaluated, the following results can be reached. In terms of mechanical properties, PMMA is in the middle-high class when only thermoplastics is considered, while it is present in the middle class in all plastics [7-11]. It exhibits diamagnetic properties when it exposed to any external magnetic field [12-13]. Base PMMA has presented the contact angle between ~64-73° [14-17]. This contact angle is accepted as a medium grade in terms of wettability, which expresses the relationship of the surface with water. The average molecular weight, which is a measure of the density of bonds formed in the structure, is in the range of 70,000-110,000 g/mol in PMMA [17-20]. Like all thermoplastics, it exhibits a relatively low thermal performance in thermal applications [21-23].

PMMA is a type of amorphous polymer can be obtained by direct exposure of MMA to irradiation or heat. Besides, PMMA can be fabricated as a result of synthesis with different types of polymerization. The atom transfer radical polymerization method is one of them and ATRP is one of the Controlled/"Living" Radical Polymerizations. Polymer synthesis in these polymerization types takes place in a controlled manner. Therefore, the ATRP method allows polymers to be obtained with narrow molecular weight distribution and long-lived polymer chains. Besides, it can be predetermined the degree of polymerization in ATRP [24-28].

In this thesis, base PMMA and PMMA/Borax composite samples were synthesized by the ATRP method. In this synthesis, copper bromide (CuBr) was selected as catalyst, PMDETA (N, N, N ′, N ′ ′, N ′, PentPentamethyldiethylenetriamine) as ligand, Tetrabutylammonium bromide (Bu_4NBr) as solvent, Ethyl α-bromoisobutyrate as initiator (EBIB) and Methyl Methacrylate (MMA) was selected as monomers due to the efficient results of these components in the literature [29-32].

There are in nature more than 150 boron minerals, containing boron element and these minerals are named with the name of cation which they combined (calcium borax, sodium borax, magnesium borax, strontium borax). Sodium tetraborate decahydrate

(Borax, $Na_2.2B_2O_3.10H_2O$) presents several features that its density is 1,73 g/cm^3 (at 20 °C) and its water solubility 38,1 g/l at 20 °C (completely soluble) [33-36]. On the other hand, the Mohs hardness of borax is presented as 2,5. Powdered borax is white and the result of the colorimetric test in borax is 91,92 for average L value (L* = 0 yields black, L* = 100 indicates diffuse white in the CIELAB color space) [37]. Hence, borax was added as reinforcement material at 5-10 (% wt.) in PMMA/Borax composite samples to increase the hardness and the wettability properties of the composite samples.

2. BACKGROUND AND LITERATURE REVIEW

2.1 Polymers

Polymers are common materials in daily life with developing technology due to their low density compared to basic engineering materials such as metal, having a structure suitable for doping and changing easily their properties with reinforces. However, one of the major disadvantages of them is their low mechanical properties compared to metals. Besides that, with various contributions, studies on increasing thermal, magnetic and optical properties have continued in recent years [38].

Polymers are macromolecular structures formed by covalent bonding of a large number of monomers and composed of many repeated subunits [11]. This is also observed in Figure 2.1 [39]. These repeat units form the most significant building block of polymer and the description of the polymers is based on these them [40]. TO give an example, Poly(methyl methacrylate) named as PMMA forms as a result of the polymerization of methyl methacrylate (MMA) and takes its name from methyl methacrylate (MMA). Polymers are divided into three in terms of repeated units. If a polymer contains one type of repeated units (monomer), it is classified as homopolymer (such as Poly-acrylic acid, Poly-methyl methacrylate). On the other hand, if a polymer consists of two different repeating units, they are called copolymers (poly(styrene-co-(methyl methacrylic). Besides, if three repeat units form a polymer, then this polymer is called terpolymer [40-41].
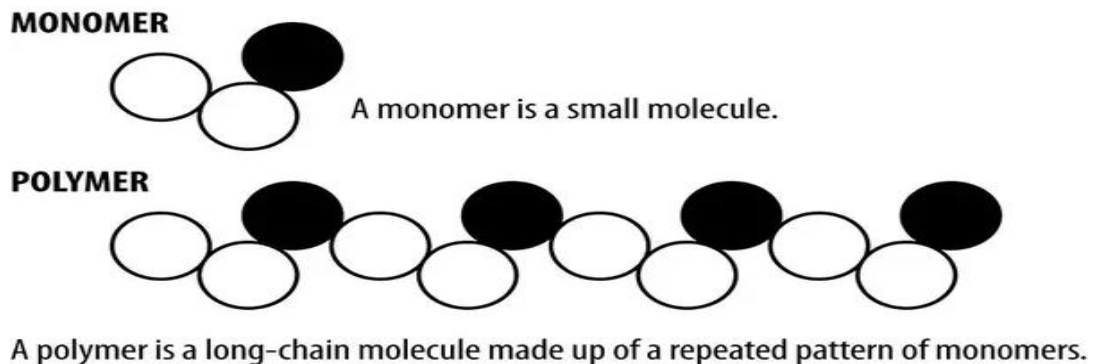
Figure 2.1: Forming of monomer and polymer [39].

2.1.1 Polymer Types

Polymers are divided into three in terms of the creation. One of them is the natural polymers. These polymers exist in nature and are extracted in nature. There is no need laboratory environment to create any natural polymers. They are usually based on water such as DNA, cellulose, and proteins. The second type of them is synthetic polymers. They derived from petroleum oil in the laboratory environment. Polymers such as nylon, polyethylene, polyester, and epoxy are included in this class. Third of them is semi-synthetic polymers. These polymers are obtained as a result of the modification of natural polymers in the laboratory environment. They are formed as a result of chemical reactions (in a controlled environment) such as vulcanized rubber (Sulphur is used in cross bonding the polymer chains found in natural rubber) [18,42].

2.1.2 Classification of Polymers

Polymers can be classified as thermoplastics, elastomers, thermosets in terms of linking chains and Figure 2.2 indicates the bonding of the chains of thermosets and thermoplastics.

Thermoplastic
B: Branch

Thermosettings
□: Crosslinking point
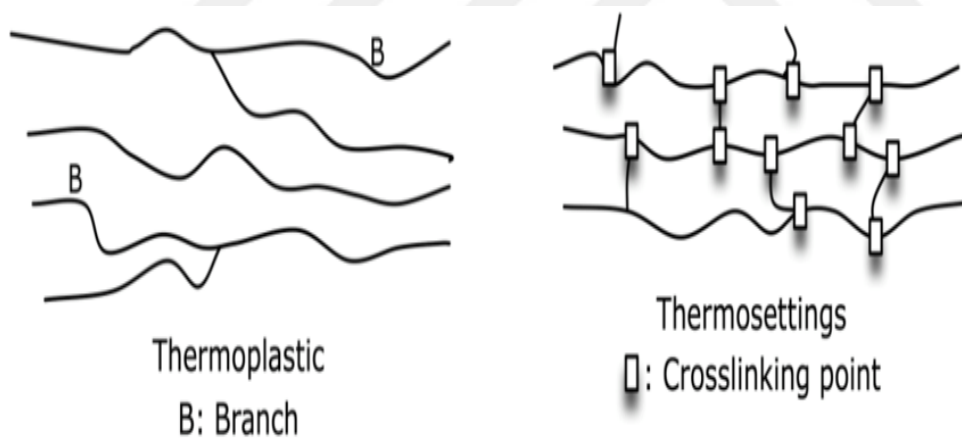
Figure 2.2: The linking of chain in thermoplastic and thermosetting [43].

2.1.2.1 Thermoplastics

Van der Waals bonds exist in the structure of thermoplastics. These bonds are relatively weak. When the thermoplastics are exposed to the heat treatment, the debonding in thermoplastics occurs easily. However, the heat applied heat treatment is eliminated, these lost bonds are formed again. This is one of the most important properties of thermoplastics. So, after using thermoplastics can be melted and reused [44].

Van der Walls bonds cause thermoplastics to exhibit relatively low mechanical performance even though they provide reusing of the thermoplastics after the heat treatment application. This low mechanical performance is one of the most significant disadvantages of these polymers. These van der Waals force which allows the chains to be connected to each other are shown in Figure 2.3 [40].
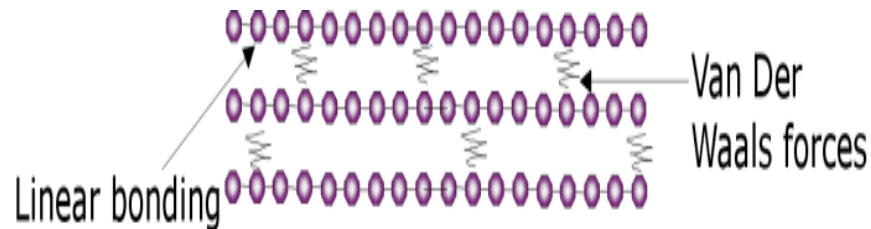
Figure 2.3: Schematic of thermoplastic [45].

2.1.2.2 Thermosets

The chains in thermosets are linked by cross-linking with each other. These cross-links are quite strong and their debonding is more difficult than the debonding of van der Walls. These strong links provide thermosets to exhibit higher mechanical behavior against mechanical loads. On the other hand, when thermosets are applied a heat application at a temperature higher than the glass transition temperature (Tg), these cross-links vanish permanently. Because of that, they can not be reused. The cross-links forming the thermosets can be seen in Figure 2.4 [45].
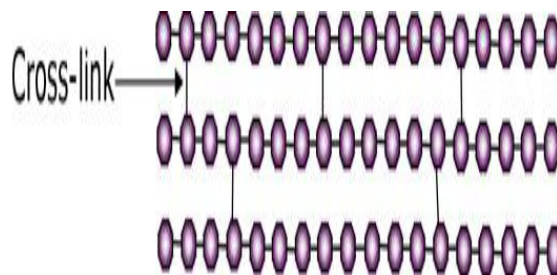
Figure 2.4: Schematic of thermoplastic [45].

2.1.2.3 Elastomers

In elastomers, chains are connected to each other by van der Waals bonds and cross-sections. Figure 2.5 indicates the cross-links and van der Walls bond-forming the elastomers [45]. The cross-links in structure provide elastomer to revert back to its initial form after deformation. It can also be said that these bonds bring in flexibility to the elastomers. On the other hand, the effect of van der Walls bonds in the structure do not provide elastomers to reused after the heat application, unlike in thermoplastics.

7
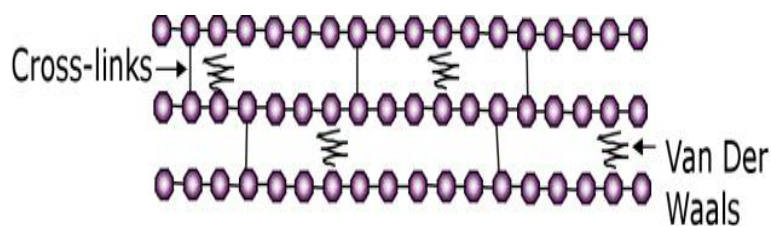
Figure 2.5: Schematic of elastomers [45].

2.1.3 Macroscopic structure of polymers

Polymers are divided into four as *macroscopic structure*. There are *linear*, the *branched polymer*, *network polymer*, and *cross-linked polymer.*

2.1.3.1 Linear polymer

A polymer is mentioned as a linear polymer when it consists of a single continuous chain of repeat units such as HPDE (High-Density Polyethylene). Some properties of these polymers can be listed below [46]. The chemical structure and macroscopic structure of HDPE, a linearly bonded polymer, is shown in Figure 2.6 [47]. Thanks to the structure of linear bonded polymers it has the following properties:

- *High tensile strength* thanks to their close packing of polymer chains
- *High density (*density of HDPE is 0,958-0,963 g/cm^3 whereas density of LDPE (Low Density Polyethylene) is 0,918-0,934 g/cm^3)
- *High melting point* (130-135 °C), whereas 110 °C is the melting point of LDPE
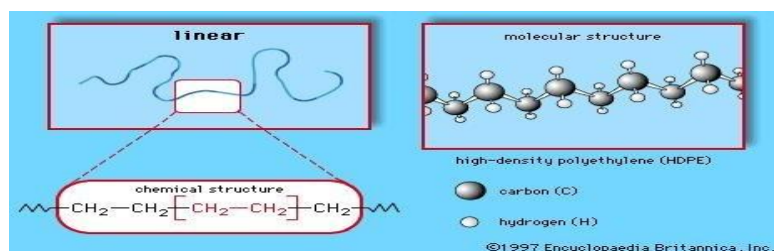
Figure. 2.6: Macroscopic structure of a linearly bonded polymer [47].

2.1.3.2. Branched polymer

Monomers coming together to form polymers are formed branched polymers at different chain lengths such as Low-Density Polyethylene (LDPE) and glycogen. Low tensile strength, low boiling point, low density are some properties of these polymers [46-48]. The microstructure of the LDPE belonging to this type of polymer is shown in Figure 2.7 [49].

8
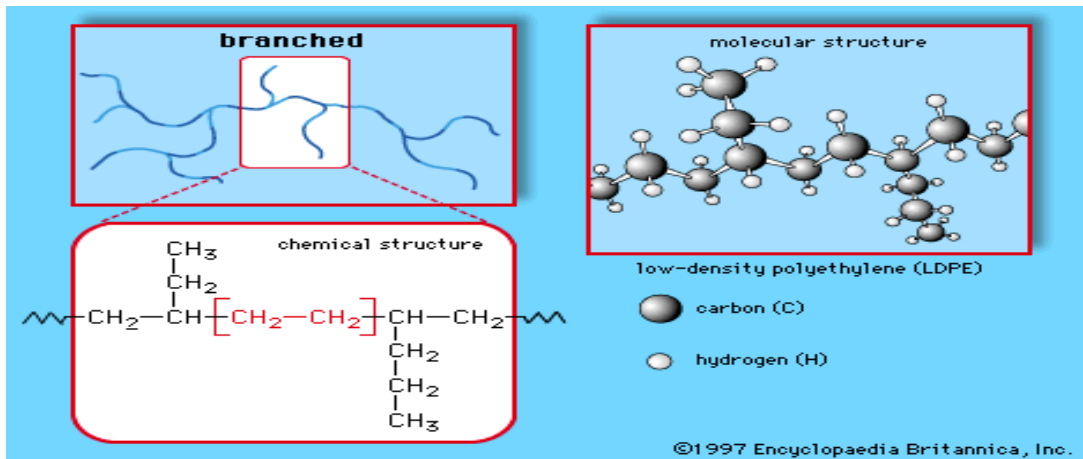
Figure 2.7: Macroscopic structure of a branched polymer [49].

2.1.3.3 Cross linked polymer

In polymer having cross-linked, there is more than one main chain and these chains are connected to each other by cross bonds, such as rubber. Thermosets and elastomers are included in this class. The breakdown of these cross-linked is relatively difficult. Because of that, polymers with cross-linked is more stable in terms of the mechanic and thermal than thermoplastics. After melting these polymers cannot be used repeatedly because of being damaged permanently in cross-linked [50-52]. The Microstructure of this type of polymer is shown in Figure 2.8 [53].
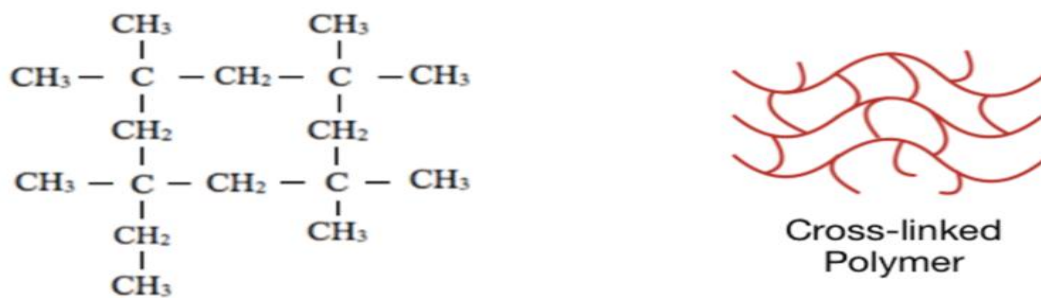
Figure 2. 8: Macroscopic structure of cross-linked polymers [53].

2.1.3.4 Network polymer

The networked polymers consist of complex three-dimensional linkages. The softening of these polymers are nearly impossible when heating without degrading the underlying polymer structure. The microstructure of this type of polymer is shown in Figure 2.9 [54].
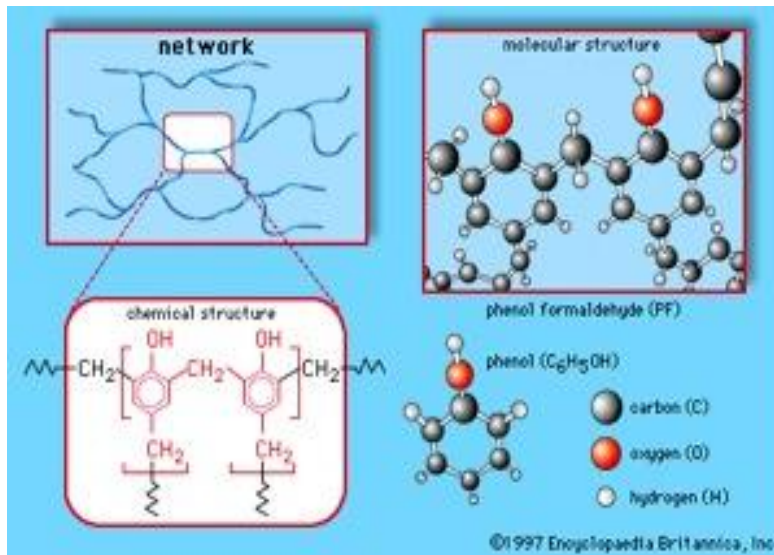
Figure 2.9: Macroscopic structure of network polymers [54].

2.2 Polymerization

Polymerization is the repetition of the "n" number of polymers consist of the chemical bonding of monomers with each other. Polymers or Oligomers are formed by repeated monomers, which are linked with covalent bonds. If the number of repeating units is less than ten, they are called oligomer ("oligo" = "few"), whereas they are called as polymers if their numbers are more than ten. It cannot be mentioned a definite limit on the number of these repeating units [55-56].

The Degree of polymerization is the average number of repeating units per chain. It is represented by DP. DP is equal to n (in Figure 2.10). For homopolymers, it can be calculated in equation 2.1.

$$Dp = Xn = M_n/M_0 \tag{2.1}$$

Where: Mn is average molecular weight and Mo is the Molecular weight of monomer.

Degree of polymerization
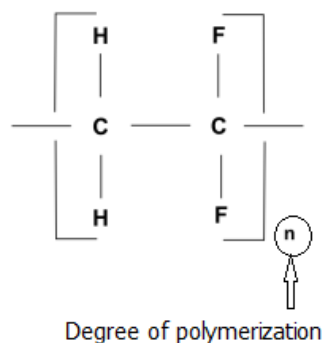
Figure 2.10: Degree of polymerization [57].

Polymerization reactions are divided into three: *Step-Growth Polymers*, *Chain-Growth (Addition) Polymerization*, and *Controlled Living Radical Polymerization*

2.2.1 Step-growth polymers

This polymerization involves a reaction between monomers from different functional groups. As these monomers come together, they react to each other and as a result of this reaction, they lose usually a small molecule such as H_2O, HCl, and NH_3, etc. [58-60]. This polymerization type can ben seen in Figure 2.11 [61]. In this example, water was produced as a result of polymerization.
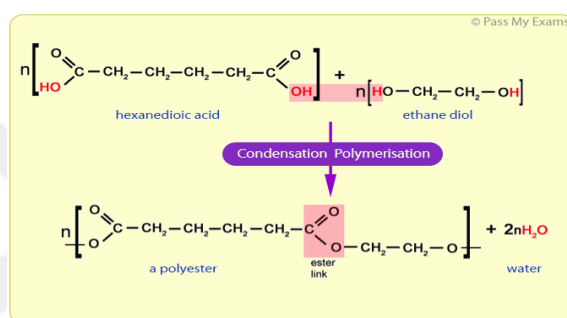
Figure 2.11: Schematic illustration of Step-Growth Polymerization [61].

2.2.2 Chain-growth (Addition) polymerization

Polymerization is formed as a result of the sequential addition of monomers without any loss in atomic numbers, unlike condensation polymerization. There are two different types of Chain-Growth polymerization as free radical polymerization and anionic addition polymerization. This polymerization is needed reactive such as free radicals, which are atoms or atomic groups containing one or more unpaired electrons, anions or, cation to initiate polymerization. There are three types of the initiator as cationic, radical, anionic. This polymerization consists of respectively three steps called initiation, propagation, and termination [62]. The formation of this polymerization is shown in Figure 2.12.
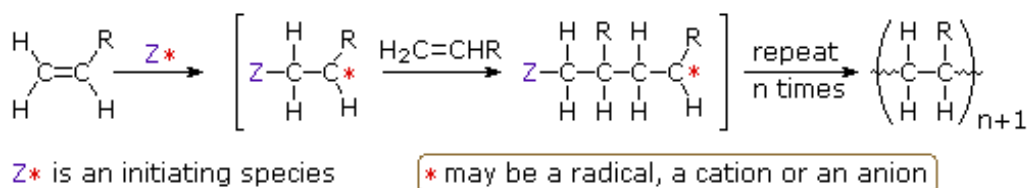
Figure 2.12: Chemical schematic of Chain-Growth (Addition) polymerization [62].

2.2.3 Radical chain-growth polymerization

Radicals are needed for reactions to take place. Free radicals are released after thermal, chemical, irradiation reaction of initiators, which contain unpaired radicals. Firstly, this free radical connects to a monomer, which is found in the ambiance of polymerization. After that, another monomer from this ambiance connects to this chain. Thus, a long chain is obtained. There are three steps in radical polymerization called initiation, propagation, and termination. It can be shown in Figure 2.13 progress stages of free radical polymerization. Here, radicals were obtained as a result of irradiation [63-64].

The termination step in radical polymerization takes place in two different ways, which are combination and disproportionation. In one of them called combination, two different active polymer chains connect to each other. In another termination called disproportionation, the hydrogen atom is transferred from a chain to another chain. After that, the active chain transforms into the passive. As shown in Figure 2.13 [65], radicals are formed due to UV rays. After forming of radicals, initiation, propagation and termination takes place respectively and the polymer is obtained.
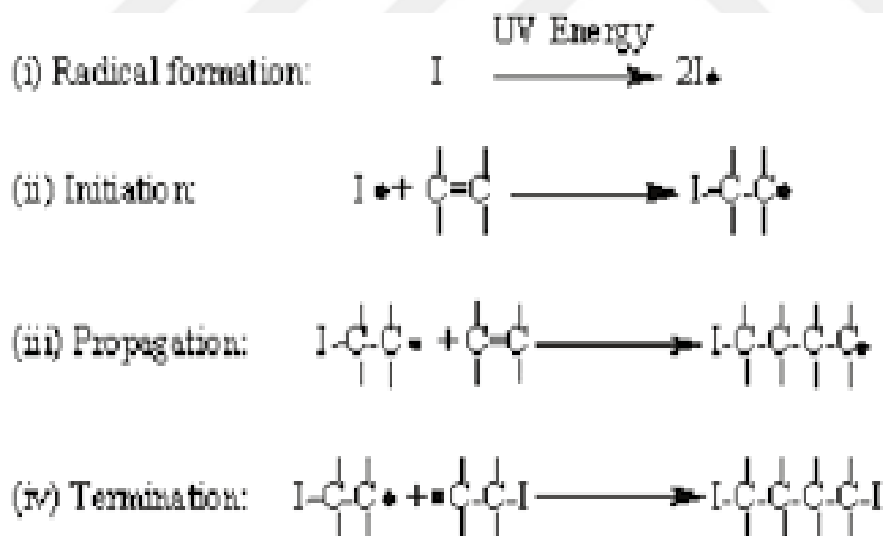
Figure 2.13: Kinetic of free radical polymerization [65].

2.2.3.1 Ionic chain-growth polymerization

Monomer molecules connect to the ionic active centers at the polymer chain, so this chain enlarges. When this ionic active center is anion, the polymerization is called as anionic radical polymerization, whereas it is called as cationic radical polymerization when the active center is cation.

2.2.4 Controlled / living radical polymerization

"Living" polymerization provides control at polymer architecture, which consists of molecular weight, molecular weight distribution (Polydispersity). The existence of premature termination is shrunk, and molecular weight proceeds linearly with time until all monomer is consumed or intentionally terminated [66].

There are three types of controlled/living radical polymerization as Nitroxide Mediated Polymerization (NMP), metal-catalyzed Atom Transfer Radical Polymerization (ATRP), and reversible addition-fragmentation chain transfer (RAFT) [24].

In Controlled Radical polymerization, chain transfer and termination reactions are eliminated, unlike radical polymerization. In these polymerizations, there is an equilibrium between growing chains and passives. Thanks to this equilibrium, the speed of polymerization decreases and the life of the growing chains can increase hours. In this way, it is possible to produce polymers whose molecular weight and Polydispersity are adjustable without being affected by chain transfer processes. The kinematics of ATRP, RAFT and NMP are shown in Figure 2.14 [25].
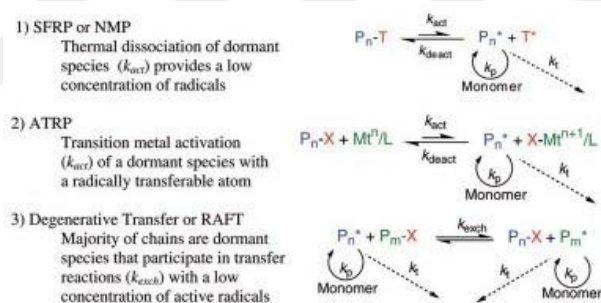
Figure 2.14: Kinematics of ATRP, RAFT and NMP [25].

Some *advances* in living radical polymerization compare to conventional free radical polymerization [26]:

- The lifetime in growing chains (propagation and termination) gets extended from <1 s to more than 1 hour in controlled radical polymerization.
- Initiation step occurs slow and the free radical initiator is generally left unconsumed at the end of conventional radical polymerization.
- The percent of dead chains in CRP is nearly < 20 % while all chains are dead in radical polymerization.
- The Polymerization process in CRP occurs generally slower than the polymerization in radical polymerization.

2.3 Atom Transfer Radical Polymerization

Atom Radical Transfer Polymerization (ATRP) is one of the types of living radical polymerization. This polymerization provides the polymers some attracted properties such as high molecular weight with low weight distribution (Polydispersity). Some monomers such as acrylate, methacrylate, acrylonitrile can be polymerized by this method. [26-27] Components, parameters and kinematic of ATRP is shown (in Figure 2.15).
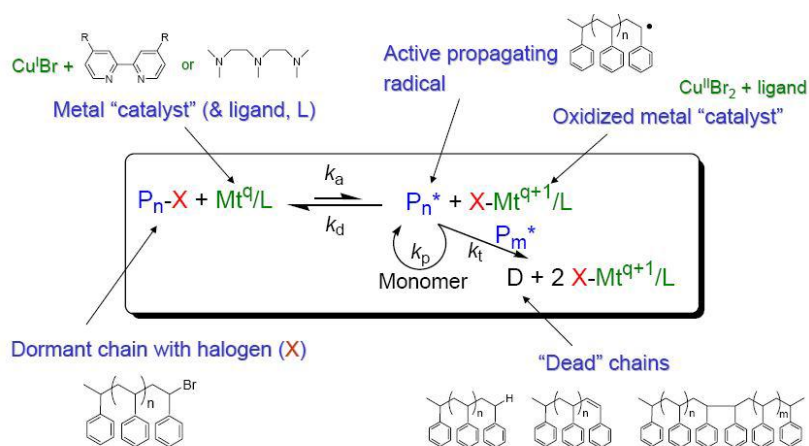
Figure 2.15: Kinematic and components of ATRP [67].

Figure 2.16 indicates k_{deact} and than k_{act}. of ATRP. As shown in Figure 2.16, the k_{deact} is considerably larger than k_{act}. Because of that, After the monomer is added to the radicals, the active radical becomes passive without passing to the termination process and this process continues until the last monomer remains in the ambiance. So, it can be obtained polymers, which have a very low Polydispersity, controlled average molecular weight [25-26].
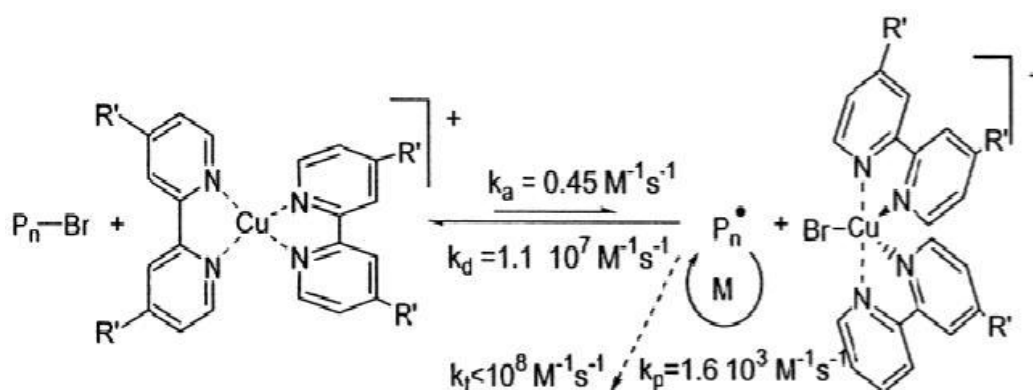
Figure 2.16: k_{active} and $k_{dactive}$ of ATRP [68].

Many different transition metals are used in ATRP as transition metals such as Cu(I), Fe(II), Ni(II), Ru(II), Re(V), Mo(V), Palladium and Co(II). Copper is one of the most common transition metals in catalysts since copper can oxidize from +1 to +2. The biggest disadvantages of this method are that copper, which is toxic, used as catalyst should be removed from the polymer and it is sensitive to acids.

2.3.1 Components of atom transfer radical polymerization

ATRP consists of six basic components: monomers, catalysts, initiators, ligand solvents, reaction temperature and reaction time. Some of them can be seen in Figure 2.17.
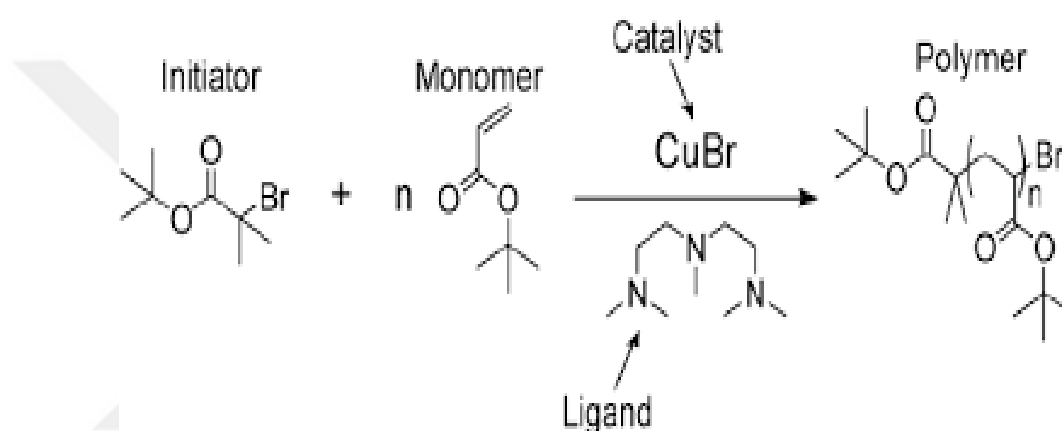
Figure 2.17: Components of ATRP [69].

2.3.1.1 Monomer

Acrylates and methacrylate's which have the ability of stabilization of propagating radicals are used as the monomer in ATRP. In this study, it was used MMA as monomer. It can be seen the chemical formula of MMA (in Figure 2.18) and some significant properties of MMA is given in table 2.1.

Table 2.1: Some significant properties of MMA [31].

Properties	Value
Density	$0,94$ g/cm^3
Molar mass	$100,12$ g/mole
Boiling point	$100,6$ °C
Melting point	-48 °C
Flash point	8°C
Polymerization heat	$2,97$J/mole
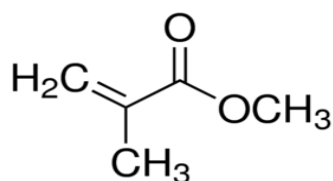
Figure 2.18: Chemical formula of MMA [70

Monomers having a major effect on the ATP reaction may affect reactions as follows:

- If a monomer with a high polymerization rate is used, it may cause an increase in the molecular weight distribution (especially at low initiator efficiency and at low conversion).
- The solubility parameters of the monomers affect the polymerization.
- Since monomers are one of the main components of polymer, other components except for monomer such as catalyst type, ligand, solvent, the temperature should be carefully selected to adjust acceptably the polymerization rate.

2.3.1.2 Catalyst

Catalysts are one of the other important components in ATRP. They react with the halogens present in the initiator and form stable complex compounds with ligands. Thus, they allow the release of radicals and so, monomers are attached to these free radicals and a long chain is obtained. They play a key role in the ATRP as it provides the forming of free radicals.

Catalyst has transition metals such as copper, nickel, iron, ruthenium. The importance of transition metals (for example, Cu-I) abstracts halogen atoms from halogen-terminated inactive polymer chains. It is oxidized to Cu(II) via single electron transfer to generate the growing radical species [25-27,67-71].

An efficient catalyst should have the following properties:

- Forming relatively strong complexation with ligands
- Having reasonable affinity towards the halogen atom
- Two readily available oxidation states separated by one electron

2.3.1.3 Initiators

Using in ATRP as initiators, alkyl halides (R-X) should be fast and quantitative. The initiators consist of radicals and halogens. One of them is radicals (R) that enable them to form longer polymer chains by linking the monomers to the chains and other

16

is Halogens (X) that provide the oxidation of transition metals and the release of radicals. Because of the above-mentioned formations, the initiators should be selected according to the catalysts and monomers. The chemical representation of some ATRP initiators is shown in Figure 2.19 [25].
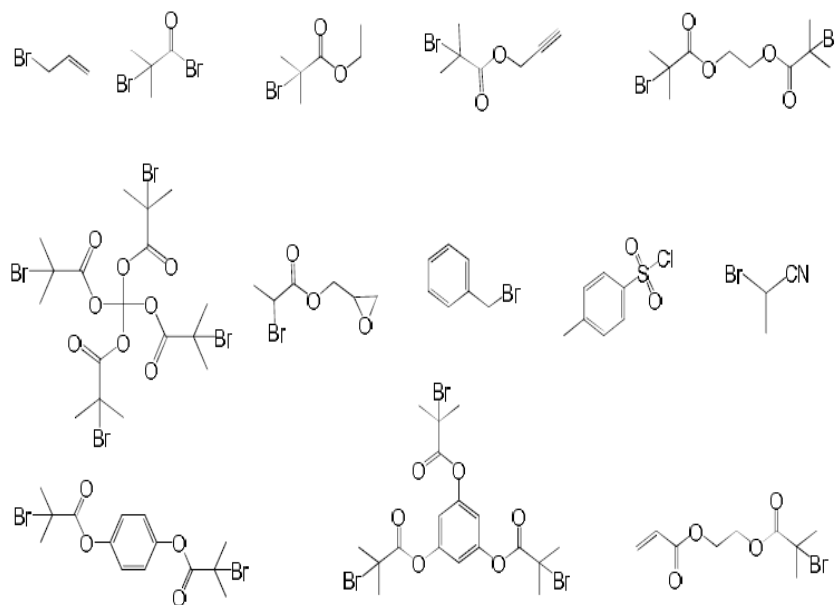
Figure 2.19: Initiator of ATRP [25].

2.3.1.4 Ligand

The main role of the ligands (in Figure 2.20) in ATRP is to dissolve the metal salt. It forms a complex compound. Thus, the catalyst becomes inactive. Since it adjusts the redox potential around the metal center, it affects the reactivity and equilibrium dynamics of the atom transfer process [71].
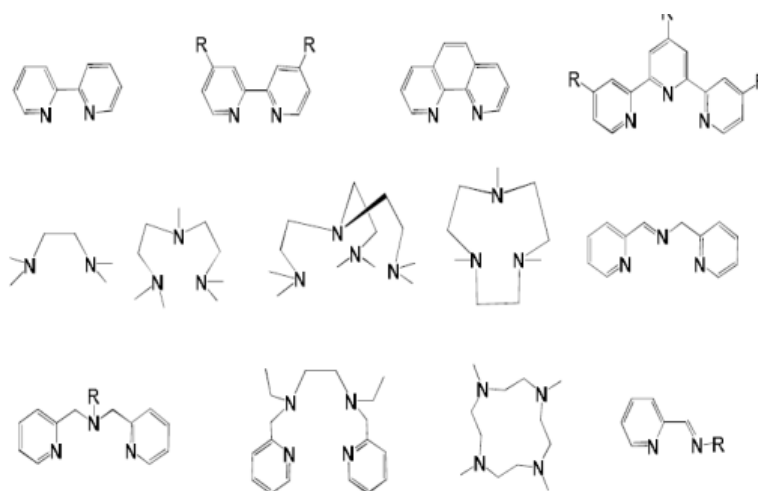
Figure 2.20: Ligands in ATRP [25].

2.3.1.5 Solvent

The main task of the solvent is to dissolve the ligand-catalyst complex in the organic medium. On the other hand, the solvents should not react directly with the catalyst. Such as alcohol, toluene, ethyl acetate, ethylene carbonate, there are different solvents.

2.3.1.6 Reaction temperature and time

Two significant parameters in ATRP such as the atom transfer equilibrium constant and the propagation rate constant increase with the increase of temperature. In addition, the solubility of the catalyst increases at higher temperatures. However, at higher temperatures, some undesirable reactions such as catalyst decomposition occur more often. Thus, it is determined an optimum temperature range. The range of useful reaction temperatures is broad, from 20°C to 150°C [25].

2.4 Use of Polymers

Polymer materials which have a relatively low density than other materials such as metals are not relatively difficult to produce. They are fabricated at relatively low temperatures than metals and it is becoming more and more popular in daily life thanks to the above-mentioned features [72-75].

The synthetic plastic has named as Bakelite was produced in 1907. Today after a century of production of Bakelite, a life without plastic is hardly possible anymore and it is a great challenge to find plastic-free alternatives. Global fabrication in 2017 has increased to 348 million tons. Of these, almost 30% were produced in China. In Europe, plastic production stabilized in 2013 following the slump in the financial crisis in 2009. Today's production in Europe amounts to around 64 million tones [76]. On the other hand, 200 million tons of plastics were produced worldwide in 2017. Almost all of the plastic materials consist of polymers.

Belonging to previous years, the production of plastics worldwide and in Europe can be seen in Figure 2.21. Approximately 36% of plastics produced in 2015 were used for packaging. Approximately 16% for building and construction, approximately 15% textiles and approximately 6% for transportation and approximately 5% for electrical/electronic [77].

Weltweite Plastik-Produktion
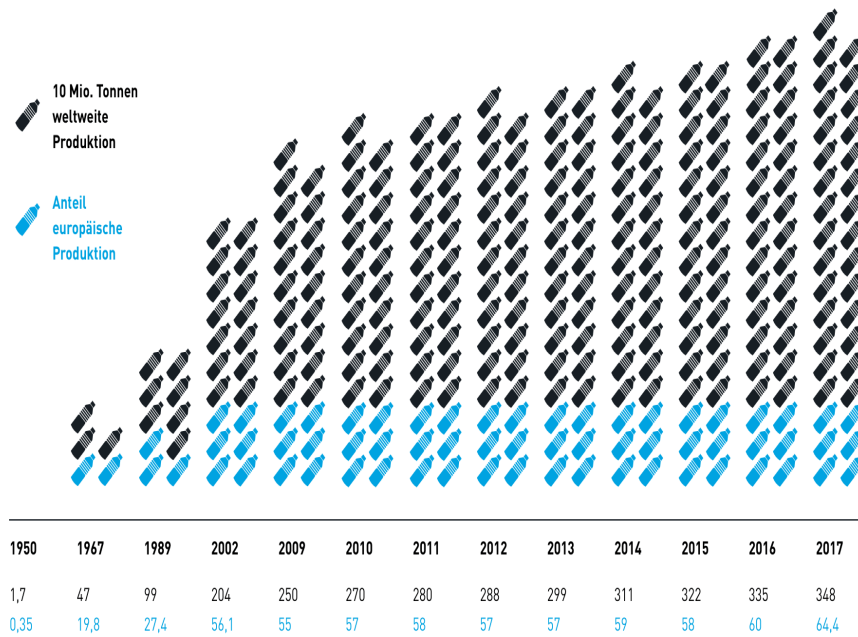
Figure 2.21: Worldwide plastics production [76].

2.5 Poly(methyl methacrylate)

Poly(methyl methacrylate) named as *PMMA* (chemical formula $((C_5O_2H_8)n)$) obtained as a result of polymerization of MMA whose chemical formula is seen in Figure 2.22 is a thermoplastic type. The chemical formula of this polymer is seen in Figure 2.23. This polymer is used quite often in daily life due to the following features:

- Having *approximately half the density* according to glass (density of PMMA is 1,27 gr/cm³ and density of glass is 2,4-2,7 gr/cm³).
- Having *optical properties* as good as glass.
- Being able to *withstand* extreme weather conditions such as snow.
- Being preferred *in the health sector* thanks to its hard structure.
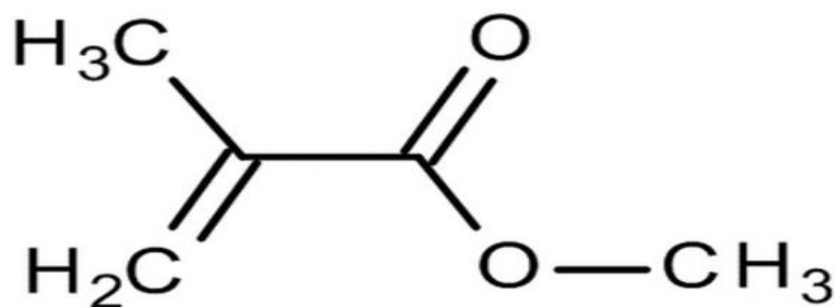
Figure 2.22: Chemical formula of MMA [77].
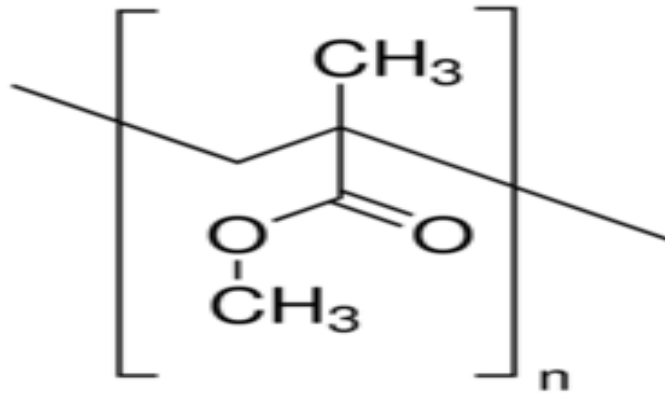
Figure 2.23: Chemical formula of PMMA [78].

2.5.1 Optical properties of PMMA

PMMA, an acrylic type, is obtained as a result of polymerization of MMA is high transparency (93% depending on thickness, for wavelengths between 430 and 1100 nm) thermoplastic type [79]. This Polymer has good properties resistance to Ultraviolet, which is harmful to human health.

PMMA has a very low refractive index (1,5). The refractive index for a material is the parameter that indicates how slowly the electromagnetic waves or light travels through the material about the movement in the vacuum. It is defined as n. To give an example, PMMA has 1,5 as a refractive index, meaning that light travels 1,5 times as rapid at vacuum.

2.5.2 Radiation properties of PMMA

PMMA's neutron absorption cross-section is very low level (for PMMA 0,13, for water 0,12, for steel 0,24, for rhenium 0,35 (cm^{-1}) [80]. The higher the newton absorption cross-section, the lower the transmission defined as the for neutron shielding. PMMA does not have acceptable values for neutron shielding and is also very brittle in electron irradiation [81]. In order to eliminate this weakness of PMMA at irradiation, various doping materials have been tried.

2.5.3 Mechanic properties of PMMA

PMMA does not have as high hardness values as thermosetting. It has average mechanic properties compared to thermoplastic materials. Mechanic properties of PMMA can be shown in table 2.2 [82].

Table 2.2: Mechanics properties of PMMA [82].

Mechanic Properties of PMMA	Value	Comparison with other Thermoplastics
Compressive (Crushing) Strength	120 MPa	middle
Elastic Modules (Young's Tensile)	3,2 GPa	low
Elongation at Break	4%	very low
Impact Strength (Notched Izod)	74 J/m	low-middle
Rockwell M Hardness	93	high

2.5.4 Thermal properties of PMMA

PMMA has 90°C Vicat softening temperature, that meaning, at atmospheric pressure at this temperature (90°C), when PMMA has applied a force of 1 Newton, this force can be penetrated 1 mm depth in PMMA. The polymer material loses its glassy property after the glass transition temperature and becomes viscous. The thermal properties of PMMA are given in table 2.3 [82].

Table 2.3: Thermal properties of PMMA [82].

Thermal Properties of PMMA	Value	Comparison with other Thermoplastics
Glass Transition Temperature	110°C	middle
Heat Deflection Temperature at 182 MPa	96°C	middle
Max. Temperature (Auto ignition)	320°C	middle
Max. Temperature (Decomposition)	360°C	middle
Melting Onset (Solids)	180°C	middle
Specific Heat Capacity	1260 J/kg-K	middle
Thermal Conductivity	0,19 W/m-K	middle
Thermal Expansion	76 μm/m-K	middle
Vicat Softening Temperature	90°C	middle

2.5.5 Electrical properties of PMMA

PMMA is a very suitable material for electrical devices due to its low water absorption capacity (5,2 g.cm/cm^2/h H$_2$0 in PMMA) and high dielectric properties (3,6 Dielectric Strength) [83]. The electrical properties of PMMA are given in table 2.4 [78].

Table 2.4. Electrical Properties of PMMA [82].

Electrical Properties of PMMA	Value	Comparison with other Thermoplastics
Dielectric Strength (Breakdown Potential)	3,6	low-middle
Dielectric Constant (Relative Permittivity) At 1 Hz	30 kV/mm	middle

Dielectrics, which are normally insulator, can be polarized by an electric field. They can store a part of the applied electrical field (relative to their dielectric properties) in the absence of electrical field. Dielectric Constant (ε) is the constant that measures the ability of a material to store electrical loads. In SI units, the ε insulating constant is farad per meter (F/m).

Relative dielectric constant (ε_r): the dielectric coefficient of any material is proportional to the dielectric constant of the vacuum. The relative dielectric constant is calculated in equation 2.2.

$$\varepsilon r = \varepsilon / \varepsilon_0 \tag{2.2}$$

Where ε_r is relative dielectric constant of any material and ε_0 is vacuum dielectric constant and its value is $8,854187817 \times 10^{-12}$ F / m.

2.5.6 Magnetic properties of PMMA

The magnetic susceptibility of PMMA is 9.06×10^{-6} in the SI Unit system which is the subject of our thesis and is quite low like the values of all other polymers (Table 2.5). Various reinforcements have been tried to increase these values [13,84-85]. As shown in Figure 2.24 [86], when diamagnetic materials like PMMA are subjected to any external magnetic field, they are magnetized in the opposite direction to that external magnetic field to which they are subjected.

As shown in Figure 2.24 [86], when diamagnetic materials like PMMA are subjected to any external magnetic field, they are magnetized in the opposite direction to that external magnetic field to which they are subjected.

Table 2.5: Magnetic susceptibility of some materials [12,87-89].

Materials	Temperature (°C)	Pressure (atm)	Volume χv (SI)
Helium [87]	-	1	-9.85×10^{-10}
Air (NTP) [12]	20	1	$3,6.10^{-7}$
PMMA [12]	22	1	*9.06×10^{-6}*
PVC [88]	22	1	-1.071×10^{-5}
Water [89]	20	1	-9.035×10^{-6}
Copper [12]	20	1	-9.63×10^{-6}
Aluminum [90]	-	1	2.2×10^{-5}
Iron [12]	20	1	20.0000
Nickel [90]	20	1	600
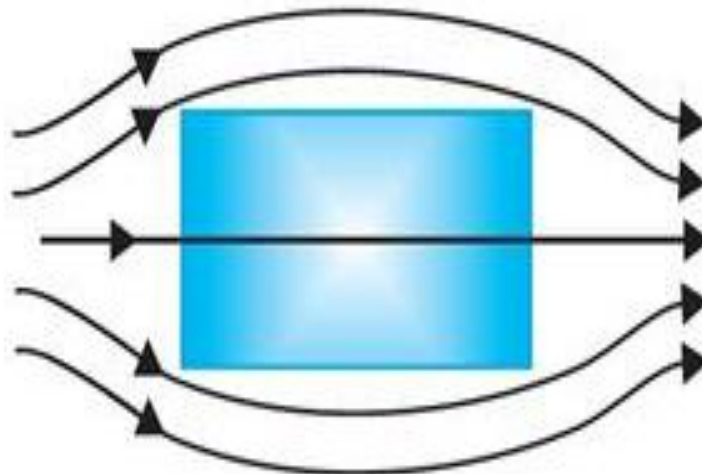
Figure 2.24: Behavior of PMMA against external magnetic field [86].

2.6 Magnetism of Materials

2.6.1 Magnetic field strength

The magnetic field strength is a vector magnitude and it is the ratio of the force acting on the pole of the magnet to the pole intensity of the magnet. H is the unit of magnetic field strength. The units of the magnetic field intensity (H) is Oersted (Oe). 1 Oe is defined as the field strength at 1 cm of the unit pole [91].

2.6.2 Magnetic flux density

Magnetic flux can be defined as the concentration of lines of force at any point. On the other hand, the magnetic flux density defined the flux per unit is represented by the symbol B, or in vector form B. For magnetic flux density, the units are gauss (G) in the CGS system of units or tesla (T) in the MKS system [91].

2.6.3 Magnetic susceptibility

Magnetic Susceptibility is expressed the behavior of the material against the magnetic field. It is calculated with equation 2.3 [92].

$$M = \chi . H \tag{2.3}$$

where M: magnetic flux density and H: magnetic filed strength. Magnetic Susceptibility of some materials can be seen in table 1.4.

Magnetic susceptibility of the materials is a measure of their magnetization. As this unit less value increases, the material becomes more magnetized when subjected to any external magnetic field.

To give an example, the materials in table 1.4 have a very low magnetic value. When these products (diamagnetic) are exposed to external magnetic fields magnetized at the low levels than materials (paramagnetic or ferromagnetic) having higher magnetic susceptibility.

2.6.4 Magnetic susceptibility

Magnetic permeability, which expresses the magnetization capacity, is a measure of how much a material can support electromagnetic flux to pass through itself within an electromagnetic field applied to it. The permeability is measured in henry per meter (H/m), or equivalently in newton per ampere squared (NxA^{-2}) in SI units.

2.6.5 Relative susceptibility

Relative Permeability is defined by a symbol μr and it refers to the permeability of the material relative to free space. It is naturally unit less. Relative Permeability of PMMA<<1, so it is defined as diamagnetic materials.

2.6.6 Classification of magnetic materials

2.6.6.1 Diamagnetism

Diamagnetic materials resist the external magnetic field exposed to them. When an external magnetic field exposed to diamagnetic materials, this material exhibits an antiparallel magnetization concerning the direction of the applied magnetic field. And this behavior against the external magnetic field can be defined as a weak form of magnetism [93]. Most elements including silver and gold, are diamagnetic in the periodic table (in Figure 2.25) [94]. It can be seen as the behavior of diamagnetic materials against the external magnetic field.
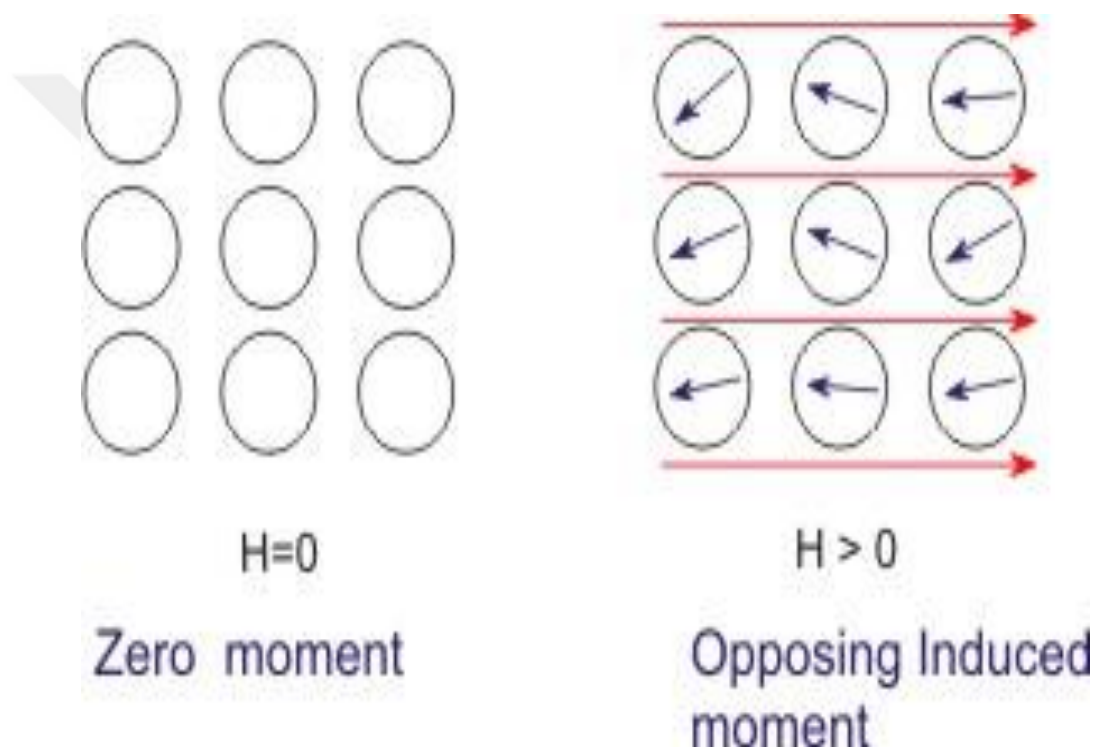
Figure 2.25. Behavior of diamagnetic materials against external magnetic field [93].

2.6.6.2 Paramagnetism

Paramagnetic materials exhibit parallel magnetization concerning the direction of the applied magnetic field when it is exposed to any external magnetic field. However, this magnetization is a weak form of magnetism [91]. The parallel magnetization occurred in paramagnetic materials disappears with the magnetic field applied to the paramagnetic materials. In other words, they are not magnetized permanently [91,94]. Paramagnetic materials contain lithium, tantalum, magnesium, and molybdenum. Relative permeability of paramagnetic is ~1. In Figure 2.26, it can be seen the behavior of paramagnetic materials against the external magnetic field.
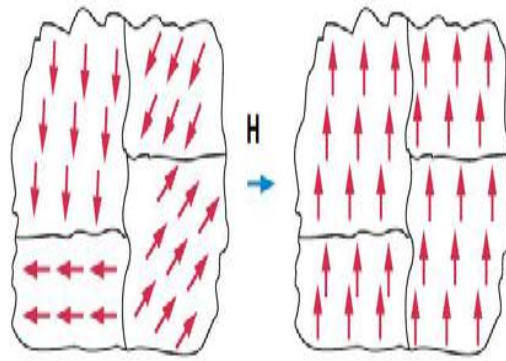
Figure 2.26: Behavior of paramagnetic materials against external magnetic field [93].

2.6.6.3 Ferromagnetism

Ferromagnetic materials are magnetized in the parallel direction of the applied magnetic field when it is exposed to any external magnetic field. The materials can be magnetized in the same direction as the magnetic field lines of that magnet when in the magnetic field of any magnet. The external magnetic field is removed and the magnetization of these continues for a certain time. Ferromagnetic materials have a curie temperature and when this temperature is exceeded, they start to show paramagnetic properties. Iron, Nickel, and Cobalt are examples of ferromagnetic materials. Relative permeability of ferromagnetic materials is >>1. In Figure 2.27 [95], it indicates the behavior of paramagnetic materials against the external magnetic field.
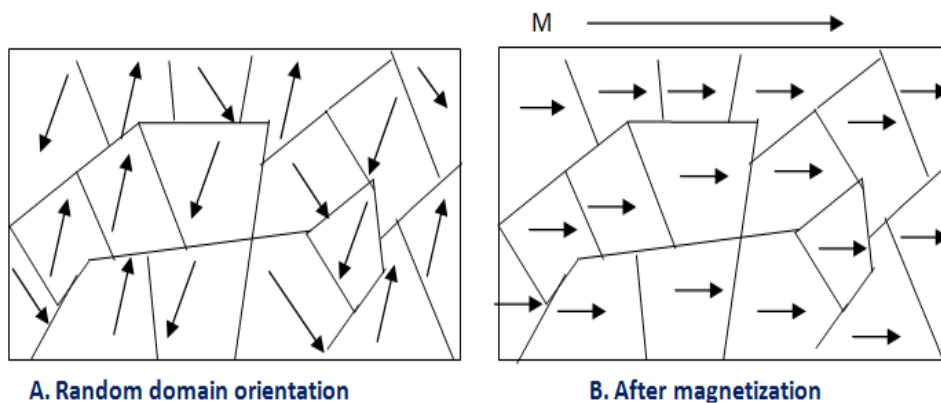
Figure 2.27. Behavior of ferromagnetic materials against external magnetic field [95].

The ferromagnetic materials have substantially greater magnetization in air (in Figure 2.28). The paramagnetic materials at the same level as the vacuum. On the other hand, diamagnetic materials produce an inverse force to the external magnetic field and are less magnetized than air.
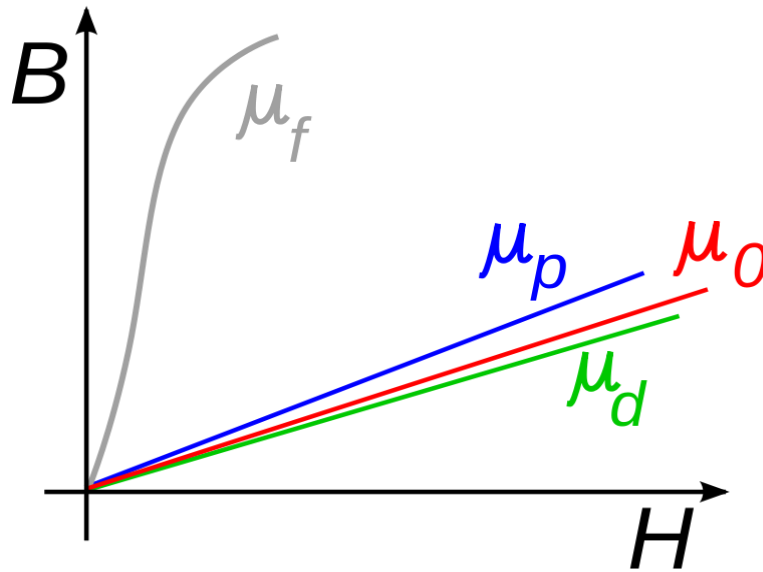
Figure 2.28: Permeability for paramagnetic, diamagnetic and ferromagnetic materials. μf: Permeability of ferromagnetic materials, μp: Permeability of paramagnetic materials, μd: Permeability of diamagnetic materials, and μo: Permeability of vacuum [95].

Finally, as shown in Fig. 2.29, when diamagnetic materials are subjected to any external magnetic field, they react in the opposite direction to this external magnetic field, while the paramagnetic materials act close to air, allowing the passage of the external magnetic field and magnetizing themselves in the same direction. On the other hand, ferromagnetic materials, are magnetized for a certain period when they are exposed to the external magnetic field and magnetize in the same direction as the external magnetic field like paramagnetic materials.
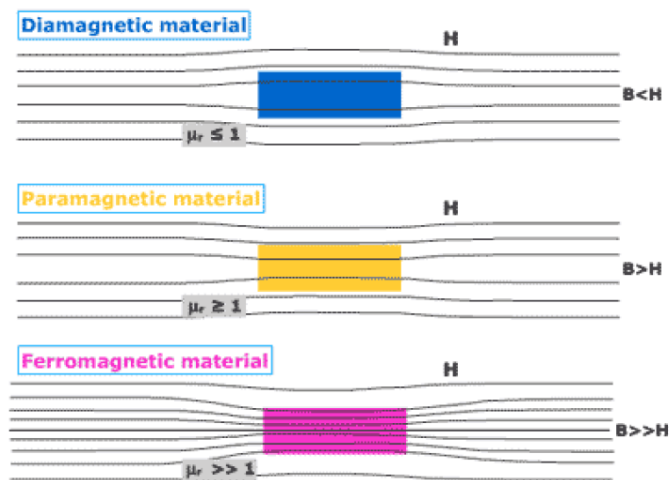
Figure 2.29. Behaviors of magnetic materials against external magnetic field [96].

2.7 Electromagnetic Spectrum

Wave is the vibration that propagates through matter or in the vacuum and transports energy. Wavelength (λ) is the distance between repeated units. It can also be defined as the distance between two crests. Frequency (F) is the cycle of a sound wave or an electromagnetic wave such as light in a second and frequency is indicated by the unit of Hertz (Hz,1/s). Amplitude (A): in a periodic motion (such as propagation of electromagnetic waves), it is defined as a maximum level of the wave [97-98]. Frequency, Amplitude, and Wavelength indicates in Figure 2.30.
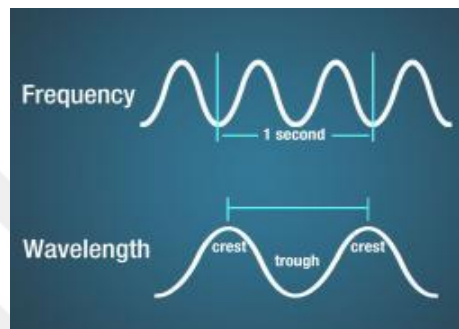
Figure 2.30: Frequency and wavelength of a sinusoidal wave [99].

2.7.1. Electromagnetic and mechanical waves

There are two different waveforms found in nature for energy transfer. While mechanical waves transfer energy as a result of disturbance or vibration in the matter (need a medium to propagate, can not travel in vacuum), electromagnetic waves make energy transfer by means of photons. Photons can propagate in vacuum. They do not need a medium to move [98]. The changes in the electrical field induce a changing of the magnetic field and vice versa. These changes in the electrical and magnetic fields form electromagnetic waves [99].

2.7.2 Photon

Photon which has no mass but is affected by gravity is the basic carrier of the electromagnetic force. It is also the main unit of light and it moves at the speed of the light in a vacuum (due to electrically unloaded and has no mass). Some significant properties of photons follow:

- Going with light speed in the vacuum
- Having stagnant mass zero
- Enter interactions as particles, propagation as waves

28

The energy of a photon is calculated by *equation 2.3*

$$E = h \, x \, f \qquad (2.3)$$

Where E energy of The Photon, Planck Constant (6.3×10^{-34} J/s) and f frequency of the photon

The electric field and the magnetic field constitute an electromagnetic wave. These two fields are perpendicular to each other, and the direction of propagation of the electromagnetic wave is perpendicular to the two. In Figure 2.31, it can be seen the schematic representation of an electromagnetic wave.
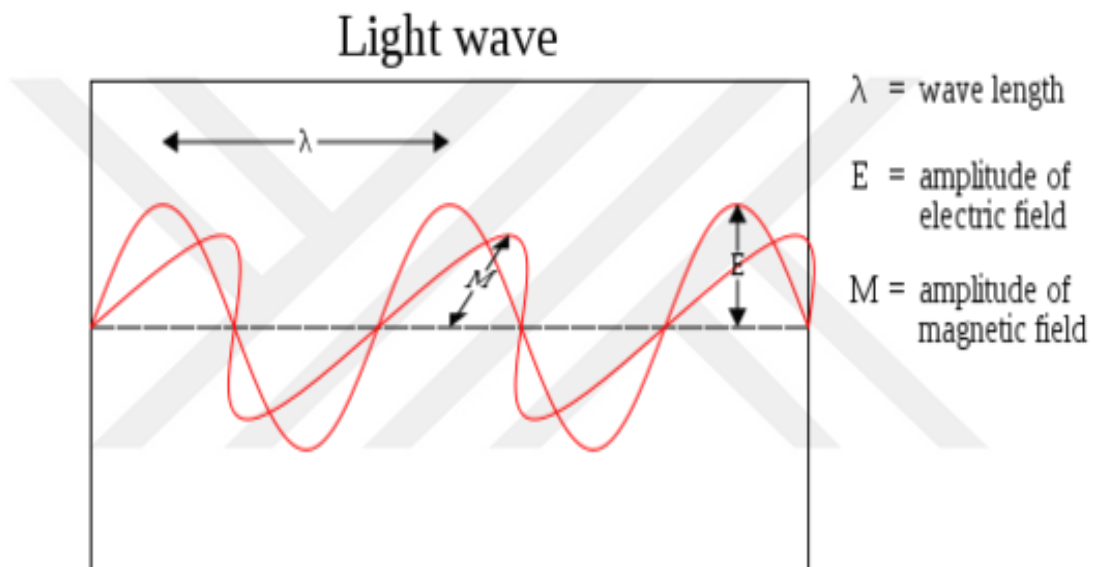
Figure 2.31. E, M and distance of electromagnetic wave [100].

There is a relationship between frequency and wavelength in an electromagnetic wave. Wavelength and frequency are inversely proportional to each other. This relationship can be seen in equation 2.4.

$$c = f . \lambda \qquad (2.4)$$

Where c is the speed of the electromagnetic wave, f frequency of this electromagnetic wave and λ wavelength of its.

In vacuum, c is the speed of electromagnetic wave equals the speed of light. It can be seen from equation 2.4, frequency of an electromagnetic wave and the wavelength are inversely proportional to each other. A high-frequency wave has a short wavelength and a low-frequency wave has a longer wavelength, based on equation 2.4.

2.7.3 Electromagnetic spectrum

The electromagnetic spectrum (in Figure 2.32) is obtained by ordering the frequencies of the electromagnetic waves. There are gamma rays with a very high frequency at the beginning of left-side and radio waves with a relatively low frequency at the right.
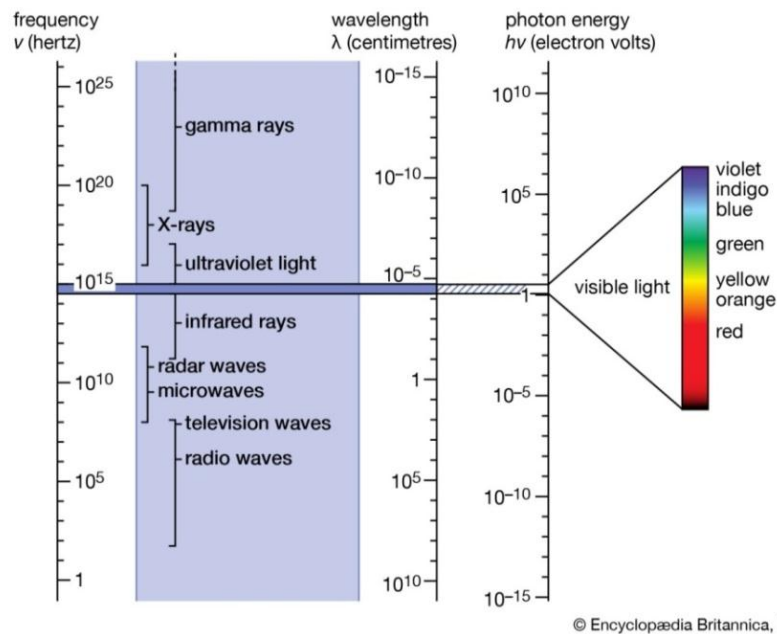
Figure 2.32: Schematic representation of the electromagnetic spectrum with frequency and wavelength [101].

2.7.4 Classification of electromagnetic spectrum

The photons in the electromagnetic spectrum are classified as gamma rays and x-rays ultraviolet waves, visible light, infrared waves, microwaves, and radio waves according to their wavelengths.

2.7.4.1 Gamma rays

Gamma rays: a few important properties of gamma rays, which is at the beginning of the left of the electromagnetic spectrum is as follows [102-105]:

- Having the highest energy in the electromagnetic spectrum (>30000 eV)
- Being highly penetrating and producing serious damage when absorbed by living tissues
- Having a very weak ionizing effect (compared to alpha)
- Being needed about 10 cm lead to stop gamma rays' effects
- Having non-effect of electrical and magnetic fields

2.7.4.2 X-rays

A few important properties of X rays, which is after gamma rays of the left of the electromagnetic spectrum is as follows [102-105]:

- It was discovered by X-ray when examining cathode rays.
- It is used as a diagnostic tool in medicine.
- It has an ionizing effect and is used to examine the crystal structure of the material such as XRD (X-ray Diffraction).
- Its energy is 100-30.000 eV.

2.7.4.3 Ultraviolet waves

UV has a wavelength between 100-400 nm and are invisible to humans. The region of UV is divided into three: as Ultraviolet A (UVA, 315-400 nm, 3-4 eV), Ultraviolet B (UVB, 280-315 nm, 4-5 eV), Ultraviolet C (UVC, 100-285 nm, 5-13 eV).

UV rays are harmful to health but, most of the UV rays coming to Earth are blocked by ozone layers, but with the thinning of the ozone layer, living things have been exposed to more UV rays in recent years. As a result of them, many diseases have started to be seen more frequently such as skin cancer, cataract.

2.7.4.4 Visible light

All of the electromagnetic waves except visible light can be undetected by the human eye and these waves are perceived by mankind in the form of colors that make up the rainbow.

It is desirable to be high transmittance properties in the visible region and to be resistant to the UV region in the materials that are used as optical materials. The light from this region has 400-700 nm wavelength, 2-3 eV.

It is desirable to be highly permeable in the visible region and to be resistant to the UV region in the materials that are used as optical materials. It can be seen in Figure 2.33 [96]. Wavelength of colors, which are found in the visible light range. The red color has 700 nm, whereas blue has 500 nm [102-105].
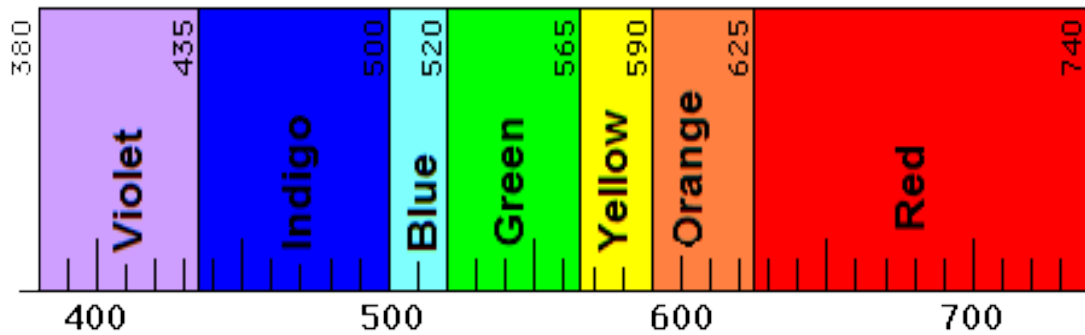
Figure 2.33: Wavelength of visible lights [106].

2.7.4.5 Infrared waves

Infrared waves having 5 μm-600 nm and 0-15-2 eV are non-ionized radiation. They can only lead to the vibration of the molecular bond of atoms. IR is used in FTIR analysis. The bonds that form the polymers have characteristic frequencies in the IR region. When IR applied to samples is the same frequency with the bonds in the structure, some of the IR lights are absorbed by these bonds. Thus, it can be determined the bond in the structure of samples.

2.7.4.6 Micro waves

Microwaves have 5 μ-0,3 m wavelength, $0,08-10^{-7}$ eV and can be produced by electronic devices. They can be used as radar waves thanks to their short wavelengths and they can be produced by electronic devices. They can be used as radar waves thanks to their short wavelengths (such as X band 9-13 GHz) and to heat food in microwave ovens [104].

2.7.4.7 Radio waves

Radio waves have the smallest frequency ($<10^9$), the largest wavelength ($>0,3$m) in the electromagnetic spectrum. Such that; they may have a wavelength as large as the length of our planet. They are generally used in the communication systems such as radio and television.

2.8 Reinforcement of Polymer by Element and Minerals

A lot of doping materials are being tried to improve the thermal, chemical, physical, mechanical properties of PMMA. Table 2.6 indicates the effect and the aims of the reinforcement materials in PMMA [107-113].

Table 2.6: The effect and the aims of reinforcement materials in PMMA [107-113]

Reinforcement Materials	Effect of Reinforcement on Structural Characteristics of PMMA	Aim of Reinforcing
$Gd_2O_3:Eu^{3+}$ [107]	Improving thermal stability	the polymer composite can be used at higher temperatures without degradation
$\{[Tb_3(L)(\mu 3\text{-}OH)_7]\cdot H_2O\}n$ (L = N,N′bis(acetoxy) biimidazole) [108]	Improving thermal stability	the polymer composite can be used at higher temperatures without degradation
$Mg_{1-x}Cu_xO$ [109]	Increase resistance to UV rays and mechanical properties	obtaining material for use as UV-filters
Nickel Chloride [110]	Increasing the dielectric constant of PMMA	obtaining material for use as insulator.
Cadmium sulphide [111]	Increasing the dielectric constant of PMMA	obtaining material for use as insulator.
(KOH and K_2CO_3): alkali salts [112]	Increasing the relative humidity (RH)	obtaining material for use as humidity sensor
AgBr/NPVP PVP:poly (4-vinylpyridinium) [113]	Increasing the mechanical properties	obtaining material for use in dental resin

2.8.1 Reinforcement of polymer by Boron element and minerals

There are also some studies about the effect of boron minerals on PMMA. Kirans et al. found that the reinforcement of BN Nano sheet increases the mechanical properties of PMMA [114]. Dogan M. et al. determined that PMMA/boron oxide nanocomposite has better properties compared to base PMMA in terms of thermal stability [115].

Yuan, Y. et al. determined that LaB_6 particles in the size of 70 nm exhibited the best absorption of VIS and NIR light which could not be achieved by the composites beyond the nanoscale [116]. In this study, borax $Na_2[B_4O_5(OH)_4]\cdot 8H_2O$ reinforced to PMMA to increase the hardness and wettability of PMMA.

The boron element at the beginning of Group 3A of the periodic table has the symbol B, the atomic number of Boron is 5 and its atomic weight is 10,81. This element is not free in nature. However, it is obtained as orthoboric acid usually in certain volcanic spring waters and as borates in borax and colemanite. In nature, it has two isotopes called B_{10} (%19,1-20,3) and B_{11} (%79,7-80,9) [28-30].

There are in nature more than 150 boron minerals, containing boron element and these minerals are named with the name of cation which they combined (calcium borax, sodium borax, magnesium borax, strontium borax). These inorganic marketed according to the amount of B_2O_3 (Boron Oxide). Table 2.7 indicates the various properties of some boron minerals.

Table 2.7: Properties of some boron minerals [28,117-118].

Name	Chemical Formula	Molecular Weight (g/m)	%B_2O_3	Density (g/cm^3)	Color	Hardness (Mohs)
Boron Oxide	B_2O_3	69,62	69,62	1,84	white	-
Borax	$Na_2.2B_2O_3.10H_2O$	381,17	37-39	1,73	white or bluish	2,5
Colemanite	$2Ca.3B_2O_3.5H_2O$	411,08	40-41	2,5	colorless	4
Anhydrous Borax	$Na_2B_4O_7$	201,27	69	2,367	-	2-2,3
Boric Acid	H_3BO_3	61,83	56	1,51	white	1

Approximately 62% of the world's boron reserves are in Turkey whereas the USA has approximately 16%. There are also important reserves in countries such as Bolivia, China, Peru, and Argentina. Turkey has of 1140 million tons of Boron mineral reserves [119].

2.9 Properties of Boron

The density of the boron element is 2,34 g/cc at 300 K and the boiling point of this element is 4002 °C. Its hardness is also 9,3 Mohs and this value is one of the highest values. The Appearance of this element is yellow-brown and non-metal crystal. These above-mentioned properties of boron can be seen in table 2.8 [120].

Table 2.8: Properties of Boron element [120].

Atomic Structure	
Atomic Diameter	1,17Å
Electron Configuration	$1s^2\ 2s^2\ p^1$
Atomic Volume	4,6 cm^3/mole
Number of Electrons	5
Electrochemical Equivalent	0,1344g/amp-h
Fusion Heat	50,2 kJ/mole
Valence electron potential (-eV)	190
Physical Properties	
Atomic Mass	10,811 g/mole
Boiling Point	4.002 °C
Thermal Expansion	0,000008/°C (at 0°C)
Thermal Conductivity	0,274 W/(cm.K)
Density	2,34g/cc (at 300 K)
Appearance	yellow-brown non-metal crystal.
Elastic Module (Bulk)	320 GPa
Hardness	Mohs: 9,3

2.9.1 Thermal properties of Boron

The thermal properties of boron are given in table 2.9. When these properties are examined, it can be concluded that boron minerals increase the thermal properties such as flame retardant of the material in which it participates as doping material. Boron Trioxide (B_2O_3) is used frequently in the glass industry due to its low melting temperature (at 430), increasing chemical resistance and most importantly increasing the thermal resistance of glass. This glass is named as borosilicate glass and these properties have enabled them to be used on NASA's Space Shuttle as a coating on the protective thermal insulation tiles [121]. Boron compounds (such as magnesium borate) do not cause toxic release if used as a flame retardant and they have low volatility. These properties make them superior to other flame retardants [121-122].

Table 2.9: Thermal properties of Boron.

Phase	Solid
Melting Point	2075 °C
Boiling Point	4000 °C
Absolute Melting Point	2348 K
Absolute Boiling Point	4273 K
Heat of Fusion	50 kJ/mole
Heat of Vaporization	507 kJ/mole
Specific Heat	1030 J/(kg.K)
Thermal Conductivity	27 W/(m.K)
Thermal Expansion	6×10^{-6} K^{-1}

2.9.2 Mechanical properties of Boron

Boron carbide has 9,2 Mohs (Table 2.10) value. It is known as the third hardest material after diamond and cubic boron nitride. Boron carbide is an important material of advanced technology today due to its many chemical properties and superior mechanical properties. Boron carbide is mainly used in nuclear reactors, light armor production and as a high-temperature material (It has 600 barn neutron absorption cross-section) [123-124].

Table 2.10: Some properties of boron carbide [124].

Boiling Temperature	3500 °C
Young's Module	450-470 GPa
Thermal Extension Constant	0,000005/K
Mohs Hardness	9,2
Neutron absorption cross section	600 barn

2.9.3 Electrical properties of Boron

It has a very low electrical conductivity at room temperature (1.0 E-12 µS/cm) which is the most important feature that distinguishes it from metals. Electrical conductivity starts to increase with temperature. Hexagonal Boron Nitride (chemical formula BN, has electrical resistance at 298K 1.7x1013 ohm-cm. dielectric constant of BN is 4. So, it can be used as electrical insulating material [125].

2.9.4 Magnetic properties of Boron

Boron element and minerals indicated usually diamagnetic properties when they exposed to an external magnetic field. Magnetic susceptibility of boron element and minerals is given in table 2.11.

Table 2.11: Magnetic susceptibility of Boron and some boron minerals [126].

Name	Chemical Formula	Magnetic susceptibly ($\chi m/10^{-6}.cm^3.mol^{-1}$)
Boron	B	-6,7
Diborane	B_2H_6	-21
Boric Acid	H_2BO_3	-34
Boron trichloride	BCl_3	-59,9
Boric Oxide	B_2O_3	-38,7

2.10 Use of Boron and Minerals

Boron and its minerals is used as a reinforcement material to improve thermal, mechanical properties and enhance shielding properties against radiation. In addition, boron and its minerals are used in various sectors such as cleaning, health, agriculture, textile and energy for various purposes [28,127-128].

3. STRUCTURAL CHARACTERIZATION TECHNIQUES FOR POLYMERS

3.1 X-RAY Diffraction (XRD)

X-rays are the photon beams with the highest energy in the electromagnetic spectrum after gamma radiation (0,125-125 Kev) and they can ionize materials by interacting with their electrons.

When crystalline materials are exposed to high energy X-ray's bombardment, they diffract characteristically this bombardment and then crystalline phases are decoded by considering this characteristic diffraction. The X-ray diffraction method (XRD) also provides information on unit cell dimension, stress in structure and ratios of crystal phases in structure [129-132].

When the crystal structures are exposed to an x-ray, they diffract x-ray uniquely. The X-ray diffraction method (XRD) is based on this unique diffraction of the crystal structures. The diffraction of the crystal phase defines as its fingerprint. Thus, crystal phases in the structure can be identified by analyzing of this diffraction. The X-ray diffraction analysis method does not destroy the sample at analysis [133].

3.1.1 Bragg's law

The target sample exposed to the x-ray beam diffracts these x-rays and new waves form from this diffraction. Even though the diffraction waves damp each other in most directions through destructive interference, they intensify constructively in a few specific directions (constructive interference) specified by Bragg's law (equation 3.1). In other words, these waves merge with one another in a phase (at certain angles) to increase wave intensity. The diffraction of this formation X-rays is called.

$$n.\lambda = 2.d.sin(\theta) \tag{3.1}$$

Where Θ is the angle between the incident beam (or the reflected beam) and crystal plane. λ is the X-ray wavelength and d is crystal plane separation. n is any integer in this equation.
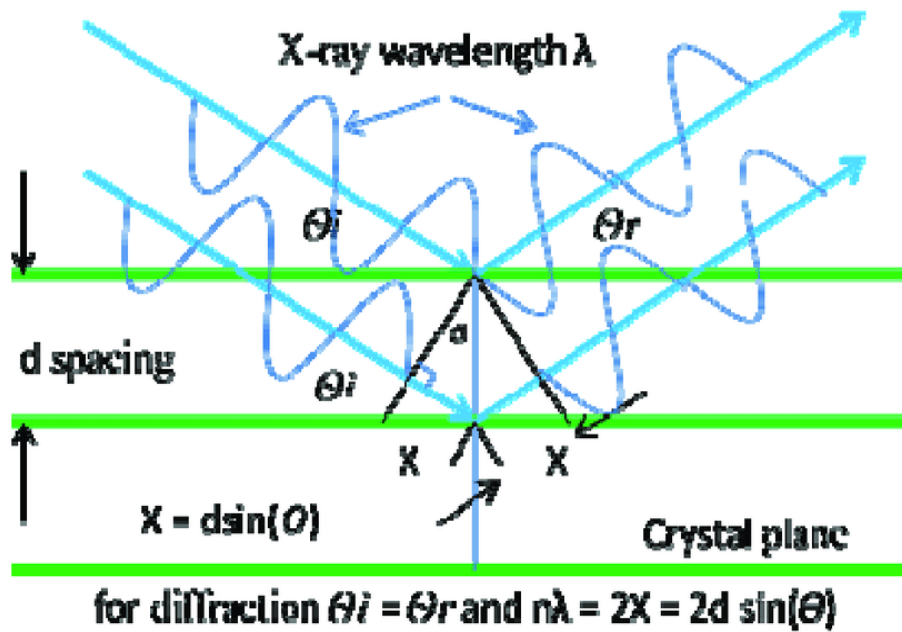
Figure 3.1: X-Ray diffraction [134].

Two conditions satisfy Bragg's law [31]:

1- The incidence angle must be equal to the scattering angle.

2- Wavelengths that have an integer number are equal to the path length difference.

Elements constitute X-ray diffractometers such as X-ray tube, a sample holder, and an X-ray detector. X-rays are produced in a cathode ray tube by heating a filament to produce electrons.

These generated X-rays are collimated and beam irradiance at the sample. The detector records the intensity of the reflected X-rays. According to the Bragg Equation, it detects intensely the reflected X-rays only at the fingerprint points. Then these X-rays convert the signal to a count rate which is then output.

3.2 Average Molecular Weight

Polymer materials that can be formed by more than one chain have a random sequence whereas molecules or atoms in crystalline materials are linked to one another in a certain order. Polymer materials consist of chains, and these chains may vary in number in terms of the monomer which is the building block of polymers. Therefore, it is not possible to mention a single molecular weight in most of the polymer materials [135]. There are four types of molecular weight at polymers.

40

One of them is number average molecular weight (Mn) which is explained: it is obtained by dividing the total molecular weight by the total number of molecules. It is obtained by methods based on the measurement of colligative properties such as freezing point descent, boiling point rise, osmotic pressure, vapor pressure drop. The number average molecular weight (Mn) is calculated in equation 3.2.

$$Mn = \frac{\sum_i NiMi}{\sum_i Ni} \tag{3.2}$$

Mi is the molecular weight of the chain. Ni is the number of chains of the molecular weight, i is the number of polymer molecules [136].

The second type of molecular weight types at polymers: Weight average molecular weight (Mw), the higher molecular weight of the molecule, the greater effect of the molecule on the average molecular weight of the polymer. Unlike the first kind of molecular weight, molecules forming polymers do not have the same effect in calculating the molecular weight. This type of molecular weight can be calculated by equation 3.3.

$$Mw = \frac{\sum_i Ni(Mi^2)}{\sum_i NiMi} \tag{3.3}$$

Mi is the molecular weight of a chain. Ni is the number of chains of that molecular weight and i is the number of polymer molecules [137].

The third type of molecular weight types at polymers: Z-Average Molecular Weight (Mz) is an uncommon type of molecular weight. It is obtained by the ultra centrifugation method. It is used to determine mechanical properties such as toughness. It can be calculated by equation 3.4.

$$Mz = \frac{\sum_i Ni(Mi^3)}{\sum_i Ni(Mi^2)} \tag{3.4}$$

where Mi is the molecular weight of a chain, Ni is the number of chains of that molecular weight, and i is the number of polymer molecules [138].

The latter, Viscosity Average Molecular Weight (Mv): viscosity is the measure of resistance to flow and the viscosity of the solid materials is calculated by dissolving in a suitable solvent. Mv is calculated in this way: the polymer material is diluted in a suitable solvent in different proportions. Solutions are obtained at different concentrations.

The viscosities of these diluted solutions are calculated, and then the molecular weight of the polymer material is calculated. The relationship between viscosity and molecular weight can be explained as follows. Flowing of large chain polymers is difficult due to entanglement and friction between the chains. That makes the solution ticker and these exhibit higher viscosities. This average molecular type is calculated by Mark-Houwink Sakurada Equations (in equation 3.5)

$$\text{Intrinsic viscosity } [\eta] = KM^a \tag{3.5}$$

Where K and α are empirically determined constants for a given polymer-solvent temperature system, M is the average molecular weight of the sample. The distribution of molecular weights in a heterogeneous polymer is Mz > Mw >Mv >Mn according to equation 3.2 -3.4. This result can be also indicated in Figure 3.2.
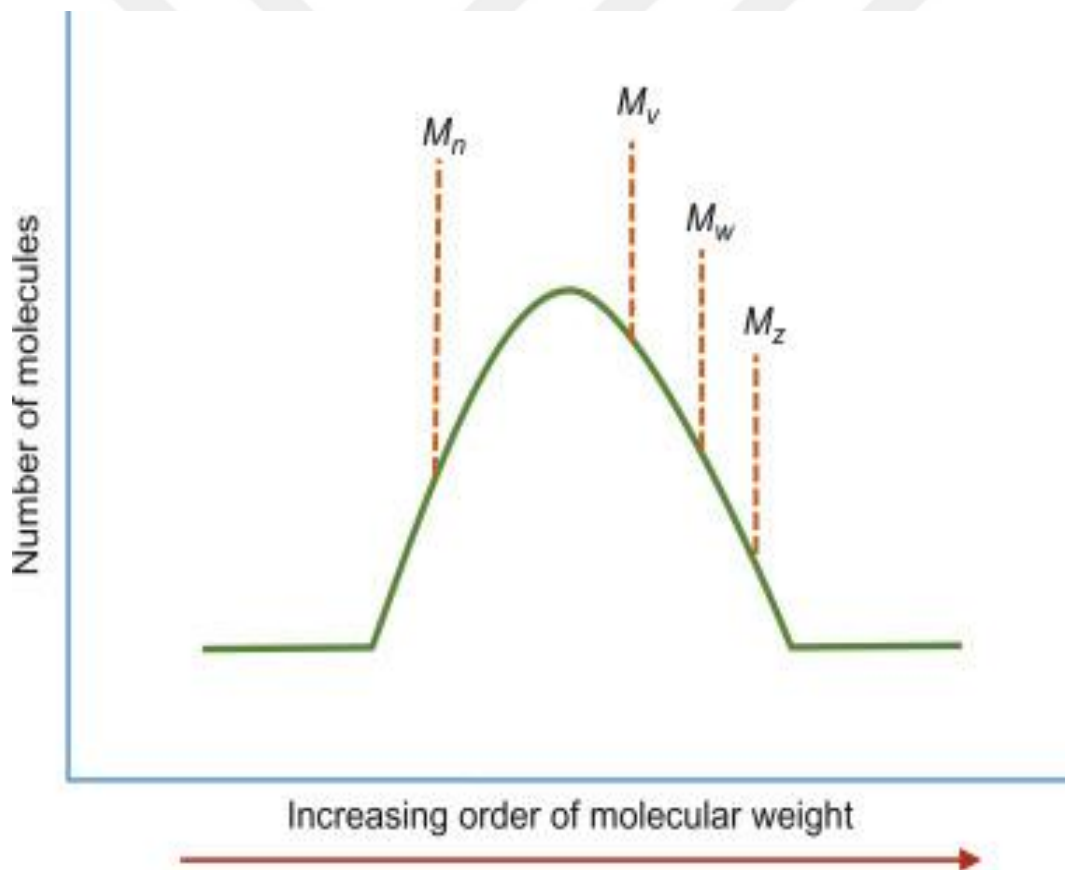
Figure 3.2: Demonstration of molecular weights in a heterogeneous polymer [139].

3.2.1 Polydispersity

Monodisperse (some natural polymer) molecular weights of all polymer molecules are the same. Polydispersity (such as most of the synthetic polymers), the molecules are distributed, unlike monodisperse.

Polydispersity Index (PDI): It is a measure of heterogeneity within the structure. If PDI is 1, then $Mw = Mn$ like some natural polymers. molecular weight is identical in all structure. On the other hand, if PDI is more than 1, $Mn>Mw$ and there is heterogeneity within the structure.

One of the most desirable properties of materials used in engineering that it has a homogeneous structure. In this context, the concept of Polydispersity for polymer materials is defined. Polydispersity is a measure of heterogeneity in the structure. As the Polydispersity increases, heterogeneity in the structure will increase, and especially mechanical differences will occur within the structure. It must be reduced the heterogeneity of the structure to eliminate these unwanted mechanical differences. In recent years, polymers have been started to produce between 1,0 and 1,2 PDI and this rate of heterogeneity has been gradually reduced. Molecular weight differences in the structure are requested to be reduced to the minimum level (in Figure 3.3).
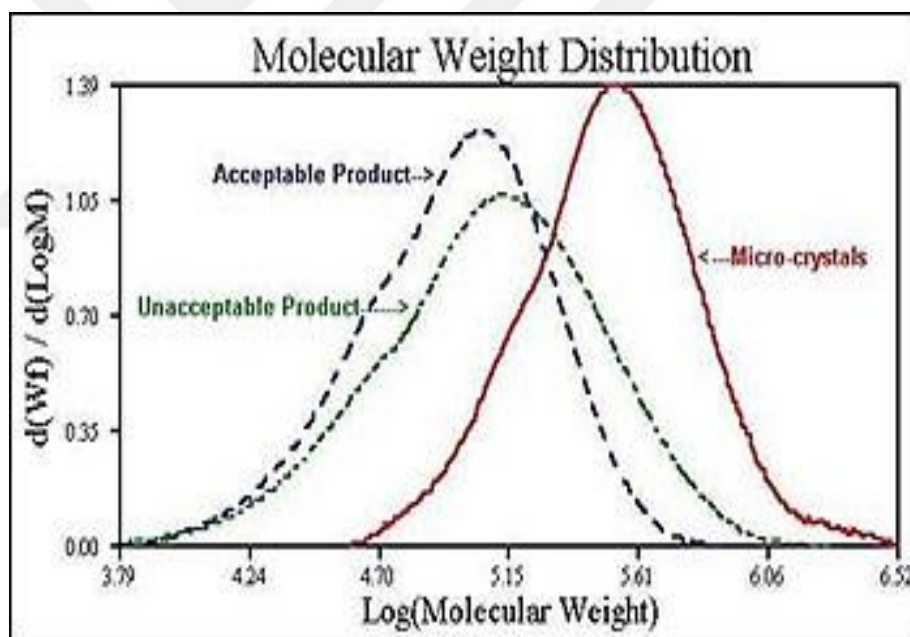
Figure 3.3: Molecular weight distribution of some polymers [140].

High mechanical properties are desirable for materials. However, it is observed that mechanical properties of polymers crawl after an approximate value of molecular weight whereas the viscosity exhibits a continuous increase with increasing molecular weight. Since the high viscosity means difficult molding of the material, optimization is needed between these values. This value of molecular weight is 10.000-1.000.000 g/mole for the polymers in Figure 3.4. The above-mentioned information is seen in Figure 3.4 [141].
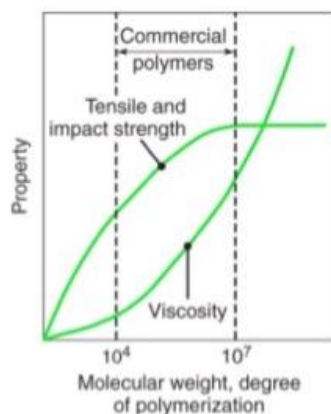
Figure 3.4: Relationship between viscosity and mechanical properties [141].

3.3 Fourier Transform Infrared Spectroscopy

Infrared radiation (IR) has 0.78 - 1000 nm wavelength and 12800 - 10 cm^{-1} wavenumber. This region consists of three ranges near wave IR, Mid wave IR and far wave IR. Midway IR (MWIR), whose wavelength is between 2,5-10 μ, is also used in Fourier Transform Infrared (FTIR). FTIR spectroscopy is a vibrational spectroscopic technique consisting of interaction between electromagnetic radiation (EMR) and specimen in the IR region. FTIR spectroscopy determined the interaction between electromagnetic radiation (EMR) and sample in the IR regions.

FTIR spectroscopy is used to identify the type of chemical bonds in a molecular by generating an infrared absorption spectrum that like a molecular finger point. This technique is more preferred in organics to determine functional groups in the structure of solid, liquid and solution organics are used in these areas: material identification and verification, identification of pollutants, textile identification: fibers, coating, quality-control of materials [142-144].

Atoms or molecules are connected to each other by bonds. Each bonds have characteristic energy levels and behaviors of these bonds under IR, which has insufficient energy to cause ionization and to excite electrons, can be likened to the movements of the springs subjected to any force. The bonds will respond with the vibrations to the radiation, which is the same level as the bond. In other saying, when the characteristic energy level of bond and the frequency of IR match up, this light is absorbed by the bond as stretching vibration (stretching and wagging). This can be observed in Figure 3.5b. If this match does not occur, the light applied to the target sample is transmitted 100 percent [131].
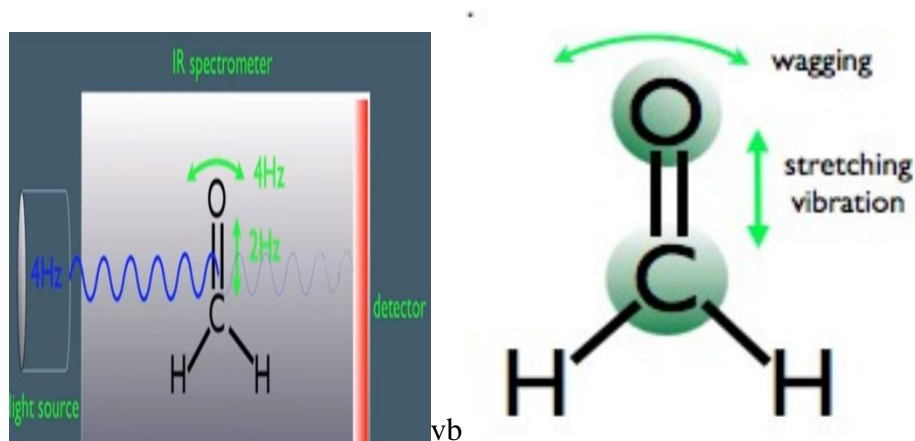
Figure 3.5a: Absorption of IR [145]. **Figure 3.5b:** Behavior of bond under IR [145].

3.3.1 Fourier transform infrared spectroscopy

Target material (sample) is exposed to an IR source whose wavenumber is between 4000-400 cm^{-1}. When the frequency of the light emitted from this source matches up the characteristic energy level of any bond in the material, this bond absorbs a portion of the light (this situation can be observed in Figure 3.5a and called as peak). Otherwise, the light applied to target materials is transmitted 100 percent. These lights reaching the opposite surface of the target material are collected by a detector. Then, spectroscopy is obtained by using a computer thanks to Fourier transform equations. the above-mentioned state is shown schematically in Figure 3.6 [146].
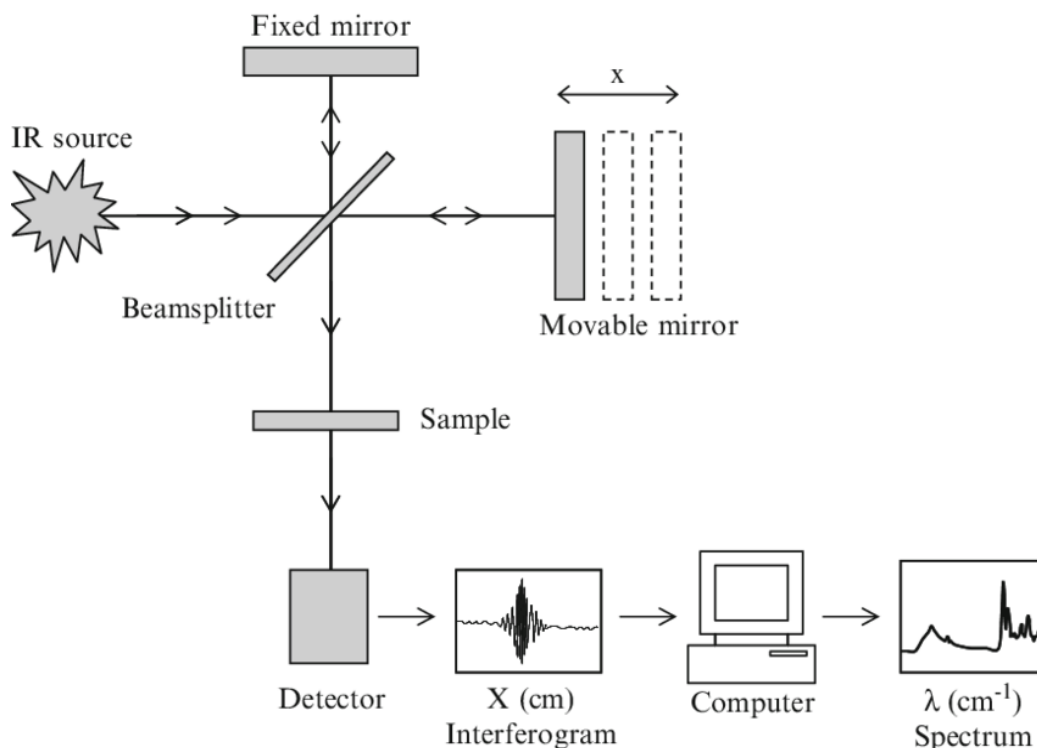
Figure 3.6: Schematic illustration of FTIR spectroscopy [146].
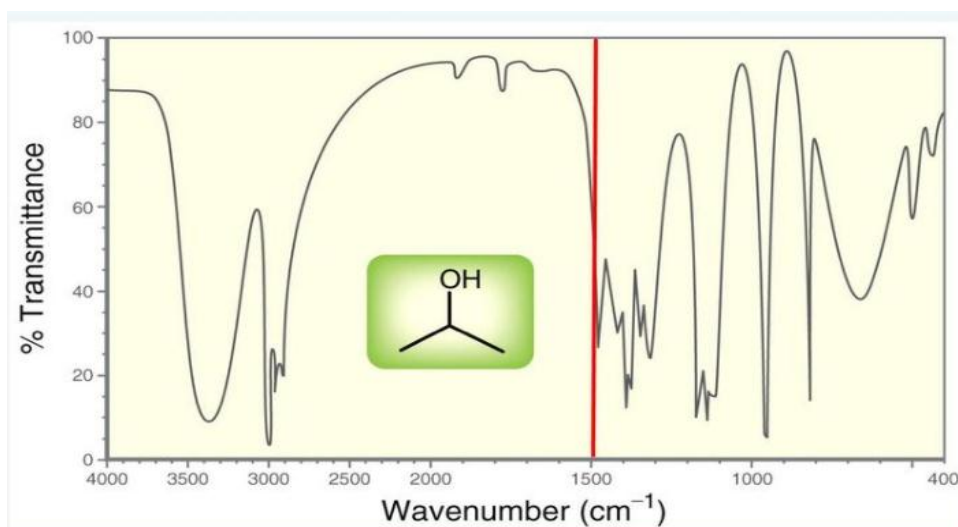
Figure 3.7: Dividing of FTIR Spectroscopy [147].

Wavenumber and Transmittance, both of them appear in each FTIR spectroscopy, Wavenumber is located on the x-axis of FTIR spectroscopy and transmittance is on the y-axis. One of them, transmittance can be expressed as how much light passes through a target material and the wavenumber $(1/\lambda)$, the unit of the wavenumber is cm^{-1}. It is directly proportional to both energy and frequency. Vibration frequency is not suitable for numerical scaling. Because of that, wavenumber is used in IR spectrometer. In FTIR Spectroscopy, Transmittance is found in Y axes, whereas Wavenumber takes place in X-axes. X-axes (wavenumber) is divided into two. The functional group region or diagnostic region has a high energy level and is used to determine the functional groups present. The wavenumber of this area is 4000-1400 cm^{-1}. The fingerprint region has a low energy level and is used for elucidation by spectral comparison. The area of this region is 1400-400 cm^{-1}. The above-mentioned situations can also be seen in Figure 3.7 (The line separating the two regions is drawn with red). In order to analyze the FTIR results more accurately and quickly, a few key points should be considered. These can be listed as follows:

- Not all bonds vibrations show absorption bend. A bond that is centered in a plane of symmetry will not show an absorption peak because when the bond stretches, its dipole moment does not change.
- The greater the dipole moment, the greater the alteration in dipole moment a bond stretches.
- The greater the alteration in dipole moment, the stronger the absorption bond.
- The stronger the bond, the higher the frequency, also wavenumber.

46

3.4 Scanning Electron Microscope

The human eye has a limited ability to see very fine details. It is able to see only visible light whose wavelength is between 380-700 nm. Mankind has used forages microscopes which is one of the optical devices to see micro details. Optical devices allow the transmission of light paths with lenses, allowing smaller details to be seen. However, these devices have led researchers to develop new systems on this basis due to the limited zooming (max 1500x) and the inability to process the resulting image. In this context, electron microscopy has been developed. Thanks to this electron microscopy, it can be zoomed 1000000 x and can be achieved a better quality, three-dimensional image. SEM (Scanning Electron Microscope) is generally used to have information about surface morphology of materials, however, it can sometimes be used for elemental analysis (Energy Dispersive X-ray (EDX) Spectroscopy). SEM is widely used in research and development studies in many branches, chip production in microelectronics, error analysis in different branches of industry, biological sciences, medicine, and criminal applications [148-152].

To have information about the morphology of the surface, the surface must be in interaction with the electrons produced and bombarded to the sample. In other words, the surface must be conductive. If the surface is not conducive, as in polymer materials, the surface is coated with micron-sized gold to make the surface conductive and surface morphology is obtained.

The tasks of the components used in SEM can be explained that an electron gun is an electron beam source, anode plate with high voltage applied to accelerate the electrons towards sample, magnetic lenses are used for obtaining a thin electron beam. Thus, electrons focus only on the sample. Scanning coils control the position of the electron beam on the sample. They let being canned over the surface of the sample. A backscattered detector and secondary electron detector are used to collect data to obtain imaging of the sample's surface. All of them can be seen in Figure 3.8a.

The interaction results between the electron beam accelerated under high voltage and the sample are shown schematically in Figure 3.8b. This interaction of electron beams with a sample can result in many different types of electrons, photons or irradiations and it supports to obtain the image of the sample's surface utilized from two types of the electron, which are backscattered (BSE) and Secondary Electron (SE). Auger electrons also occur as a result of interaction between the surface of the sample and

electron beam. These electrons are formed as a result of the non-elastic interference of sample atoms with external orbit electrons and high- energy beam electrons. They can penetrate only until a few nanometers in the material. Backscattered electron belongs to the primary electron beam and it occurs the result of elastic interactions between the beam and the sample. BSE originate from deeper regions of the sample (0,1-1 μm), whereas SE originates from surface regions (1-10 nm). Therefore, BSE and SE carry different information about the surface of the sample. BSE images indicate high sensitivity to differences in atomic number: the increased of the atomic number causes the brighter the material appears in the image. As a result of electron-sample interaction, which is the above-mentioned, several signals are generated. These signals are then detected by appropriate detectors such as BSE and SE detectors. then these signals are converted into images by computer and SEM images are obtained [153].
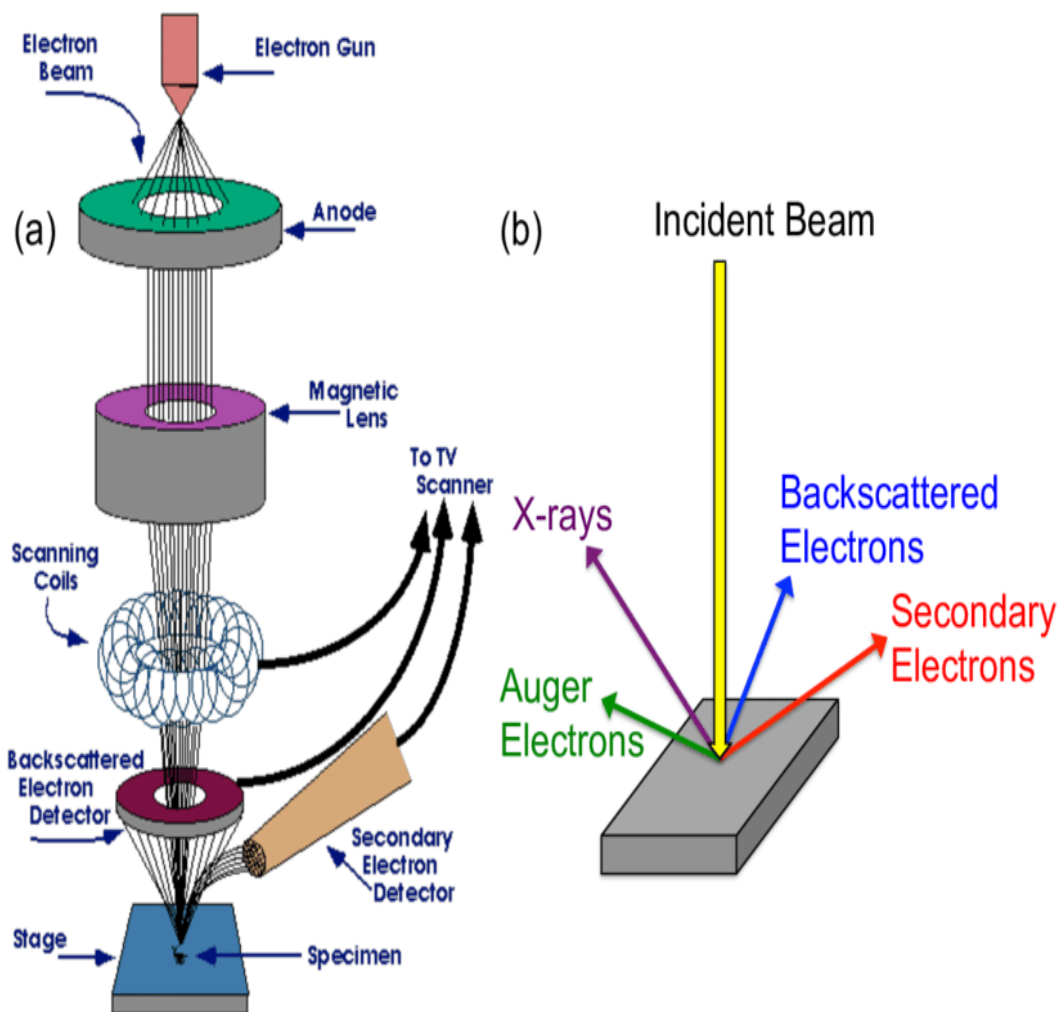
Figure 3.8a: Schematic drawing of the typical Scanning Electron Microscope (SEM). Figure **3.8b:** Sample-beam interactions within a SEM [154].

3.5 Contact Angle

The contact angle is identified as the angle between the solid surface and the liquid. It takes different values depending on the surface properties and solid surfaces are referred to as low or high energy, and on high energy surfaces, water spreads uniformly on the surface and forms a thin film. In this case, solid has a very low contact angle. The contact angle is indicated by θ and is calculated by the Young-Dupre Equation (equation 3.6) shown in Figure 3.9 [155]. The greater the cohesion force which is determined as the gravitational force of a substance between its molecules than the adhesion force which is determined as the gravitational force that exists between two different substances and allows these two substances to stick together, the greater the contact angle is. These two forces can be shown in Figure 3.10 [157-158].

Young's Equation

$$\gamma^{sv} = \gamma^{sl} + \gamma^{lv}\cos\theta$$
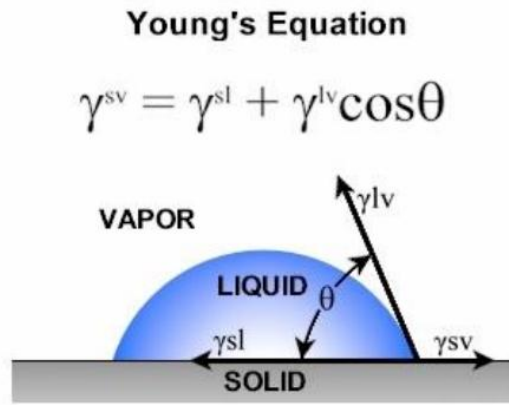
θ is the contact angle

γ^{sl} is the solid/liquid interfacial free energy

γ^{sv} is the solid surface free energy

γ^{lv} is the liquid surface free energy

Figure 3.9: Young-Dupre Equation [155].
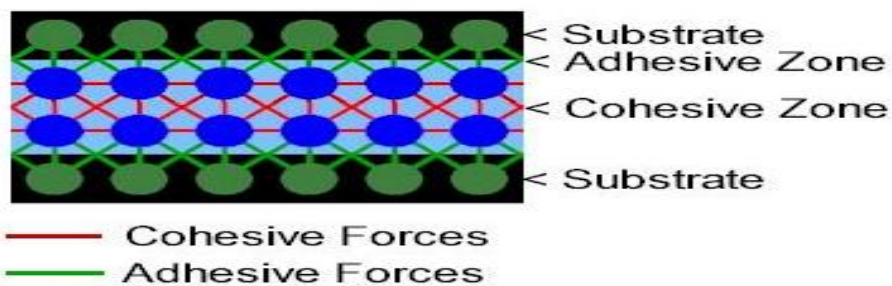
Figure 3.10: Adhesive and cohesive Force [156].

The most commonly used wetting material is water. The angle of water with the surface of the material is also a measure of the hydrophilicity of the surface. The hydrophilic surface is the case where the water droplet has a low water contact angle and the water droplet spreads or wets the surface. Hydrophobic surfaces are surfaces on which the water droplet does not spread on the surface and does not wet the surface. If the contact angle is less than 5°, then the solid material is called super hydrophilic. For smaller than 90°, it is called hydrophilic. In these cases, the surface energy of the solid material is high and the lower the contact angle value, the greater the adhesion force between the surface of solid and water. On the other hand, if the contact angle value is more than 90°, the solid material called hydrophobic. In these cases, water is not able to spread on the surface of solid material. Lastly, if this angle is more than 150°. the material is called as super hydrophobic. In these cases, it is also impossible that water survives on the surface of these super hydrophobic materials. These descriptions can also be observed in Figure 3.11.
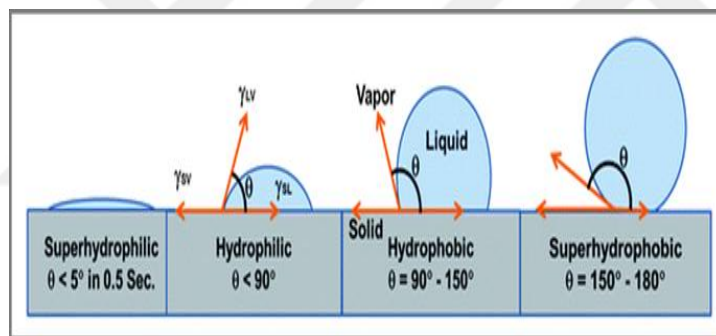
Figure 3.11: Type of materials according to contact angle [159].

3.5.1 Relationship between wettability and contact angle

Wettability is one of the significant properties that give important information about the relationship between the material and the liquid. This property is based on surface energy and surface roughness. When the surface energy of materials is higher, the hydrophilicity property of these materials is enhanced. The more a surface gets wet, the smaller the contact angle of the surface is. In other words, wettability and contact angle are inversely proportional to each other. It is expected that the materials used especially electrical cables in the underground or in cold environments such as space hard to intervene should have a very high contact angle. In these cases, when selecting the material, it must have a super hydrophobic property, whose contact angle is more than 150 ° [160-162].

3.5.2. Static water contact angle

The static contact angle meter measures the angle at which the surface of the liquid and the solid surface are made, which gives us information on how much the surface will become wet when subjected to the liquid used. The higher the angle, the less liquid the surface holds. Components of the device of static contact angle measurements are shown in Figure 3.12 [163]. The image formed as a result of the contact of distilled liquid dripped into the sample with the aid of the syringe is taken by the high precision camera and the contact angle value is obtained by means of a computer.
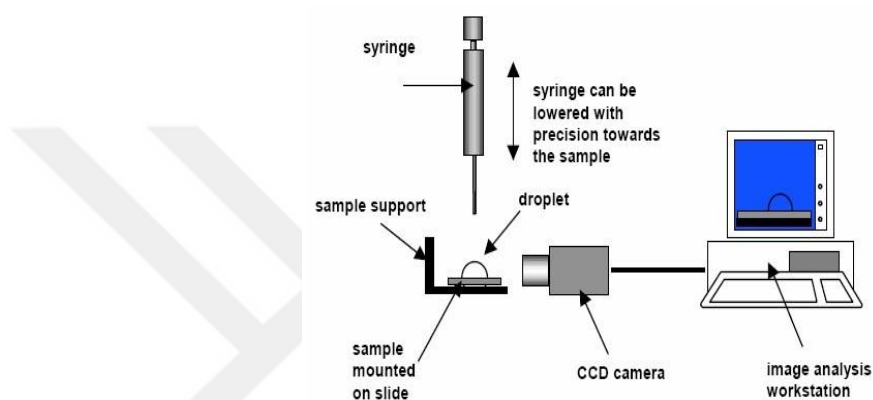
Figure 3.12: Components of the device of static contact angle measurement [163].

3.6 UV-VIS Spectrophotometer

Ultraviolet-visible spectroscopy states the interaction of light with matter. This interaction between light and material is of three types: absorption, transmittance, and reflectance. Absorption of UV lights results in the excitation of the electrons from the ground state towards a higher energy state. The energy difference between the ground state towards and the high state is actually equal to the energy from the absorbed ultraviolet radiation (the Beer-Lambert Law). This situation indicates in Figure 3.13.
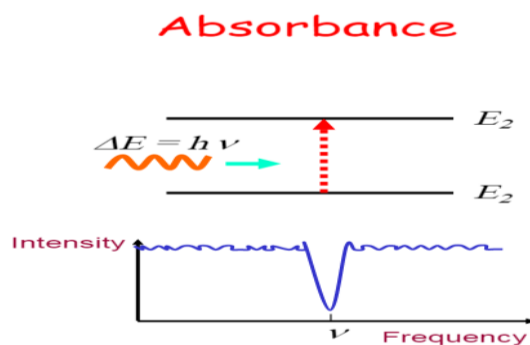
Figure 3.13: Absorbance of irradiation [164].

UV -VIS spectroscopy is generally used to be identified as functional groups in the sample material. Each functional group absorbs at a different energy level. In other words, this absorption value is characteristic of functional groups. UV Zone is divided into three zones: UVA, UVB, and UVC this identification is usually in the UVC zone whose wavelength is 100-280 nm. Since FTIR is able to detect the functional groups, it is used UV-VIS spectrophotometer to compare the optical properties of the industrial PMMA which have a very high transmittance in the visible region and base and PMMA/Borax composite samples synthesized by ATRP method in this study. UVA (320-400nm) and UVB (280-320) rays that reach the earth through the ozone layer and visible rays were taken into consideration in these examinations. [165]

The device of UV-VIS Spectrophotometer consists of several main parts: Source, Monochromator, Sample and Detector (in Figure 3.14). Source: A stable source of radiant energy at the desired wavelength. The monochromator is used to set apart a small section of a spectrum (300-1100 nm in this study). The sample is a material to measure its optical properties in the area of UV-Visible light or identify its functional groups. The detector converts the radiant energy into a user data signal (usually electrical). [166]
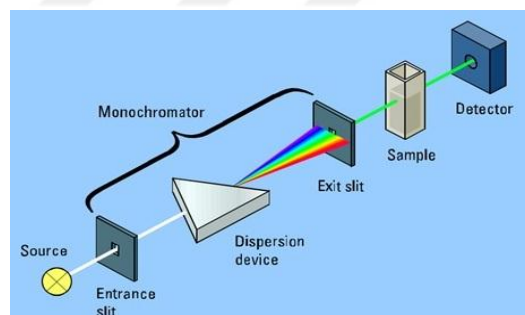
Figure 3.14: Block diagrammatic representation of UV-Vis spectrometer [167].

3.7 Measurement of Magnetic Properties

The sample is magnetized by a homogeneous magnetic field produced from two electromagnet coils in the *Vibrating-Sample Magnetometer* (VSM) device [168-169]. The constant collecting moments are constant and a vibrating, vertical transient small constant amplitude magnetic field is applied [170-172]. Due to this vibration of the magnetized sample, an induced electromotive force (emf) is generated that generates voltage difference and current in the collecting coils. The induced voltage for a single turn on the pickup coil is indicated in equation 3.7**.**

$$V = -\frac{d}{dt}\oint A \cdot ds = -\oint \dot{R} \cdot [(ds \times grad) \times A]_{t=0} \qquad (3.7)$$

In the above equation A: the vector potential R of the magnetic induction current of the sample is the time-dependent distance between the sample and the collection coils.

The induced current is proportional to the induced emf, which is proportional to the magnetization value of the sample. An amplifier is used to amplify the induced current, then the components of the areas forming the interfaces are processed by the computer to produce results and draw graphs.

3.7.1 Determination of magnetic properties

The Physical Property Measurement System (PPMS) is used as a measurement system (in Figure 3.15) that analyzes the electrical (super conductivity, dielectric constant), magnetic and thermal properties (thermal conductivity, Seebeck & Nernst effects) of materials. The PPMS system is the Quantum Design- PPMS DynaCool-9 model and devices can be adjusted at 1.8-400 K temperature and magnetic field up to 9 Tesla (T) can be applied to the materials.

The sample whose magnetic properties are to be determined is pulverized (provided that it is not less than 1 g) and this pulverized sample mount on "pucks" which inserts in the system. After that, the external magnetic field between -9 T and 9 Tesla applied to the samples and their magnetization is determined in this region. Finally, the data obtained is then collected by a computer and is created a graph with magnetization on the x-axis and an external magnetic field on the y-axis emerges. [172]

Figure 3.15: Quantum Design Model: PPMS DynaCool-9 [173].
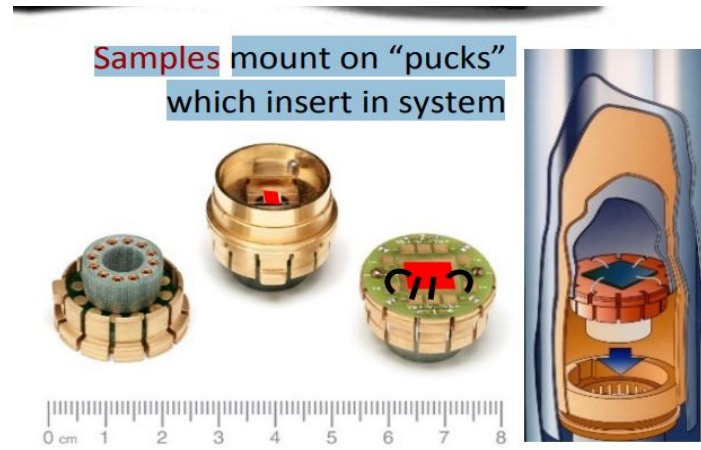
Figure 3.16: Pucks of PPMS [172].

4. EXPERIMENTAL

4.1 Materials

PMMA synthesis was carried out by using the following materials in table 4.1. The reinforcement of PMMA was performed by Sodium Borate (sodium tetraborate decahydrate ($Na_2B_4O_7 \cdot 10H_2O$) (named as borax) with ≥99.5% purity at different amounts.

Table 4.1: The materials used during PMMA synthesis.

Name, Chemical Formula, Purity, Molecular Weight and Manufacturer	Task in ATRP	Amount in Synthesis
Methyl methacrylate (MMA) Chemical Formula : $C_5H_8O_2$ Molecular Weight: 100,121g/mole Purity: ≥99.0%, Sigma Aldrich	Monomer	95,6966
Tetrabutylammonium bromide Chemical Formula: Bu_4NBr Molecular Weight: 322.37 g/mole Purity: ≥99.0%, Sigma Aldrich	Solvent	4 ,124 g
Copper bromide Chemical Formula: CuBr Molecular Weight: 143.45 g/mole Purity: ≥99.99%, Sigma Aldrich	Catalytic	0.216 g
Pentamethyldiethylenetriamine (PMDETA) L.C.F: $[(CH_3)_2NCH_2CH_2]_2NCH_3$ Molecular Weight: 173,3g/mole Purity: ≥99.%, Sigma Aldrich	Ligand	332 μl
Argon Chemical Formula: Ar Purity: ≥99.99%, Özvarış Firm	Noble Gas	▬
Sodium tetraborate decahydrate Linear Formula: $Na_2B_4O_7 10H_2O$ Molecular Weight: 381,37g/mole Purity: ≥99.5%, Sigma Aldrich	Doping Material	-5.2651 g for 5 (%wt.) -11,1164 g for 10 (%wt.)

4.1.1 Equipment and devices for synthesis

It was used some equipment for polymer synthesis, which was listed as follows:

- Atmosbag 1 and Atmosbag 2 were used to prevent oxidation of copper (in Figure 4.1a and 4.1b).

- Precision balanced for precise weighing of materials used in the synthesis (in Figure 4.2a)

- Vacuum pump to prevent the formation of the bubble after pouring in polymer molds (in Figure 4.2b)

- Finally, the magnetic stirrer (in Figure 4.3a) and the rotary stirrer (in Figure 4.3b) to allow the solution to stir more rapidly and homogeneously.

Figure 4.1a: AtmosBag 1. **Figure 4.1b:** AtmosBag 2

Figure 4.2a: Weighing Instrument. **Figure 4.2b:** Vacuum Pump.

Figure 4.3a: Magnetic Stirrer. **Figure 4.3b:** Rotary Stirrer.

4.1.2 Preparation of base and composite Poly(methyl methacrylate) by ATRP

Solvent, catalyzer, doping material (used except the synthesis of base PMMA) under storage conditions were placed in the two hands AtmosBag 1 (in Figure 4.1a) and all the air in the AtmosBag 1 was evacuated by the vacuum pump (Figure 4.2b). The presence of air in the AtmosBag 1 also means oxygen. In this case, it causes oxidation of copper used as a catalyst. Therefore, should make sure that there is almost no air left in the AtmosBag 1. After this process, Argon gas was filled in the AtmosBag 1. Afterward, solvent, catalyzer, and doping material were weighed with 10^{-4} g accuracy in the weighing instrument (in Figure 4.2a). Materials were calculated with reference to 102,24 ml MMA (95,6966 g). 4,124 g Bu_4NBr as solvent, 0.216 g CuBr as Catalyst and 5.2651 g borax as doping material in 5 (wt.%) borax added PMMA, 11,1164 g borax in 10 (wt.%) borax added PMMA were used. Thus, a solid mixture was obtained. Immediately after, the weighed materials were placed in the glass and then sealed with paraffin. Finally, the sealed with paraffin glass was removed from the AtmosBag 1. The glass with paraffin removed from the AtmosBag 1 was placed in the AtmosBag 2 (in Figure 4.1b). The processes which are the evacuation of air in the AtmosBag 2 and blowing argon gas were repeated. After these processes, paraffin was removed to add material to the mixture and monomer MMA (102.24. ml,) was mixed with solid chemicals. Then, PMDETA as ligand (332 µl, was added to the mixture. After this step, a degassing process with a gas-tight syringe was carried out for 5 minutes.

Finally, EBIB (236 µl) was added to the mixture as the initiator and the glass was sealed with cork stopper and paraffin The glass was shaken several times to start the reaction quickly. Then, it placed on the magnetic stirrer (Figure 3.3a) operating at 40°C and 720 rpm/min. All the mixtures turned green in 15 minutes like in Figure 4.4. This meant that the catalyst dissolved in the mixture and ATRP started. The solution was removed from the magnetic stirrer for 15 minutes per hour and placed on a rotary stirrer. The purpose of this process is to prevent the formed copper ligand complex compound from settling at the bottom of the solution and to make the structure more homogeneous. As polymerizations occurred in the mixtures within the glass, the mixture began to solidify and the mixture was poured into glass molds. The end of the pourable phase of the solution was selected to prevent oxidation. This section (from magnetic stirrer until pouring) lasted 6 hours for doped borax-PMMA

and 7 hours for base PMMA. The samples in this study poured into glass molds are taken to other round glasses (air entry to the glass is prevented by paraffin) and vacuum is applied at 70 kilo Pascal for about half an hour. Thus, air bubbles in the structure are minimized and a more mechanically stable polymer is obtained. The samples which were kept in this glass in the airless environment for two days were obtained as the final product. The whole process of polymer and polymer composite synthesis is shown in Figure 4.5.
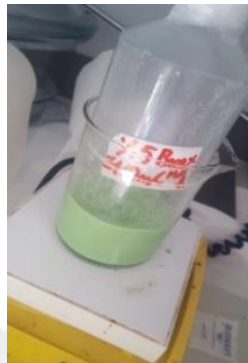
Figure 4.4: The situation of synthesis of PMMA with respect to elapsed time for 15. Minute.
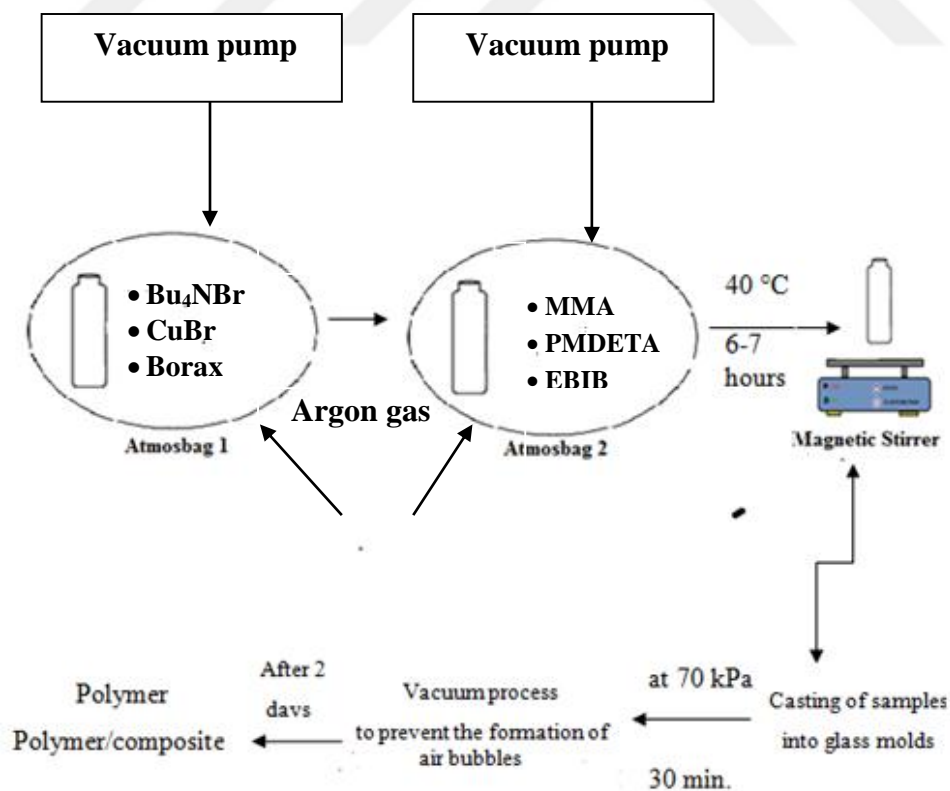
Figure 4.5: Schematic representation of synthesis of base and composite samples ATRP method.

The produces in this study indicates in Figure 4.6 were used in X-ray powder diffraction (XRD), Fourier-transform infrared (FTIR) spectroscopy, scanning electron microscope (SEM), UV-VIS spectroscopy, static contact angle, and determination of shore hardness. On the other hand, pulverized base and composite samples (Figure 4.7) were used in the determination of magnetic properties, thermogravimetric analysis, and average molecular weight.

Figure 4.6: Final products as solid states.
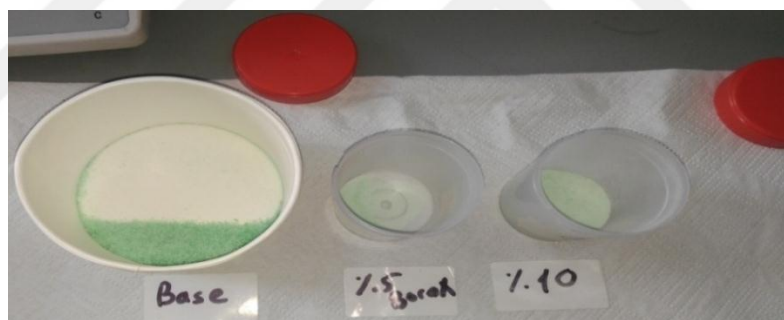
Figure 4.7: Pulverization of final products.

4.2 Characterization of Base and Composite Samples

4.2.1 X-ray Diffraction of base and composite samples

X-Ray Diffraction (XRD) was used to determine the crystalline structures present in the solid-state samples synthesized and rendered in Figure 4.8 In these determinations, X'pert pro device was used and these examinations were carried out at ITU Prof.Dr. Adnan Tekin Applied Research Center of Materials Science and Production Technologies (ATUM). The above-mentioned solid samples are three, base PMMA, 5 (wt.%) borax added PMMA and 10 (wt.%) borax added PMMA. XRD device in this study has a scanning speed of 2°/min and operating at 40 kV and 40 mA.

X-ray beam from an X-ray scanner was applied to the samples with a constant force of 40 kV and 40 mA between 5-70°. In Bragg's law, the angle calculations are based on the incident x-ray beam rather than the sample. Therefore, the incident beam always is taken into consideration in the measurement instead of the sample. For that, although the incident x-ray beam makes one Theta (degree) with the sample, the detector will make 2 Theta (degree) with the detector. For the above-mentioned reason, in X-ray diffraction graphs, the angle is expressed as 2 thetas.

Figure 4.8: X'pert pro X-ray Diffraction device.

4.2.2 Determination of the intrinsic viscosity and molecular weight of base and composite

The Examinations were carried out in Istanbul University Physical Chemistry Research Laboratory and viscometer branded SV-10 (in Figure 4.9) was used for the measurements of viscosity average molecular weight of base PMMA and PMMA/Borax composite.

The samples to determine average molecular weight are base PMMA, 5 (wt.%) borax added PMMA and 10 (wt.%) borax added PMMA. All of them were pulverized previously. The fact that the measuring surface on the device is made of gold material had minimized the possibility of contamination and this has resulted in more accurate measurements.

Figure 4. 9: Viscometer used in this study.

The determination of the average molecular weight in samples was performed in the following order:

4.2.2.1 Weighting of polymer samples by using sensitive balance to be measured viscosity

Different amount of samples belonging to base and composite Poly(methyl methacrylate) by ATRP was weighed respectively on the precision scale, whose brand is Radwag AS 220 / C / 2 and whose accuracy is 10^{-4} g.

4.2.2.2 Preparation of toluene as solvent

Toluene (from Merc) was chosen as the solvent, and some information on toluene is available in table 4.2. 50 ml of toluene was used as solvent in each sample-solvent and the used toluene was measured in the measuring cylinder.

Table 4.2: Information about Toluene [174].

Cast Number	108-88-3
Chemical Formula	C_7H_8
Density	0,87 gr/cm^3
Degree of purity	99%
Molecular Weight	92,14 g/mole

4.2.2.3 Solution preparation and measures taken to maintain the amount of solvent

The concentration of the solutions consisted of measured toluene and base and composite and the amount of them is shown in table 4.3. Each of the solutions with a magnetic stir bar making the solutions homogeneous is placed in the conical flask. Since toluene is a volatile material, this flask was sealed to be airtight. Any loss in toluene results in a difference between the target concentration and the concentration of the solution. This also leads to erroneous results.

Table 4.3: Concentration of the solution consisting of base and composite PMMA and toluene.

Amount of Polymer (g)	Toluene (Solvent) (ml)	Concentration (g/ml)
0,1	50	0,002
0,3	50	0,006
0,5	50	0,01
0,8	50	0,016

The flask was placed on a magnetic stirrer set at 250 revolutions per minute at room temperature to obtain homogeneous solutions. This process can be seen in Figure 4.11a-d. Figure 4.10a belongs to the solution containing 0.5 g of PMMA with 10 (wt.%) borax whereas 4.11 b, c, and d belong to solutions containing 0.1 g, 0.3 g and 0.5 g of base PMMA, respectively.

(a)   (b)

(c)   (d)
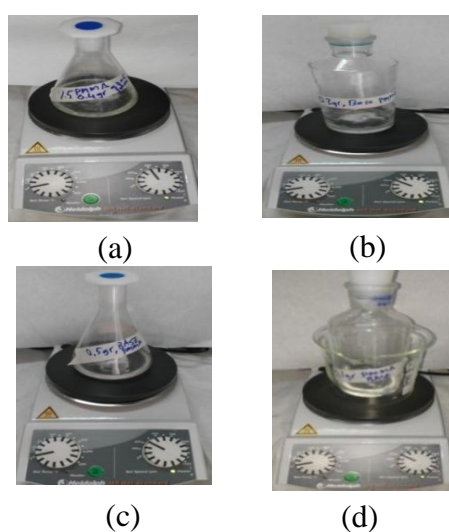
Figure 4.10 a-d: Homogenization of solutions on the magnetic stirrer.

4.2.2.4 Measuring the viscosity of the solutions

When the solutions became homogeneous, the flask was taken from the magnetic stirrer and the viscosities of the solution at different concentrations were measured by means of a viscometer. This step can be seen in Figure 4.11. This figure belongs to the measurement of the solution containing 0,8 g base PMMA. The measurements were carried out with AND-SV-10 viscometer. This viscometer has accuracy with 0.01 centipoise (cP) for the measurements.

Figure 4.11: The measurement of viscosity of solution containing of 0,8 g base PMMA.

4.2.2.5 Equations and expressions used to measure the viscosity average molecular weight of solution

The viscosity of the solutions having different concentrations was used to obtain relative viscosity, specific viscosity, reduced viscosity, inherent viscosity, intrinsic viscosity. How these viscosity values are calculated were shown in equations 4.1-.4.5.

The calculated intrinsic viscosity used in the Mark-Houwink Equation (equation 4.6). Finally, the average molecular weight is calculated using this equation. Where η (the intrinsic viscosity), M (Molecular weight) and α, K constants for the particular polymer-solvent system. The appropriate solvent for the synthesized base and composite samples in this study were toluene and its equations constants were presented in table 4.4 [161]. The result with the viscosity molecular weight test was determined by using Mark-Houwink equation.

$$\text{Intrinsic viscosity } [\eta] = KM^a \tag{4.6}$$

Where η was determined as the cut-off point of y axes, k was constant for toluene (0,007 mL/g), α was constant for toluene (0,71) as solvent, M= Average molecular weight.

Table 4.4: Equation constants for various polymer-solvent pairs [175].

Polymer-solvent system	K x 10^3 mL/g *(Eq. constant)*	α *(Eq. constant)*
PMMA-Acetone	7.70	0.700
PMMA-Benzene	5.20	0.760
PMMA-Toluene	*7.00*	*0.710*
Poly vinyl acetate-Acetone	10.20	0.720
Poly vinyl acetate-Benzene	56.30	0.620
Poly vinyl acetate-Acetonitrile	41.50	0.620
Poly vinyl alcohol-Water	45.30	0.640
Poly styrene-Benzene	10.60	0.735
Poly styrene-Toluene	11.00	0.725

After intrinsic viscosity [η] was determined by Mark-Houwink Equation molecular weight was determined [176]. For this purpose, the relative viscosity (η_{rel}) (eq-4.1) was calculated from the ratio between the viscosity of solvent (η_o) and the viscosity of the polymer solution (η) and Relative viscosity (η_{sp}), [η] and inherent viscosity (η_{inh}) were determined by using eq. 4.2-5 [177-179].

Relative viscosity:

$$\eta_{rel} = \frac{n}{n_0} \tag{4.1}$$

Specific viscosity:

$$\eta_{sp} = \frac{n}{n_0} - 1 = \eta_{rel} - 1 \tag{4.2}$$

Reduced viscosity:

$$\eta_{sp} = \frac{n - n_0}{n_0 * C} = \frac{\eta_{sp}}{C} \tag{4.3}$$

Inherent viscosity:

$$\eta_{inh} = In\frac{n/n_0}{C} = In\frac{\eta_{rel}}{C} \tag{4.4}$$

Intrinsic viscosity:

$$\left(\frac{\eta_{sp}}{C}\right)_{C \to} 0 = ln\left(\frac{\eta_r}{C}\right)_{C \to} 0 = [\eta] \tag{4.5}$$

4.2.3 Implementation of FTIR spectroscopy in base and composite samples

In order to determine the bonds existing in the structure of the synthesized polymer samples in this study, FTIR Spectroscopy was applied. The above-mentioned solid samples are three, base PMMA, 5 (wt.%) borax added PMMA and 10 (wt.%) borax added PMMA. The FTIR spectroscopy analysis was carried out with a branded PerkinElmer device (in Figure 4.12) in ITU Polymer Chemistry Laboratory and infrared rays with wavelengths between 4000-400 cm^{-1} were applied at the samples.

Figure 4.12: FTIR Spectrometer device branded PerkinElmer used in this study.

4.2.4 Examination of surface morphology of base and composite samples

SEM Analysis of the samples in this study was carried out at KOC University Surface Science and Technology Center (KUYTAM). There are several steps for preparing the samples (base PMMA, PMMA with 5 (wt.%) borax, PMMA with 10 (wt.%) borax for SEM analysis. Firstly, cleaning of the polymer using deionized water, ethanol. After the cleaning process, samples were dried. Secondly, the samples were prepared as shown in Figure 4.13 and placed in the SEM device shown in Figure 4.14. Then, samples were subjected to the electron beam to obtain surface morphology. Since our samples have not been conductive materials, the overcharging problem was encountered. Therefore, no images of the surfaces of the samples could be obtained. To solve this problem, the surfaces of the samples were coated with 10 nm gold and then vacuum was applied. The applied coating process is shown in Figure 4.15. After this coating process, the samples in Figure 4.16 were subjected to electron beam again to obtain surface morphology (SEM) and Energy Dispersive X-Ray Spectroscopy (EDS or EDX) was performed for elemental analysis.

Figure 4.13: The preparing of the samples for SEM.

Figure 4.14: The scanning electron microscope (SEM) using this study.

Figure 4.15: The process of coating the surfaces of samples with gold and then vacuuming of PMMA's.

Figure 4.16: Coating of surfaces with gold.

4.2.5 Examination of static contact angle in base and composite samples

The measurements of contact angle of the sample were carried out in the Drinking Water Laboratory of Yıldız Technical University Faculty of Civil Engineering and the examination was carried out for the following three samples: Base PMMA, PMMA with 5 (wt.%) borax, PMMA with 10 (wt.%) borax. The surfaces of the samples must be completely flat and smooth. Otherwise, a smaller value is obtained from the contact angle that should actually be present. The surfaces of the samples were provided to have these properties as much as possible. The sequence of the examination was performed as follows for all three samples:

Firstly, syringe was filled with ultra distilled water and the sample was mounted on a slide and then a drop of the water from the syringe was dropped onto the surface the sample like (in Figure 4.17). The relation of this drop with the surface of the sample was taken with a sensitive camera as an image (the situation in the 12th second was taken into consideration as the image). Finally, this image was analyzed on a computer and the static contact angle of the sample was obtained (in Figure 4.18).
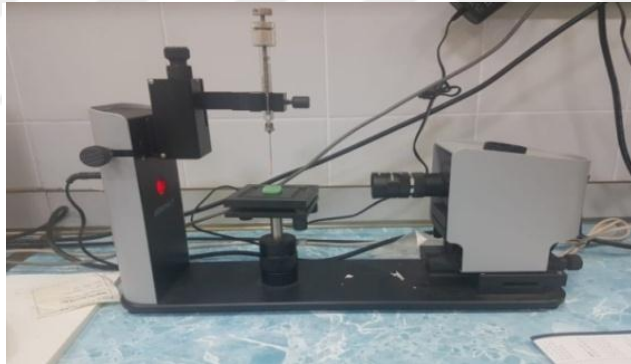
Figure 4.17: Examination of static contact angle of PMMA with 10 (wt.%) borax.
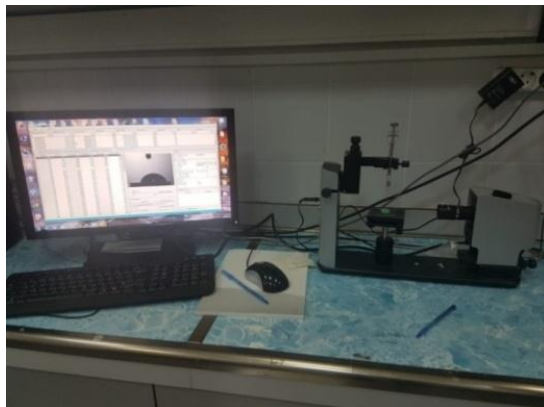
Figure 4.18: The analyzing of image by computer.

4.2.6 Ultraviolet and visible spectroscopy in base and composite samples

Industrial PMMA is colorless and one of the most prominent features is its optical property. These measurements were made in order to determine the optical properties of the samples. UV-Vis Spectrometer was used for the determination of optical properties and experiments were performed in Istanbul Technical University Energy Institute Radiology Laboratory. T80 branded spectrometer was also used as UV-VIS spectrometer.

A total of five samples were examined, one of which belonged to base PMMA and three belonged to PMMA with 5 (wt.%) borax (in Figure 4.19). One belongs to PMMA with 10 wt.% borax (in Figure 4.20). All samples were measured with a precision caliper and were found to have 2 mm thickness. The beam with the wavelength in the range of 1100-400 nm (1100-780 nm Near IR, 780-380 Visible range and 380-300 UV-A ranges) was applied to the samples at 1 nm intervals and the optical properties (such as Transmittance (T%) and Reflectance (R%) were measured. The absorbance was determined by using T% and R%.
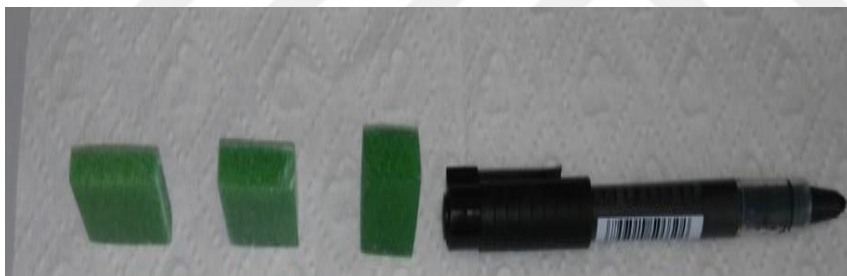
Figure 4.19: Determination of the optical properties of PMMAs with 5 wt.% borax in UV-A, VIS and near IR range.
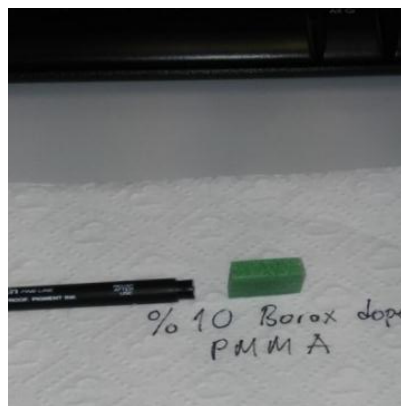
Figure 4.20: Determination of the optical properties of PMMA with 10 wt.% borax in UV-A, VIS and near IR range.

The sequence of the examination was performed as follows for all five samples. Firstly, the device has been calibrated and then a transmission apparatus is installed to determine the transmittance properties. After that, the transmittance properties of the space selected for reference were measured in the wavelength range mentioned above. Then, the transmittance of the five samples was again measured as applied to space.

After the examination of transmittance properties of PMMA's, the transmission apparatus was then removed and this time the reflector apparatus was installed to measure the reflective properties (in Figure 4.21). Then the reflective properties of the selected space as a reference at the same wavelength were also measured. The same measurement was applied to all five samples.

Figure 4.21: Placing the reflector in the device.

4.2.7 Examination of magnetic properties in base and composite samples

The magnetic properties of PMMA/Borax composite synthesized in this study were investigated in the central research laboratory of Çukurova University (ÇÜMERLAB), whereas the determination of these properties in synthesized base PMMA was carried out at International Center for Materials Nanoarchitectonics in Japan. Quantum Design PPMS DynaCool device was used to determine magnetic properties. Less than one gram of the previously powdered samples was weighed on sensitive scales. These prepared samples were placed in capsules (in Figure 4.22). These weighed samples in the capsule were placed in the puck in the device for the determination of their magnetic properties. An external magnetic field between +20000 Oe and -20000 Oe was then applied to the samples, which were ready for the measurement of their magnetic properties, and their response (magnetization) to this external magnetic field was measured. (0 Oe to 5,000 Oe with an increment of 100 Oe, other fields up to 20,000 Oe with an increment of 1000 Oe).

Figure 4.22: Inserting base PMMA into capsule.

4.2.8 Thermogravimetric analysis of base and composite samples

Polymers lose thermal stability at lower temperatures than metals, and as a result of that breaks in the bonds that form them. On the basis of polymers, thermoplastic materials like PMMA lose their thermal stability at lower temperatures than thermosets due to van der Walls bonds. For this reason, it is of great importance to determine the thermal stability of the polymers using thermal analysis methods. Thermogravimetric Analysis (TGA) is one of them.

Thermogravimetric analysis (TGA) is a kind of quantitative analysis. It is obtained with the change of the weight in the mass of the sample as a result of increasing the temperature at a certain rate. This loss of mass may be caused by the evaporation of volatile components, dehydration, thermal distortion, pyrolysis, chemical reactions.

There are three samples as base PMMA, 5 wt.% borax doped PMMA and 10 (wt.%) borax doped PMMA for Thermogravimetric analysis and all samples were already pulverized and prepared as 10 mg. The temperature was increased to 5 degrees per minute. Thermogravimetric analysis (TGA) was carried out at the Materials Production and Preparation Laboratory in ITU. The device used is Likron SDT-Q600 brand and indicated in Figure 4.23.

Figure 4.23: TGA-DSC device used in this study.

4.2.9 Determination of Shore D hardness in base and composite samples

Shore Hardness Test, which is one of the hardness tests using dynamic load, is a method used to determine the hardness values of polymer materials having less hardness than metals. In this determination, pressing force is applied to the shore meter manually and as a result of this pressing force, the needle tip in shoremetre pricks on the surface of the sample. As a result of this pricking, if the sample is a hard material, a small part of this dipping energy causes deformation in the material. A large part causes the needle tip to recoil. In this method of hardness measurement, the energy causing the recoiling is determined and the hardness value of the material is calculated. That is, the harder the material is, the more recoiling occurs. In other words, it has a higher hardness value than the others having more recoiling.

The measurement of surface hardness of base and composite samples (base PMMA, 5 wt.% borax doped PMMA, and 10 wt.% borax added PMMA) was carried out in Hardness Measurement Laboratory of Metallurgical and Materials Engineering Department of Istanbul Technical University. In soft polymers, is used the shore a scale, whereas relatively hard polymers used the shore d scale. Since the synthesized polymers in this study were hard, Shore D scale was used for shore hardness determination. This determination was applied 5 times to the regions on the surface of samples. These were chosen from the different regions on the surfaces durometer (shore meter) used in this study is Durotech brand, MD-1 model and DIN 58505 standards. This durometer can be seen in Figure 4.24.

Figure 4.24: The Shore D measurement of PMMA with 10 (wt.%)
borax addition.

5. EXPERIMENTAL RESULTS

5.1 FTIR Spectroscopy Analysis of Base and Composite Samples

FTIR spectroscopy about Borax, base PMMA and PMMA/Borax composite samples was presented in Figure 5.1 The vertical axes in Figure 5.1 have represented the transmittance (T%), while the horizontal axis has represented the wavenumber (cm^{-1}). The wavenumbers of the peaks belonging to samples (base, with 5 (wt.%) borax and with 10 (wt.%) borax) and the bonds corresponding to the characteristic peaks were given in table 5.1.

When the peaks of base and composite samples were examined, it was determined that the peaks were very similar to each other. O-H bonds formed in the 3420's were observed in FTIR spectroscopy of borax and all PMMA/borax composites. Although this bond formed all of the samples, it was also observed prominently in FTIR spectroscopy of borax, whereas it was partially observed in PMMA with 5% borax. Apart from this bond, the peaks were given below were formed in all PMMA /Borax composites and have only slight differences in terms of transmittance percentages. Therefore, the below peaks, the wavenumber and the vibration form of the bond has represented all of polymer and polymer composites in this study.

The peaks formed at 2994 cm^{-1} and 2952 cm^{-1} belong to C-H stretching, 1772 cm^{-1} C = 0 stretching 1484 cm^{-1} and 1435 cm^{-1} C-H bending or scissoring, 1271 cm^{-1} and 1240 cm^{-1} C-0 stretching, 1190 cm^{-1} C-O-C bending, 1144 cm^{-1} C-H_2 bending and finally, the peak formed at 1063 cm^{-1} belongs to the C-0 stretching (in table 5.1).

Table 5.2 indicated the results of the FTIR analysis of borax. As a result of this analysis, it was detected that the peak between 3600-3200 cm^{-1} has represented 0-H stretching and it belongs to the moisture in the borax ($Na_2[B_4O_5(OH)_4].8H_2O$). The peaks at 1695 and 1650 cm^{-1} have represented H-0-H bending. Besides the peaks at 1425 and 1360 have belonged to $B0_3$ asymmetric stretching the peak at 1161 cm^{-1} has belonged to B-0-H bending and the peaks at 1000 and 950 cm^{-1} have symbolized $B0_3$ symmetric stretching.

Table 5.1: Wavenumber of peaks and bonds formed in base and composite samples as a result of FTIR spectroscopy.

Wavenumber (cm^{-1})	Bond
3427	O-H stretching
2994	Csp^{3}H Stretching
2952	Csp^{3}H Stretching
1722	C=O (Strong) Stretching
1484-1435	C–H bending or scissoring
1271	C-O Stretching
1240	C-O Stretching
1190	C-O-C Bending
1144	C-H$_2$ Bending
1063	C-O Stretching

Table 5.2: Wavenumber of peaks and bonds formed in borax as a result of FTIR spectroscopy.

Wavenumber (cm^{-1})	Bond
3600-3200	O-H stretching
1695 and 1650	H-0-H bending
1425 and 1360	B0$_3$ asymmetric stretching
1161	B-0-H bending
1000 and 950	B0$_3$ symmetric stretching
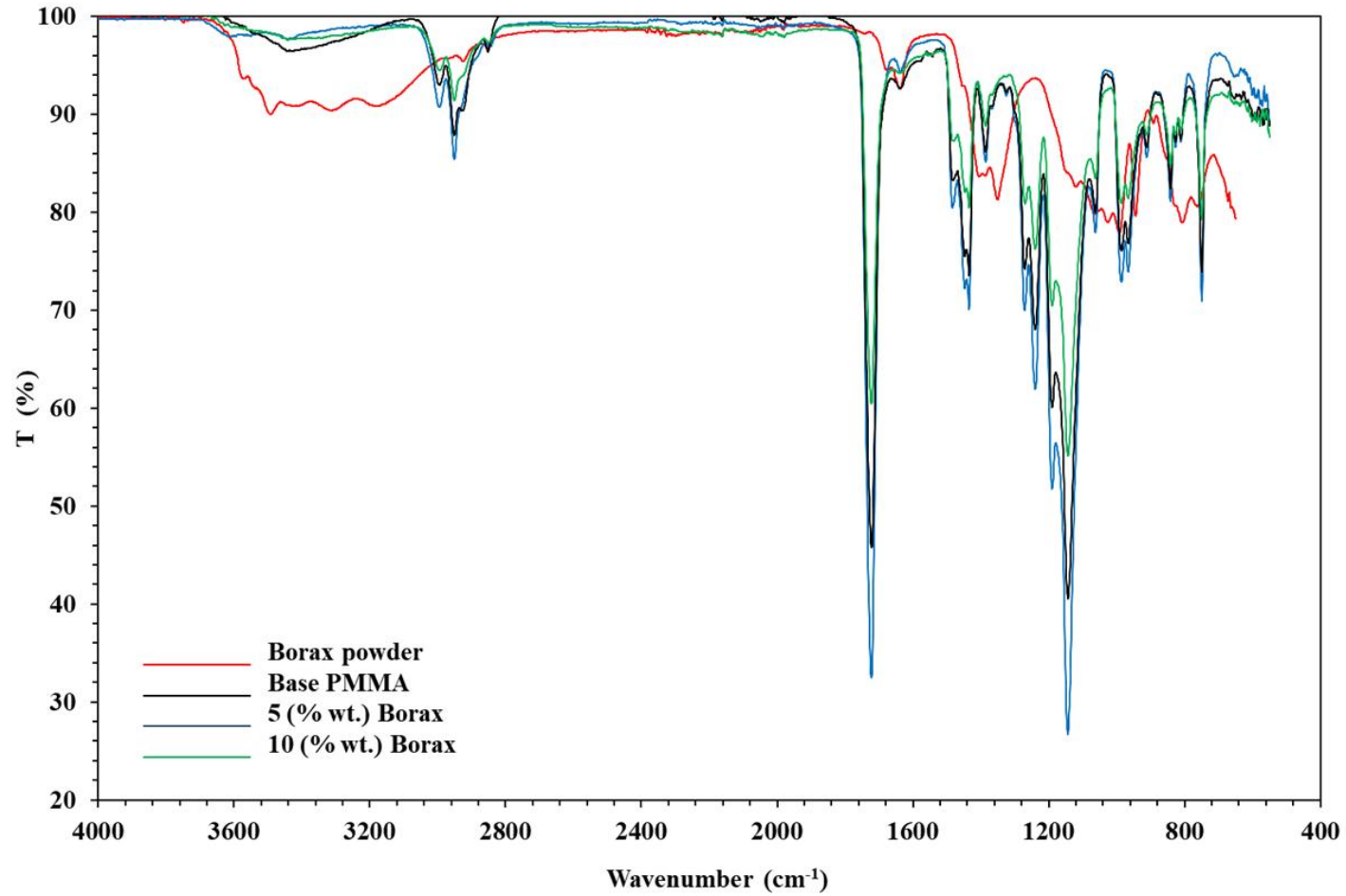
Figure 5.1: FTIR spectroscopy of Borax and base and composite samples

5.2 Determination of Average Molecular Weight of Base and Composite Samples

The viscosity values of the solutions of base PMMA were measured by using the viscometer. For this purpose, relative viscosity, specific viscosity, reduced viscosity, inherent viscosity, and intrinsic viscosity parameters were determined to evaluate the viscosity of the solutions of PMMA. All of them were calculated by using respectively the equations 4.1- 4.5. The viscosities of the solutions consisting of base PMMA were given in table 5.3.

Table 5.3: Viscosities of solutions consisting of base PMMA.

Concentration (g/ml)	Solvent Viscosity (cP)	Solution Viscosity (cP)	Relative Viscosity (η_{nr})	Specific Viscosity (η_{sp})	Reduced Viscosity (η_{red})	Inherent Viscosity (η_{inh})
0,002	0,58	0,64	1,10	0,10	51,72	49,22
0,01	0,58	0,78	1,34	0,34	34,48	29,63
0,016	0,58	0,88	1,52	0,52	32,33	26,06

Intrinsic viscosity is a measure of a solute's contribution to the viscosity of a solution. In order to calculate this viscosity of samples, firstly the reduced viscosity and inherent viscosity of solutions at different concentrations were calculated and as a result of these calculations, two one-dimensional equations were formed. The only variable in these equations is the concentration of polymer and polymer composite. In this equation, the x-axis has represented the concentration of the solution (g/ml) and the y-axis has represented the intrinsic viscosity.

Two intrinsic viscosities based on reduced viscosity and inherent viscosity were obtained for each solution. Due to two types of intrinsic viscosity were obtained, these two representations were also considered. Of these one-dimensional curves, the curve with a higher R represents better the viscosities of solutions. Therefore, the intrinsic viscosity from reduced viscosity was accepted the intrinsic viscosity of the solution. This has indicated in Figure 5.2. Then, by using the obtained intrinsic viscosity in the Mark-Houwink Equation (equation 4.6), the average molecular weight of base PMMA was determined. The equations used to determine the average molecular weight of base PMMA was used in the same way and the average molecular weight of 5 wt.% borax added PMMA (Table 5.4) and 10 wt.% borax added PMMA (Table 5.5) were obtained. Based on this information, the intrinsic viscosity-concentration points in Figure 5.3 for

5 wt.% borax added PMMA were obtained, as well as the intrinsic viscosity-concentration points in Figure 5.4 for 10 wt.% borax added PMMA. These obtained intrinsic viscosities were used in the Mark-Houwink Equation and the average molecular weights of the synthesized polymers in this study were calculated.
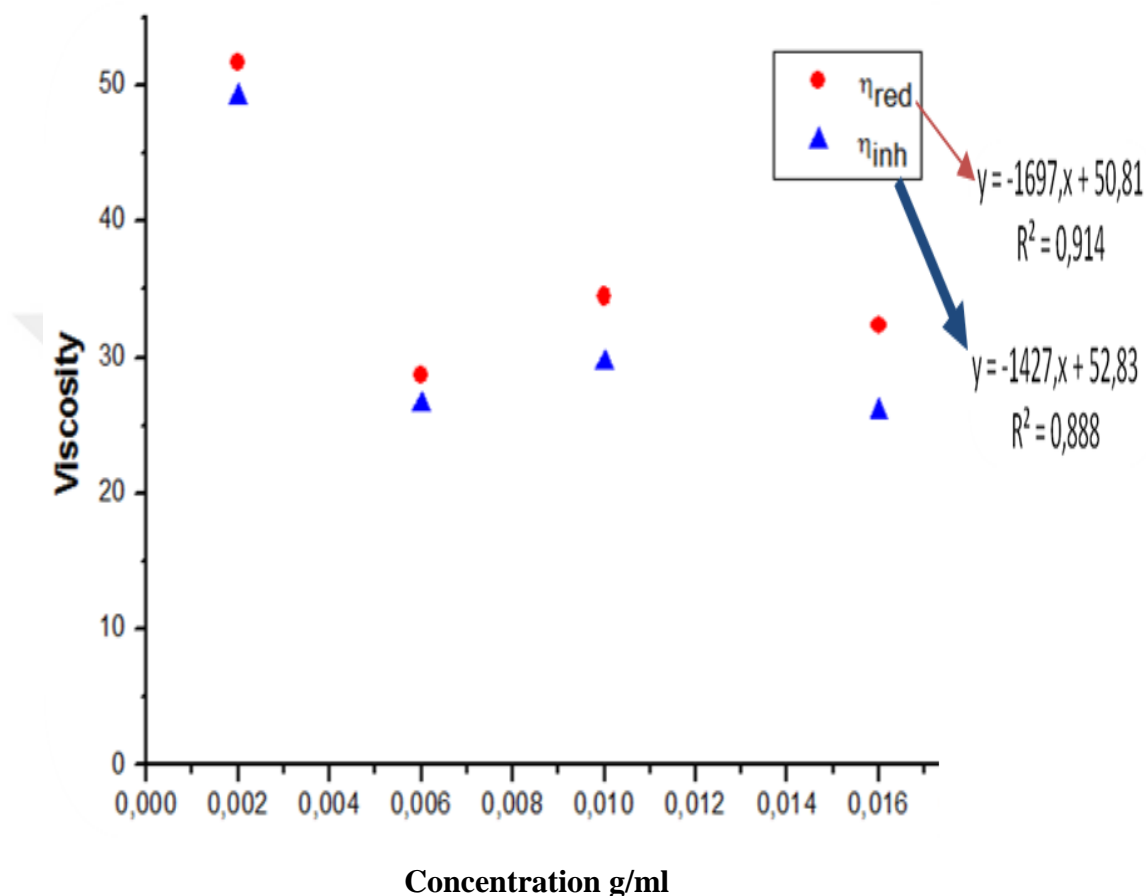
Figure 5.2: Intrinsic viscosity of base PMMA.

Table 5.4: Viscosities of solutions consisting of PMMA with 5 wt.% borax at different concentrations.

Concentration (g/ml)	Reduced Viscosity (η_{red})	Inherent Viscosity (η_{inh})
0,002	51,72413793	49,22003641
0,004	43,10344828	39,76617366
0,008	40,94827586	35,42030141
0,016	31,25	25,34156926
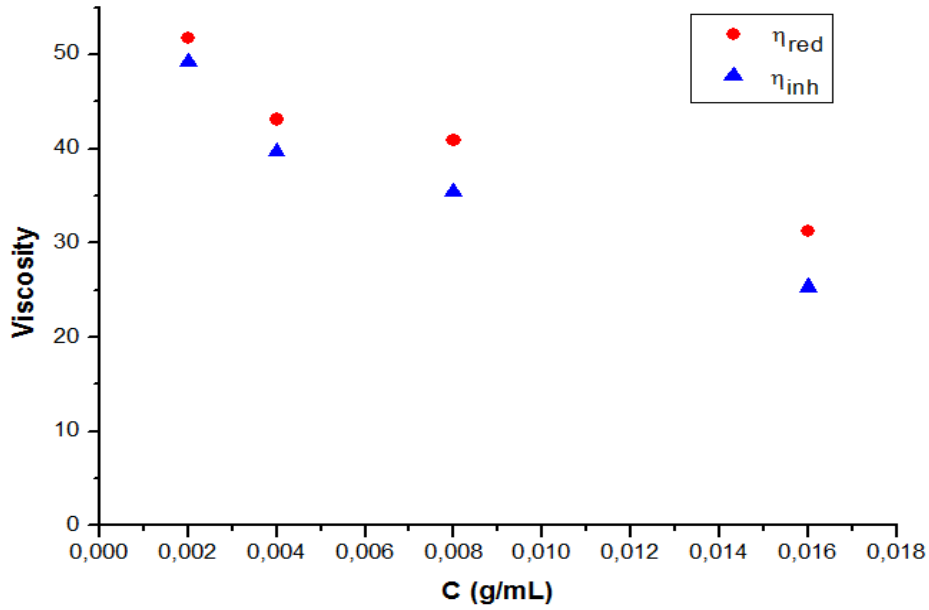
Figure 5.3: Intrinsic viscosity of PMMA 5 wt.% borax.

Table 5.5: Viscosities of solutions consisting of PMMA with 10 wt.% borax.

Concentration (g/ml)	Solvent Viscosity (cP)	Solution Viscosity (cP)	Relative Viscosity (η_{nr})	Specific Viscosity (η_{sp})	Reduced Viscosity (η_{red})	Inherent Viscosity (η_{inh})
0,002	0,58	0,69	1,18	0,18	94,82	86,83
0,04	0,58	0,76	1,31	0,31	77,58	67,57
0,008	0,58	0,81	1,39	0,39	49,56	41,75
0,016	0,58	0,86	1,48	0,48	30,17	24,61
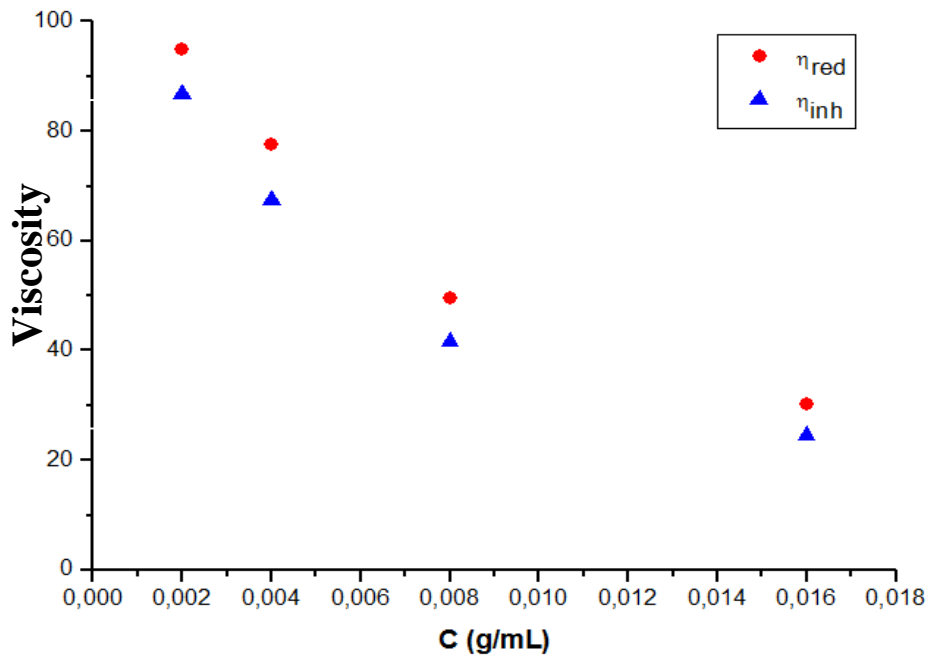
Figure 5.4: Intrinsic viscosity of PMMA 10 wt.% borax.

Table 5.6 indicates the average molecular weights of synthesized base and composite samples in this study. Concerning these results: The viscosity average molecular weight of PMMA with 5 wt.% borax was almost equal to base PMMA, while this molecular weight of 10 wt.% borax added PMMA had more than 2.5 times the average molecular weight than that in base PMMA. Although there was no consistent link between the reinforcement rates it has indicated that it was a positive contribution of borax reinforcing. What caused this situation, it can be determined by examining the relevant parameters such as the structure of the borax, the synthesis parameters or toluene selected as the solvent by testing the relevant parameters.

Table 5.6: Average molecular weight of the samples.

Sample	Molecular Weight (g/mole)
base PMMA	~270.000
5 wt.% borax added PMMA	~280.000
10 wt.% borax added PMMA	~675.000

5.3 Determination of Static Contact Angle of Base and Composite Samples

The contact angle of base and composite samples as base PMMA, PMMA with 5 wt.% borax and PMMA with 10 wt.% borax was determined in this study. All of the three samples were synthesized by ATRP. Their contact angles were also measured were given in table 5.7, whereas their figures were given in Figure 5.5a-c (In the calculations, the situation of water drop in 12 seconds after dropping on the sample surface was taken into consideration).
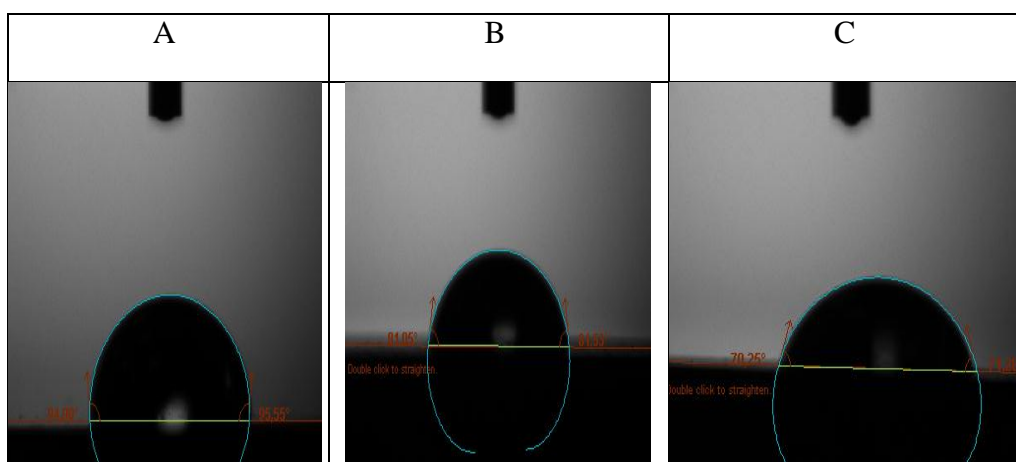
Figure 5.5a-c: a**:** Contact angle of base PMMA, b: contact angle of 5 (wt.%) borax added PMMA and c: 10 (wt.%) borax added PMMA.

Table 5.7: Contact angle of base and composite samples in this study

Sample	Contact Angle (°)
base PMMA	~95
5 wt.% borax added PMMA	~ 81
10 wt.% borax added PMMA	~71

The base PMMA, whose contact angle was measured about 95°, has called hydrophobic, while borax added PMMAs are called hydrophilic (the angle of PMMA with 5 wt.% borax was measured about 81° and the angle of PMMA with 10 wt.% borax ~71°). Methyl methacrylate (MMA) was used as monomer synthesized PMMA by ATRP and this monomer constituted ~ 95% by weight of PMMA. The solubility of MMA is 15 g/l at 20°C whereas the solubility of borax in water 38.1 g/l at 20°C [31,180]. Hence, it was assumed that borax used as reinforcement in this polymer leads to the rise of hydrophilic property in PMMA.

It was deduced from the results of contact angle measurement in PMMA/Borax composite samples that the borax reinforcement in PMMA caused to decrease in the contact angle. This has meant that the borax-added surface retains more water when exposed to water. It was assumed that the reason why the contact angle of base PMMA was considerably high was increasing the average molecular weight. The reason for this idea was that the increased molecular weight led to an enhancement in the cohesion force, resulting in greater resistance to the adhesion force.

5.4 Evaluation of Magnetic Properties in Base and Composite Samples

The external magnetic field between 20.000 Oe and -20.000 Oe was applied to three polymer samples such as base PMMA, PMMA/borax composite samples (at 5 and 10 (wt.%)) were given in Figure 5.6 and Figure 5.7. M-H curve of base PMMA was shown in Figure 5.6, and the M-H curve of composite samples was given in Figure 5.7. In these figures, the x-axis has represented the external magnetic field (Oe), while the y-axis has referred to the magnetic moment the samples have against this magnetic field (emu/g). The magnetic moment value of the capsule is subtracted from the total magnetic moment of the samples since the magnetic behavior of all samples is calculated in the capsule. After this subtraction, the M-H curves of the samples were formed.

The M-H curve of base PMMA was indicated in Figure 5.6. Base PMMA was subjected to an external magnetic field between -20.000-20000 Oe. Base PMMA had a reverse magnetic moment of 0.01 emu /g when exposed to an external magnetic field of 20,000 Oe, base PMMA was magnetized inversely against to this magnetic field. The magnetization reaction of PMMA is a characteristic behavior belonging to diamagnetic materials. In this context, base PMMA can be accepted as one of the diamagnetic materials.

Figure 5.7 explained the M-H curve of PMMA with borax addition at 5 wt.% and 10 wt.% amounts. The M-H curves of PMMA/Borax composite samples divided into three regions since they had different behavior against to external magnetic field at these regions. One of these regions was centered between -2.500 Oe and +2.500 Oe. PMMA/Borax composite samples at 5 and 10 (wt.%) borax exhibited paramagnetic properties with the rise of the external magnetic field in the first region.

The second region appeared between (-5.000) – (-2.500) Oe and (+2500) - (+5000 Oe). In the second region, while the applied external magnetic field increased, the paramagnetic properties decreased of PMMA/Borax composite at 5 wt.% and 10 wt.%.

The third region distinguished at the ranges between (-20.000) – (-5.000) Oe and (+5000) - (+20.000) Oe. PMMA/Borax composite samples at 5 and 10 (wt.%) borax exhibited diamagnetic properties when they were exposed to the external magnetic field in the third region.
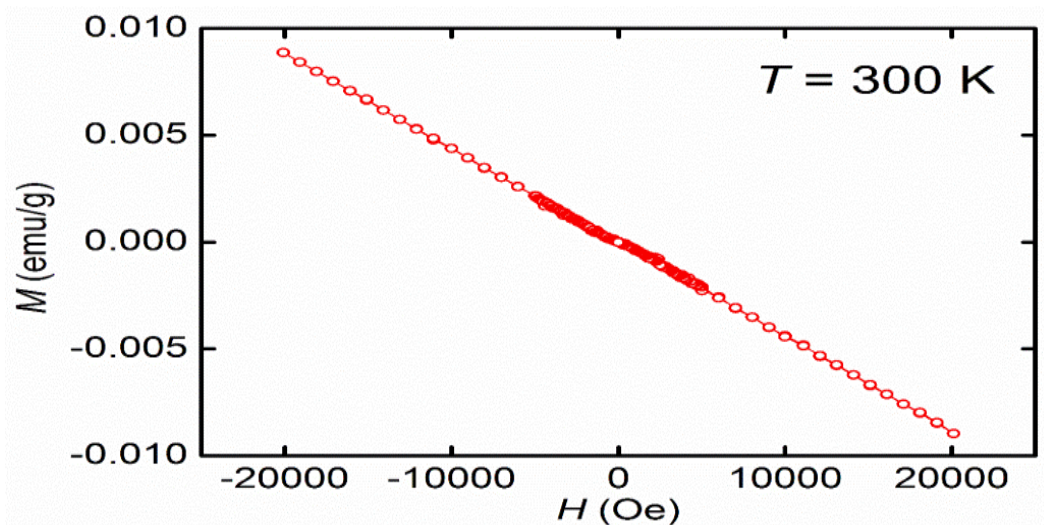
Figure 5.6: M-H Curve of base PMMA.
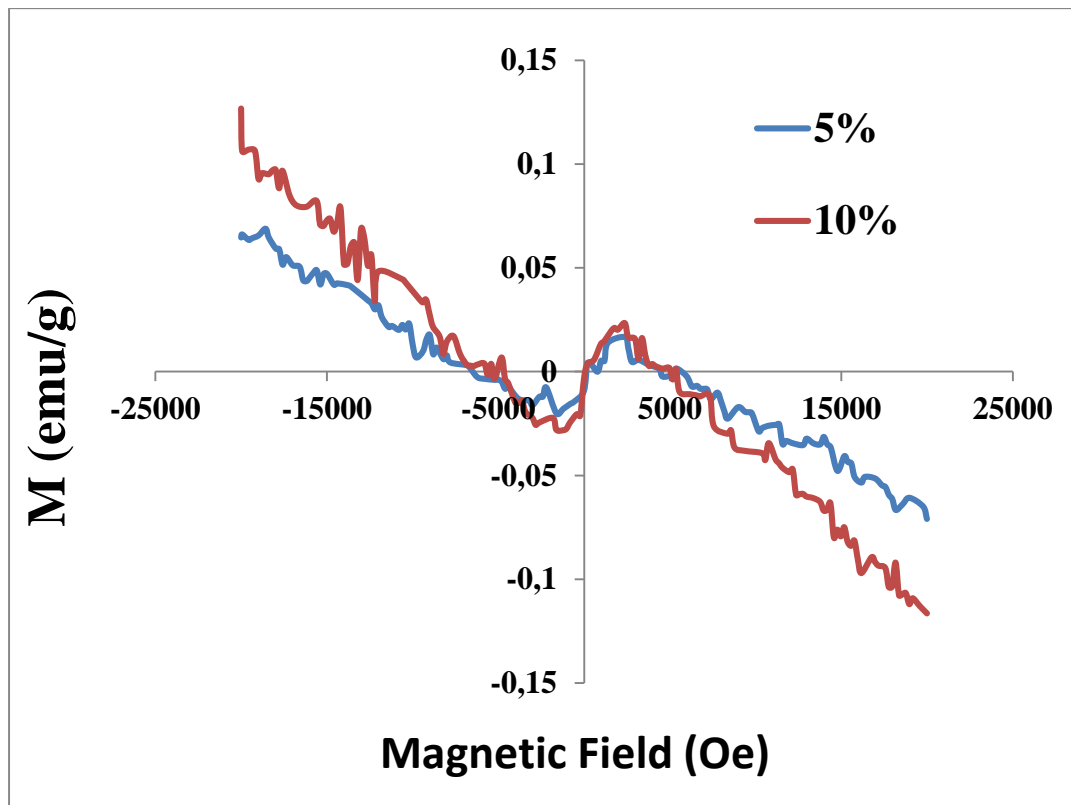
Figure 5.7: Magnetic Field-Momentum curve of PMMA reinforced by borax at 5 wt.% *(blue)* and 10 wt.% *(red)*.

5.5 Evaluation of Optical Properties in Base and Composite Samples

The optical properties of base PMMA and PMMA/Borax composite samples at 5 wt.% and 10 wt.% amounts were examined as transmittance T (%), reflectance R (%) and absorbance A (%). The transmittance of the samples was presented in Figure 5.8.

The measurement of the UV-VIS spectrophotometer was extended from a part of the UV range at 300 nm to the near-infrared region of 1100 nm for all samples. The base PMMA with 2 mm thickness had 3% transmittance between 320 and 360 nm and the base PMMA presented the cut-of beyond~310 nm.

The transmittance was measured as 80% between ~360-400-nm. at the visible range. Besides, T% of base PMMA exhibited an increase between ~380-550 nm. It had ~58% transmittance at~ 550 nm (which is max. visual eye sensitivity at this wavelength) in visible range. T% of base PMMA exhibited a decrease between 550-700 nm. When the curve of base PMMA was examined it had 55% transmittance at ~ 1100 nm in the near-infrared (NIR) range.

The T (%) values of PMMA/Borax composite samples at 5 wt.% and 10 wt.% borax amounts have presented in Figure 5.8. The PMMA/Borax composite samples with 2 mm thickness had 3% transmittance between 320 and 360 nm and the composite samples presented the cut-of beyond~310 nm. Both of the composite samples exhibited the same behavior with an increase to 80 %between 360-400 nm (in the IR region and visible range). However, T% of these composite samples was decreased considerably to 2% between the beginning of visible range (~400 nm) to NIR (1100 nm).

Finally, base PMMA and PMMA/Borax composite samples presented similar behavior for the cut-of beyond ~310 nm. As the reinforcement of borax in PMMA, the transmittance of PMMA decreased depending on the white of powdered borax with 91,92 average L value ($L^* = 0$ yields black, $L^* = 100$ with the diffuse of white according to the CIELAB color space) [32,181]. The optical property of borax as translucent to opaque has affected considerably transmittance of the polymer composite. Hence borax addition caused to decrease in the transmittance of PMMA/Borax composite samples due to the improvement of the opaque property of polymer composite.

Figure 5.9 indicated the wavelength of the colors belonging to the visible range. When base PMMA was examined according to the information in this Figure, it was determined that the transmittance percent of base PMMA increased sharply when approaching the yellow zone (~550 nm) and decreased when it went away from the yellow zone.
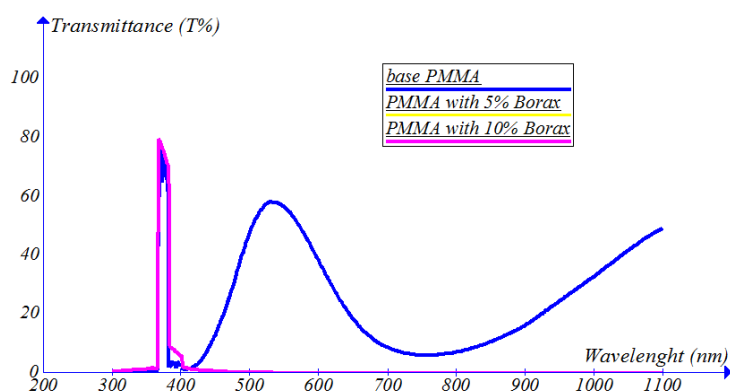
Figure 5.8: Transmittance of base and composite samples exposed to light at 300-1100 n. Blue: base PMMA. yellow: PMMA with 5 wt.% borax and pink: PMMA with 10 wt.% borax .
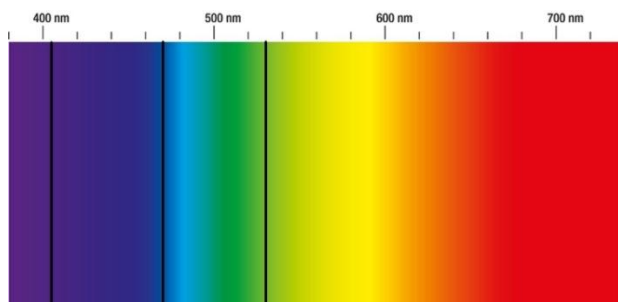
Figure 5.9: The Wavelength of color takes part in the visible range of the spectrum [182].

The reflectance R (%) values of PMMA/Borax composite samples at two different borax amounts (such as 5 and 10 wt.%) have determined between 300-1100-nm in Figure 5.10. R% of the polymer composite increased slightly from 300 nm to 380 nm and it increased considerably at 380 nm. The composite sample reflected ~94% of the light having this wavelength (380 nm). However, R% of this composite samples decreased from 380 nm to 550 nm and it was measured 3% between 550-1100 nm.

R% of PMMA with 10 wt.% borax has similar R% properties with PMMA with 5 wt.% borax. The borax addition at 10 wt.% caused to rise the reflectance of the composite depending on the increase the scattering effect due to the increase of borax powder amount in the composite structure. %R of PMMA with 10 wt.% borax was measured a few percent's lower than 5 wt.% borax added PMMA. To give an example, the reflection of 10 wt.% borax added PMMA at 300 nm was measured ~2 %, whereas this value was ~4% for 10 wt.% borax added PMMA.
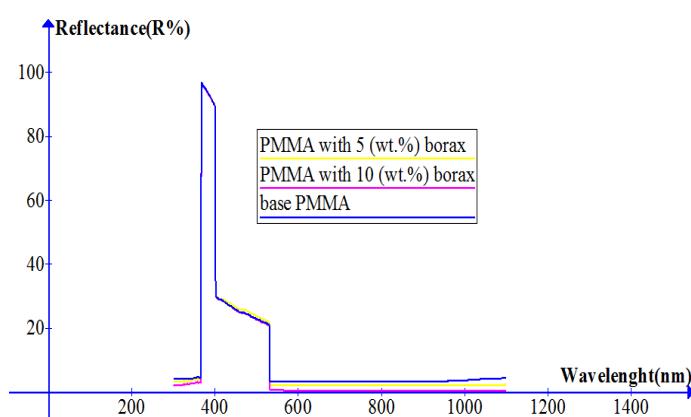
Figure 5.10: Reflectance of base and composite samples exposed to light at 300-1100 nm , *yellow*: PMMA with 5 wt.% borax, *pink* : PMMA with 5 wt.% borax.

84

The absorbance A% of composite samples was determined according to eq.5.1 and the absorbance was calculated considering the transmittance and the reflectance.

$$100\% = Transmittance\ T\% + Refletance\ R\% + Absorbance\ A\% \qquad (5.1)$$

The absorbance of PMMA with 5 and 10 wt.% borax was determined as ~95% from 300 to 380 nm in the UV range (in Figure 5.13). The absorbance of the composite samples decreased considerably at 380 nm and reached to 0% at 380 nm. The absorbance of the samples exhibited a considerable increase at 400 nm and it was measured as~65%.

The increase in the absorbance of the composite samples determined as ~97 % at 550 nm and The absorbance at ~97 % has presented a broadened absorption band between 550 and 1100 nm.

It was assumed that the effect of multiple scattering of light between 550 and 1100 nm caused to self-absorption on the PMMA/Borax composite depending on the borax addition to PMMA (at two different borax amount such as 5 and 10 wt.%).
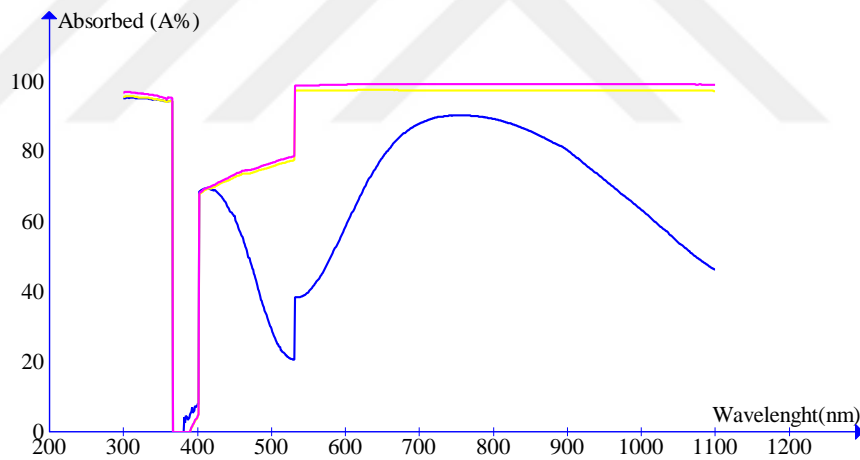
Figure 5.11: Absorbance of base and composite samples exposed to light at 300-1000 nm. Blue: base PMMA, *yellow*: PMMA with 5 wt.% borax, *pink:* PMMA with 5 wt.% borax.

It was observed a result of these examinations that the reinforcing borax in PMMA decreased the transmittance rate of PMMA, thus increasing the amount of light absorbed by the PMMA as the amount of borax as the additive material in PMMA increases. As a result of this examination, it was determined that the behavior of PMMA against light turned from optical material to opaque material with borax reinforcement.

5.6 Evaluation of Thermogravimetric Analysis in Base and Composite Samples

Figure 5.12 indicates Thermogravimetric Analysis (TGA) thermogram of borax, base and composite samples (base PMMA, PMMA with 5 wt.% borax and PMMA with 10 wt.% borax). TGA thermogram o were used to measure the mass change associated with the increase in temperature (This loss is an indication of thermal stability).

When the TGA thermogram of base and composite samples were examined, the first serious mass loss of the samples occurred around 200°C. The reason for this was the evaporation of the moisture present in the structure. The amount of this mass loss due to moisture was measured as 12 % at 200 °C. As the borax ($Na_2B_4O.10H_2O$) structure contained moisture, the amount of mass loss increases as the percentage by weight increases in the composite. In addition, the dramatic mass loss observed between 350-400 °C in all three samples represented the change of state of the samples.
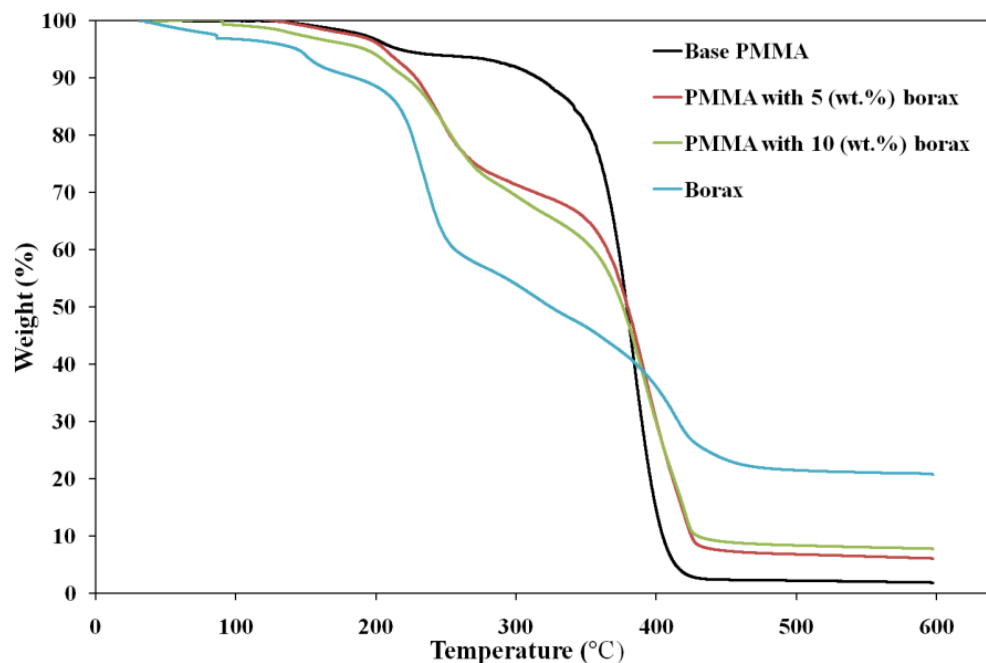
Figure 5.12: TGA of borax, base and composite samples in this study

Table 5.8 has presented the changes in the thermal degradation for PMMA/Borax composite at the different borax amount that is based on the results obtained from TGA. This table indicated the temperatures at which the specific percentages are lost in the mass of the sample. With respect to this table obtained from TGA, it was detected that 5% mass-loss of base PMMA occurred at 203 °C, 10% mass-loss of this polymer at 311 °C, 20% mass-loss of this polymer at 353 °C, and 30% mass-loss in

this polymer occurred at 362 ° C. Besides, it was detected from TGA that 5% mass-loss of PMMA with 5 wt.% borax occurred at 203 °C, 10% of mass-loss at 226 ° C, and 20% of mass-loss at 252 ° C and 30% of the mass-loss occurred at 308 °C. 5% of mass-loss of PMMA with 10 wt.% borax occurred at 192 ° C, 10% mass-loss of this polymer at 221 ° C, 20% mass-loss at 254 ° C, and 30% of mass-loss occurred at 296 °C.

Table 5.8: The changes of thermal degradation for base and composite samples.

PMMA/Borax Composite for (borax wt.%)	Weight loss at ~5%	Weight loss at ~10%	Weight loss at ~20%	Weight loss at ~30%
base	208°C	311°C	353 °C	362°C
5 wt.%	203°C	226°C	252°C	308°C
10 wt.%	192°C	221°C	254°C	296°C

5.7 Evaluation of X-ray Diffraction of Base and Composite Samples

X-ray diffraction peaks of borax ($Na_2B_4O.10H_2O$) were determined at ~15, 18, 25 and 30 (2θ degree) in Figure 5.13a. The similar peaks were determined for borax at PMMA/Borax composite samples in this study.

The amount of borax was increased in PMMA the intensity of diffraction peaks start to increase in this study (Figure 5.13b) until about 25°. On the other hand, when the XRD curve of the base PMMA was examined, three broad prominent humps are visible. There are around 10°–25°, 25-35°, 35-45° and this result is consistent with the literature [183-184]. It is confirming the presence of PMMA. Furthermore, when the curve of the base PMMA is compared with other doped PMMA, more pronounced peaks are encountered.

XRD curves of PMMA/Borax composite samples were evaluated together because they have very similar results. (Although there are some shifts up to 25 °, almost equivalent results are encountered after this value). The intensity of the humps, which detected also in the base PMMA, in borax added PMMA decreased. Besides that, in spite of some shifts, peaks in base PMMA were also observed in composite samples.
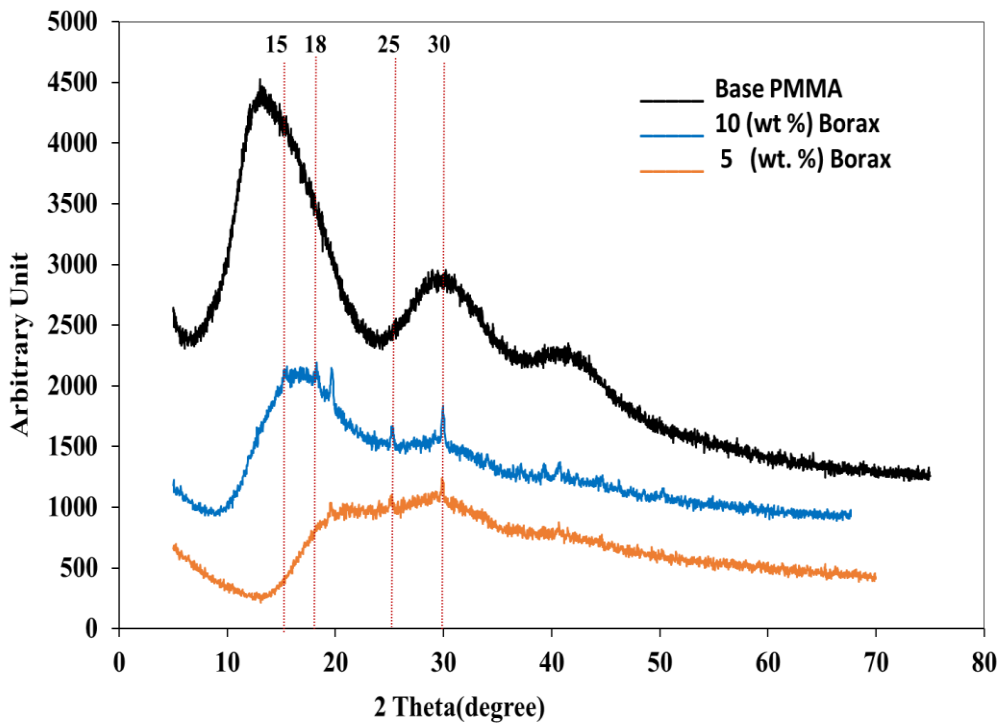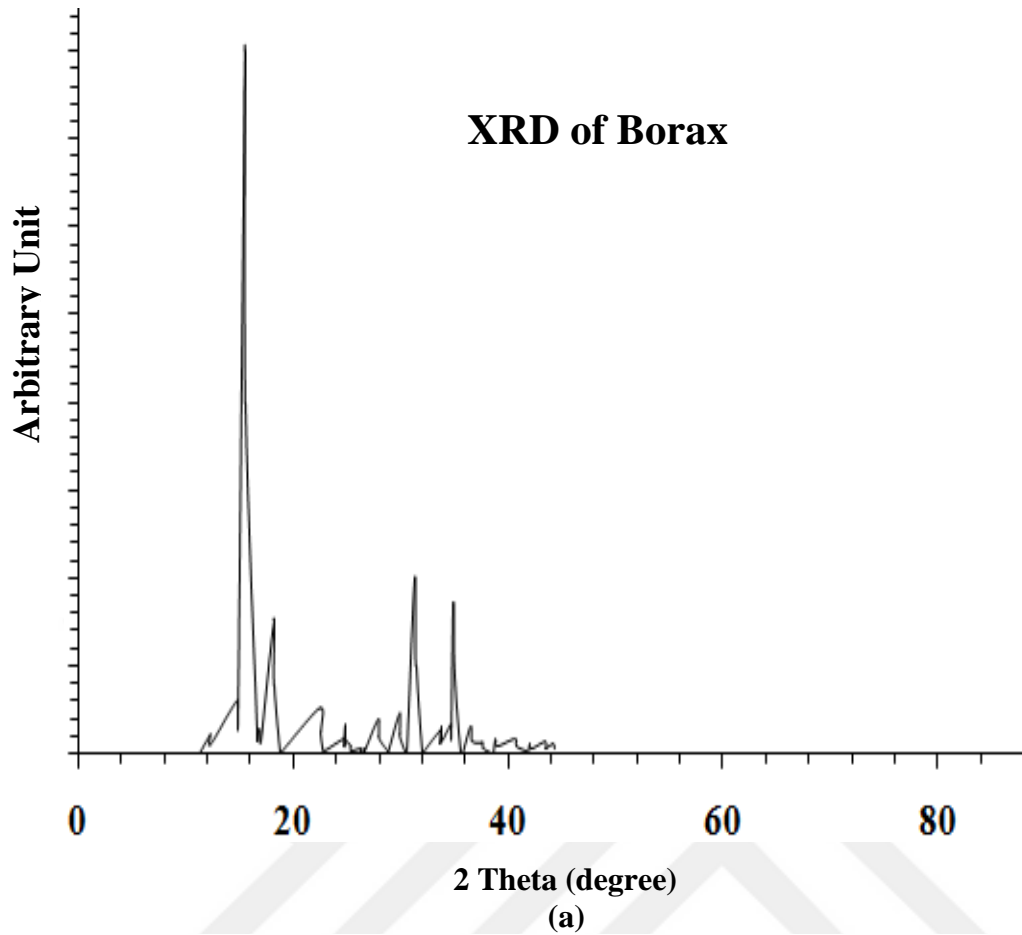
Figure 5.13a-b: a: XRD of borax. b: XRD patterns of base and composite samples

5.8 Scanning Electron Microscope of Base and Composite Samples

The SEM Images of Borax ($Na_2B_4O_7.10H_2O$) with purity at $\geq$99.5% named borax was presented with 1000 x magnification in Figure 5.14(a) and Figure 5.14(b) with 2500 x magnitude. SEM images with 20.000 X magnifications of base and composite samples were included in FIG. 5.19a-c. To evaluate the relative integrity of the surface of PMMA samples with and without borax doping, the surfaces were subjected to simple grinding by a mesh abrasive paper before SEM examinations. As shown in Fig. 5.15a, base PMMA sample has a highly flat surface morphology and was free from any scratches and detachments from the surface.

However, the surface gets progressively deteriorated as the content of borax in PMMA increases. For example, shallow and randomly oriented flaws originating from the grinding were seen on the surface of PMMA with 5 wt.% borax sample (Fig. 5.15b). On the other hand, the highest amount of borax addition led to deeper cracks aligned in the transverse direction of the grinding (Fig. 5.15c). This observation might be taken as the relative measure of surface integrity of PMMA samples and showed that the samples were more brittle with the increasing amount of borax doping.
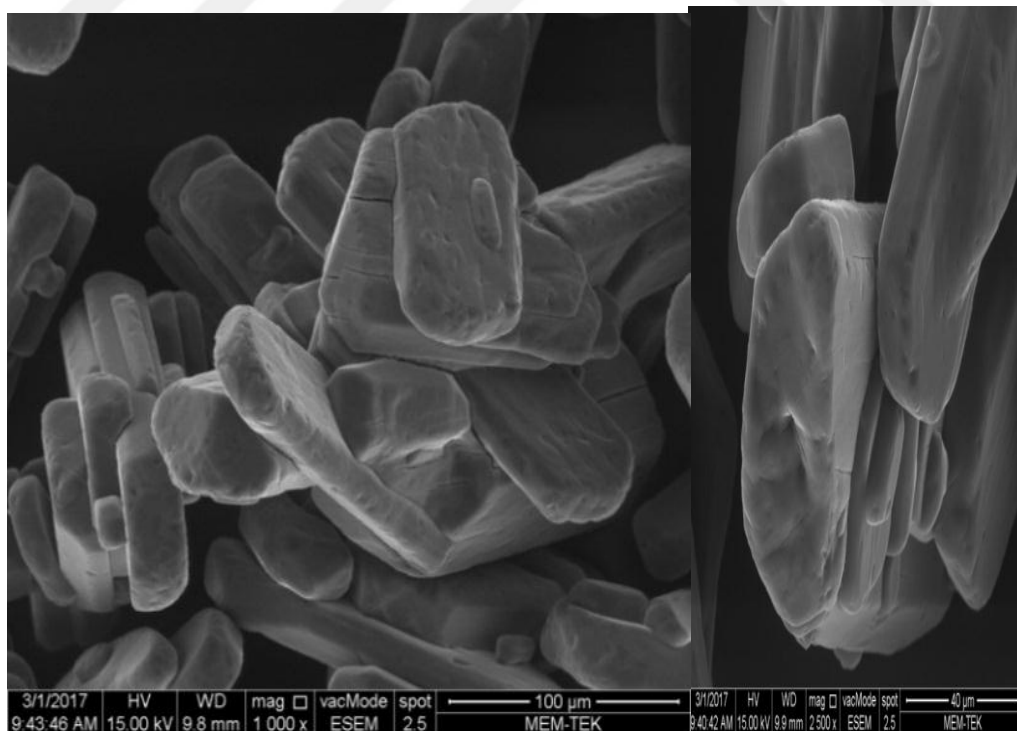
a   b

Figure 5.14 a-b: SEM Images of Borax
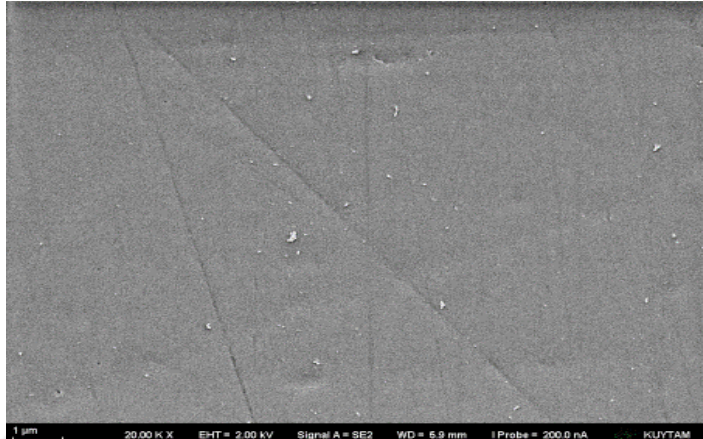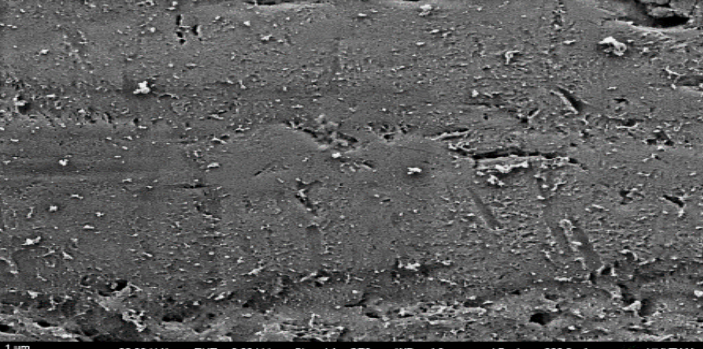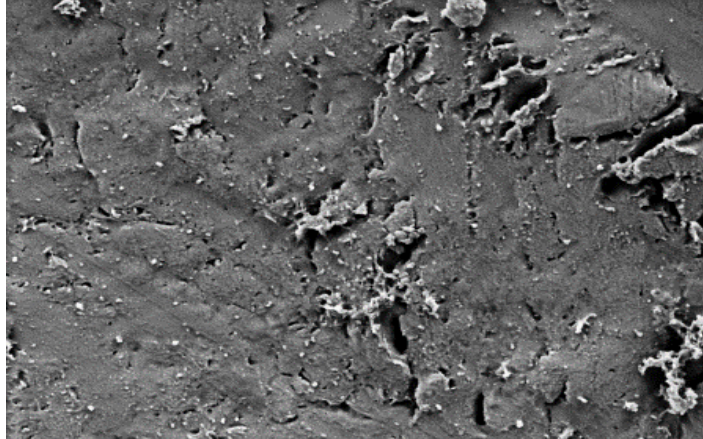
PMMA/Borax Composite	SEM Image
a *Base*	
b *5 (wt .%borax)*	
c *10 (wt. %) borax*	

Figure 5.15a-c: a: SEM image of base PMMA, b: SEM image of PMMA with %5 borax, c: SEM Image of PMMA with %10 borax.

To determine the elemental composition of the samples, the samples were subjected to a scanning electron beam following SEM. Base PMMA's surface was applied Energy Dispersive X-Ray Analysis (EDX) is shown in Figure 5.16 and the result of the analysis was indicated in Figure 5.17. As a result of this analysis, carbon, copper, oxygen, and bromine were found in the structure of base PMMA. All of these elements were expected to be found in the structure of base PMMA. Of these, carbon was present in the structure of Tetrabutylammonium bromide $(CH_3CH_2CH_2CH_2)4N(Br)$, which used as solvent, PMDETA $(C_9H_{23}N_3)$, which used as ligand, EBIB $((CH_3)_2CBrCOOC_2H_5)$, which was used as initiator, while oxygen was present in the structure of EBIB. Bromine was present in the structure of Bu_4NBr used as solvent and copper bromide (CuBr) used as catalyst, while copper was present in the structure of catalyst (CuBr).
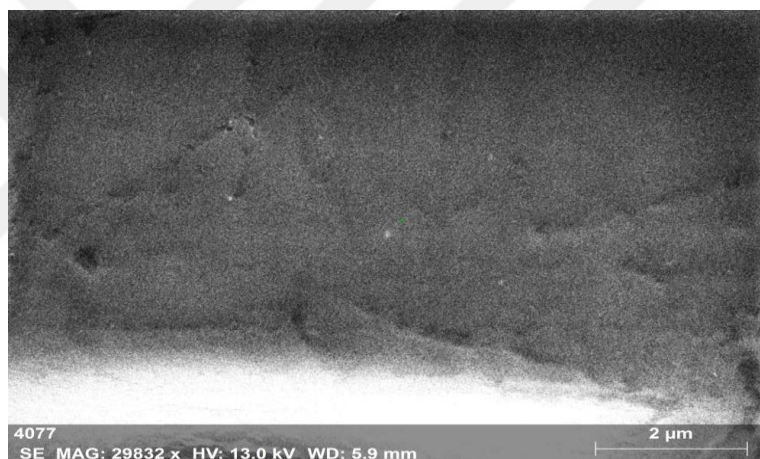
Figure 5.16: Image of EDX applied surface of base PMMA.
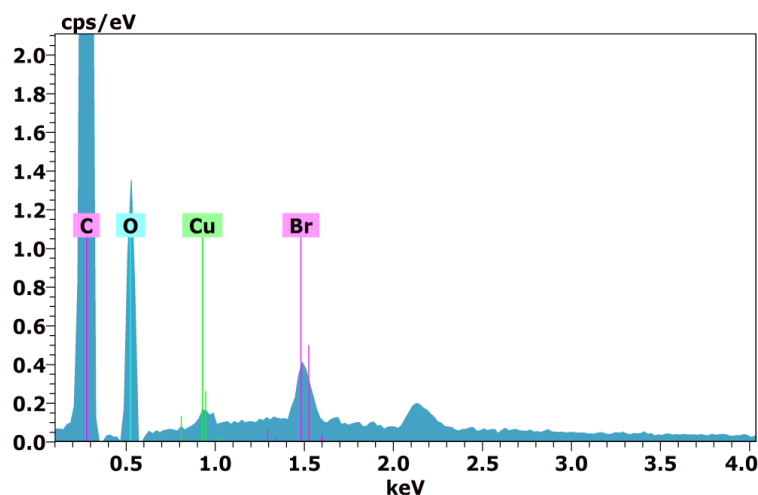
Figure 5.17: EDX of base PMMA.

The surface of PMMA with 5 (wt.%) borax was applied electron scanning beam (in Figure 5.18). The result of the analysis was indicated in Figure 5.19. As a result of this process, carbon, copper, oxygen, and bromine were found in the structure of this doped PMMA like in base PMMA. However, the boron element used as reinforcement material was not found in the structure as a result of EDX.

Figure 5.18: Image of EDX applied surface of PMMA with 5 (wt.%) borax.
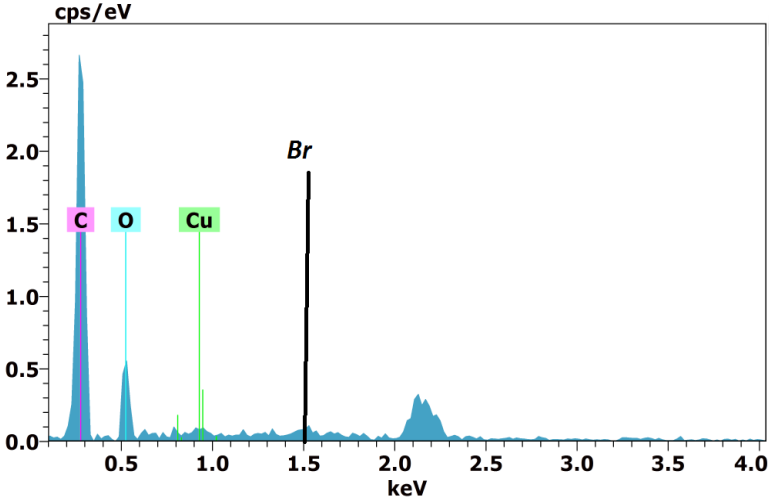
Figure 5.19: EDX of PMMA with 5 (wt.%) borax.

The surface applied electron scanning beam of PMMA/Borax composite with 10 (wt. %) borax is shown in Figure 5.20. and the result of the analysis was shown in Figure 5.21. As a result of this process, carbon, copper, oxygen and bromine were found in the structure of this doped PMMA like in base PMMA. However, the boron element used as reinforcement material was not found in the structure as a result of EDX.
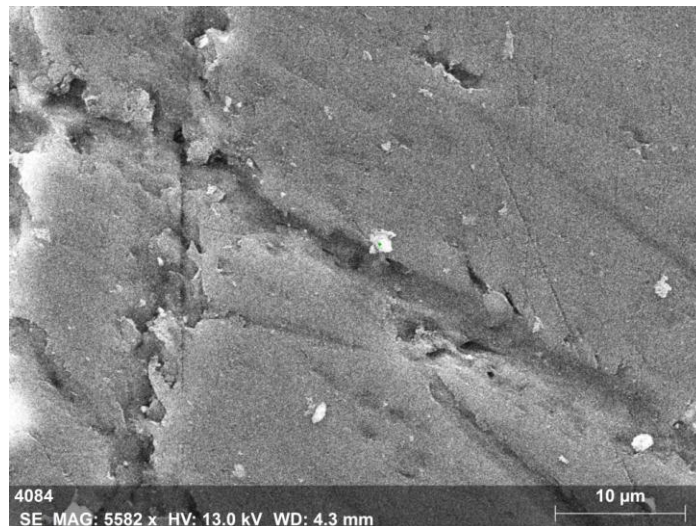
Figure 5.20: Image of EDX applied surface of PMMA with 10 (wt.%) borax.
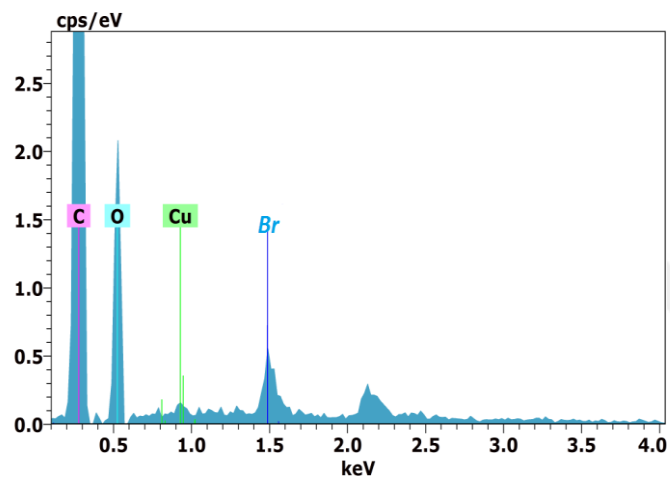
Figure 5.21: EDX of PMMA with 10% borax.

The boron element used as doping material in this study was not found by EDX analysis. The particle size of the boron is very small, which has led to this situation and this is quite common in literature. In order to solve this problem, X-ray Photoelectron Spectroscopy (XPS) was used for the determination of the boron element in the surface of samples (in Figure 5.22 and 5.23).

According to the peak with their binding energy of 192.01 eV at XPS analysis, the borax crystal was assigned to be $Na_2B_4O_7.10H_2O$ at PMMA/Borax composite with 10 (wt.%) borax amount. Boron in PMMA/Borax composite at 5 (wt.%) borax amount can not be determined at XPS analysis as this borax amount is lower than the detection limit of X-ray photoelectron spectroscopy (XPS). Similar results of boron in borax are determined in literature [185].
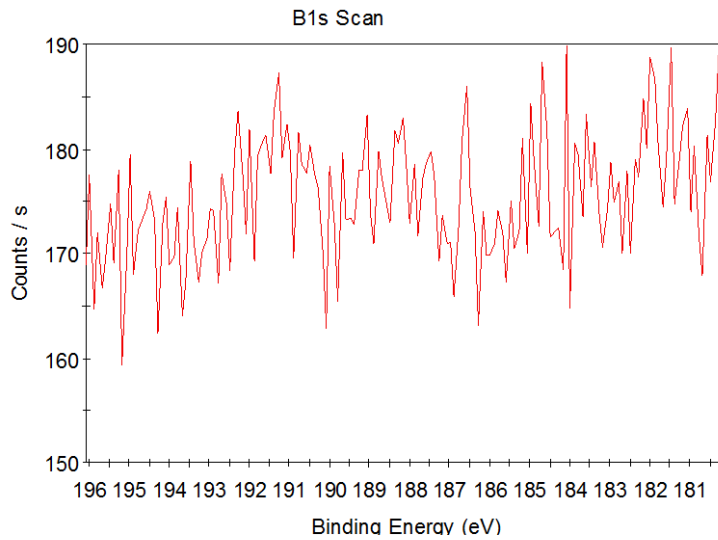
Figure 5.22: XPS of PMMA with 5 (wt.%) borax amount.
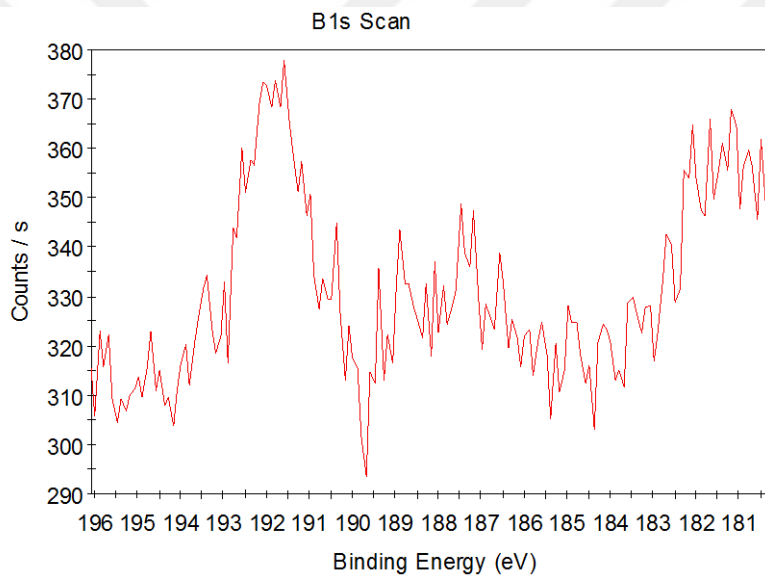
Figure 5.23: XPS of PMMA with 10 (wt.%) borax amount.

5.9 Shore D Hardness of Base and Composite Samples

In the Examination of five Shore D hardness values of the samples, it was obtained the same values 75 for base PMMA. Besides, the Shore D hardness was measured all time as 88 for PMMA with 5% borax and it was measured three times as 86 and two times as 85 for PMMA with 10% borax. When the 5 results of each sample were examined, almost the same results were measured for each. This is an indication that the structure is very homogeneous. This is highly desirable in polymer materials and this has been achieved.

The arithmetic means of these five results were taken into consideration and then the Shore D hardness values of the samples were calculated. As shown in Figure 5.24, Shore D hardness value of base PMMA is 75. Besides, this value was measured as 88 for PMMA with 5% borax and 86 for PMMA with 10% borax.

Figure 5.24: Shore D Hardness of base and composite samples in this study.

When the effect of borax-reinforcement on hardness in PMMA was examined, it was observed that reinforcement of borax increases hardness up to ~%5 (88 Shore D) and after this reinforcing ratio and it caused a small decrease in hardness value in PMMA (at 10% reinforcing ratio, 86 Shore D).

6.DISCUSSION

6.1 Identification of Poly(methyl methacrylate) bonds

The identification of poly(methyl methacrylate) bonds was performed by using FTIR Analysis. The wavenumbers of the identified peaks indicated by FTIR analysis for base PMMA and PMMA/borax composite synthesized in this study (in table 5.1a). When the results were compared with the literature [186-190], similar identical peaks were determined in this study. The characteristic bonds of PMMA and PMMA/Borax composite samples have formed smoothly.

6.2 Optical properties of Poly(methyl methacrylate)

One of the most important properties of industrial PMMA is its high transmittance (%90-93) in the visible region (380-780 nm) [191-193]. The color of the base PMMA synthesized by the ATRP method changed green due to copper used as the catalyst in the ATRP method.

The transmittance, T (%) was 60% at ~550 nm (the maximum human visual sensitivity) in the visible range. On the other hand, the borax selected as the reinforcement material caused to decrease in the transmittance of PMMA. The average L value scale used in the colorimetry test is a measure of the color of the sample. Powdered borax is white and the result of the colorimetry test in borax is 91,92 for average L value (L* = 0 yields black, L* = 100 indicates diffuse white in the CIELAB color space) [32]. The optical property of borax is translucent to opaque [181]. Therefore, the result of these properties of borax caused decreasing the transmittance of PMMA/Borax composite. and improved its opaque property.

6.3 Contact Angle in Poly(methyl methacrylate)

The borax free-PMMA in this study presented hydrophobic properties with 95° contact angle. The contact angle of base PMMA was considerably high when it was compared with the literature (Table 6.1) [14-17]. This higher contact angle will result in less wetting.

When it is used particularly outdoor in rainy weather, it will have less mass increase due to less water absorption as its surface will hold less water when it is used outdoors. This less mass increasing will cause to save fuel when this polymer was used in transportation technologies etc.

Table 6.1: Comparison of contact angle of PMMA between the literature and this study [14-17].

Material	Information of PMMA	Contact Angle (°)
PMMA [14]	Industrial Insulation Chennai Company, India (PDI=1.82)	~73
PMMA [15]	Mw=93.9 kg/mole Industrial Insulation Chennai, India	~60-70
PMMA [16]	Free radical synthesis	64
PMMA [17]	by Sigma Aldrich Homopolymer (Mn 90 kg/mole) PDI=1.09	69
base PMMA (in this study)	ATRP Method (Mw=270 kg/mole)	~95
PMMA with 5 (wt.%) borax (in this study)	ATRP Method (Mw=275 kg/mole	~81
PMMA with 10 (wt.%) borax (in this study)	ATRP Method (Mw=670 kg/mole	~71

The contact angle of PMMA with borax at 5 (wt.%) was determined as 81°. Besides, the contact angle of PMMA with borax at 10 (wt.%) was 71° in this study. Borax addition caused to decrease in the contact angle of polymer surface in this study. The similar changes of contact angle were determined between the literature [194-196] and this study depending on borax addition to PMMA. The hydrophobic property of base PMMA has turned into hydrophilic property due to the borax addition.

Therefore, the addition of borax in PMMA synthesized by the ATRP method has supported fabricating more hydrophilic self-cleaning surface. It was assumed that dirt or contaminants were reduced or disintegrated into smaller particles upon contact with the polymer surface since the development of the hydrophilic surface permits the self-cleaning behavior of PMMA/Borax composite samples.

6.4 Magnetic Properties of Poly(methyl methacrylate)

PMMA is magnetized at a very low level when it is exposed to an external magnetic field like almost all of the polymers. While PMMA often exhibits diamagnetic properties, it has been observed in the literature that in some cases it can have a low level of paramagnetic properties due to the effect of materials used during its synthesis (such as copper used in ATRP) [181]. A number of reinforcements have been tried to enhance this low magnetic property of PMMA [197].

Figure 6.1 was indicated the magnetic properties of PMMA synthesized by ATRP like that in this study. The maximum magnetization in the study was observed at approximately 0.00015 emu/g at 1600 Gauss (1 Gauss= 1 Oe), which was considerably lower than the magnetization of synthesized PMMA in this study (0.14 emu/g at 20.000 Oe). Besides, the maximum magnetization of PMMA/ Fe-oxide nanocomposites was measured is approximately 0.02 emu/g at 20.000 0e (in Figure 6.2) [198]. Although borax addition supported to increasing magnetic properties of PMMA, PMMA/Borax composite has not been at the high level in terms of magnetization. In this context, this can be tried to be reinforced with additional material to increase the magnetic properties of this composite.
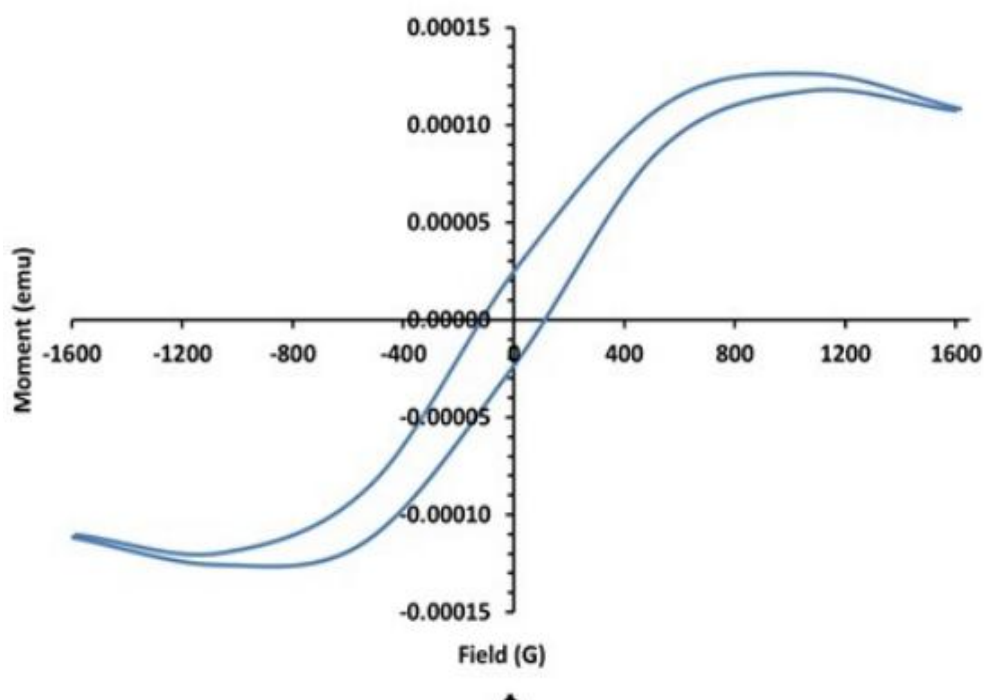
Figure 6.1: VSM profile of magnetic moment (emu) versus applied field (G) curve of PMMA by ATRP [197].
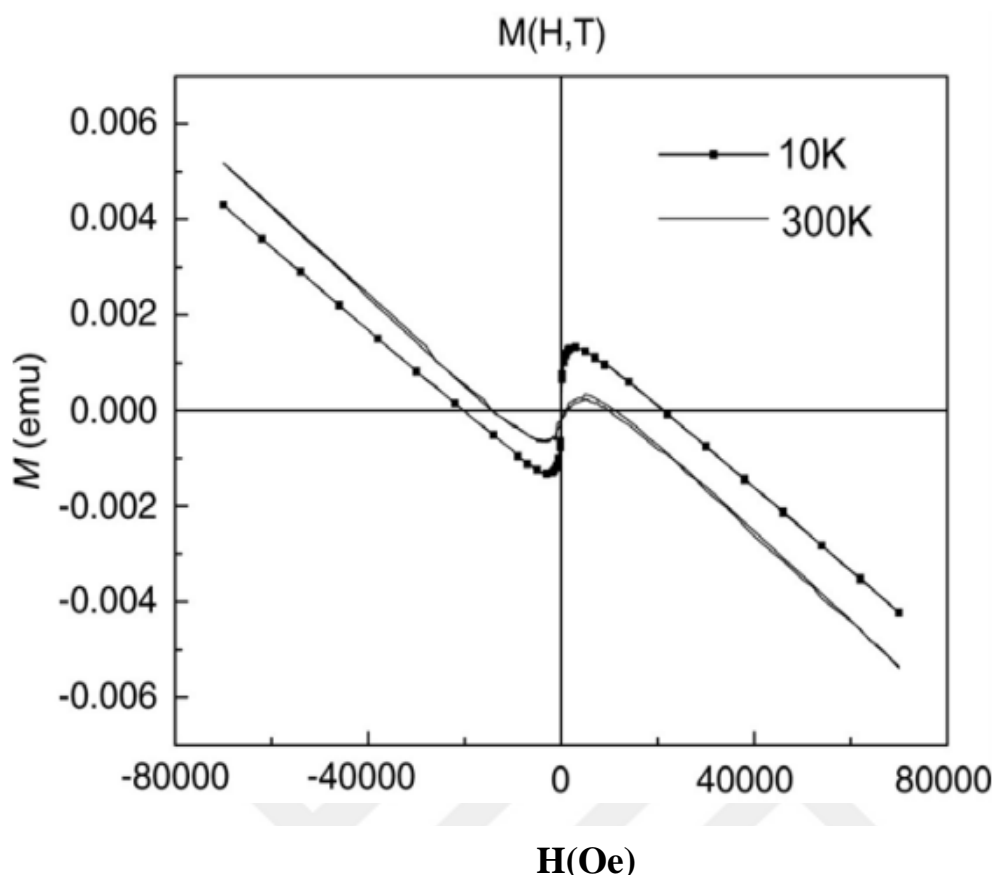
Figure 6.2: M–H curves at 10 and 300 K for PMMA/Fe-oxide nanocomposites. (0.05 wt. %, the loading is calculated based on considering all Fe oxide to be Fe_2O_3 [198].

6.5 Average Molecular Weight in Poly(methyl methacrylate)

One of the most important properties of the ATRP method is that the polymerization is carried out in a controlled manner. As a result, it allows obtaining the polymers with high average molecular weight. To observe this positive effect of the ATRP method, the average molecular weight of the synthesized polymers was measured in this study. As a result of these measurements, it was determined that base PMMA in this study had an average molecular weight of 270.000 g/mol. Besides, this value of PMMA/Borax composite at 5 (wt.%) borax amount was determined as 275.000 g/mol. The average molecular weight of PMMA/Borax composite at 10 (wt.%) borax was determined as 670.000 g/mol and this results supported by the changes of average molecular weight of PMMA [199].

When these results were compared with the literature (Table 6.2), it was determined that PMMA/Borax composite in this study was synthesized with a considerably high average molecular weight according to the literature [17, 19-20, 200].

Table 6.2: Average molecular weight of PMMA in the literature and this study.

Material	Average Molecular Weight (g/mole)
PMMA [200] (by GPC)	120.000
PMMA [17] (PMMA prepared from the block copolymer micelle/ homopolymer)	90.000
PMMA [19] (PMMA synthesized by the catalyzed recyclable Ni–Co alloy nanoparticle)	129.500 (PDI=1,30)
PMMA [20] (ARGET ATRP)	42.500 (PDI=1.36)
Base PMMA by ATRP (in this study)	270.000
5 (wt.%) borax doped PMMA by ATRP (in this study)	275.000
10 (wt.%) borax doped PMMA by ATRP (in this study)	670.000

6.6 Thermal Stability of Poly(methyl methacrylate)

One of the most important disadvantages of polymeric materials is that they lose their thermal stability at relatively low temperatures compared to metals. Therefore, it is expected that the material selected as the additional material support to increase thermal stability in polymer. In this context, the effect of borax addition on thermal stability was investigated in PMMA by thermal gravimetric analysis. When the borax amount increased in PMMA the thermal stability of polymer composite decreased slightly from 208°C to 192°C for weight loss at ~5%. When these results were compared to the literature [21-23,201], it was observed that base PMMA was consistent with the literature in terms of thermal stability, whereas this property in borax added PMMA exhibited at lower levels than that in literature.

6.7 Hardness in Poly(methyl methacrylate)

In table 6.3, the Shore D hardness of base PMMA in this study and in the literature, as well as these hardness value of PMMA/Borax composite samples are indicated. When the values were examined together, it was observed that the base PMMA synthesized in this study had a hardness value of at least 18 percent higher than the literature. In the same way, PMMA with 5 % borax has a hardness value of at least %38 higher than PMMA in the literature. It is known that increases the average molecular weight in polymers synthesized by the ATRP method also increases mechanical properties. In this study, this known situation was encountered.

Table 6.3: Shore D hardness of some base PMMA in the literature [7-10].

Material	Shore Hardness (D)
base PMMA [7] by melt intercalation method	~58
base PMMA [8]	~70
base PMMA [9]	~61
base PMMA [10] by cold curing	~62
base PMMA by ATRP in this study	75
5 (wt.%) borax doped PMMA by ATRP (in this study)	88
10 (wt.%) borax doped PMMA by ATRP (in this study)	86

7.CONCLUSION

One of the most important advantages of the ATRP method chosen as synthesis method in this study is that it provides the synthesis to be carried out in a controlled manner and gives the polymers synthesized by this method with very high average molecular weight and very low Polydispersity index. To determined the above positive effect of the ATRP method on polymerization, the viscosity average molecular weight of PMMA and borax doped PMMA was measured. The molecular weight of base PMMA synthesized by the ATRP method was measured as 270.000 g / mol. The results about the improvement of the average molecular weight indicated the positive effect of the ATRP method on the average molecular weight of PMMA. The average molecular weight reached about 670,000 g/mole in PMMA/Borax composite at 10 (wt.%) borax amount. The reinforcement with borax in PMMA has a positive effect at 10 (wt.%) borax amount for the enhancement of the average molecular weight of PMMA/Borax composite.

The hardness values of PMMA/Borax composite samples were measured by the Shore D scale. The hardness of Base PMMA was measured as 75 Shore D, whereas hardness of PMMA/Borax composite at 5 (wt.%) borax amount was measured as 88 Shore D. The hardness of PMMA/Borax composite at 10 (wt.%) borax amount was measured as 86 Shore D. The optimum borax amount in terms of hardness was determined at a range between ~ 5 and 10 (wt.%) borax amount. These results from viscosity average molecular weight and hardness tests were indicated the accuracy of ATRP selected as the synthesis method and the selection of borax as doping material in PMMA. Besides, the five measurements taken from the samples in hardness test measurements are almost the same, indicating how homogeneous the structure is. Although no experiments were carried out for Polydispersity in this study, these results were strongly suggestive of positive results about Polydispersity.

The wettability of the PMMA/Borax composite samples was determined by the measuring of the contact angles of a drop of distilled water deposited on the surface of the samples. Wettability measurements of the samples were done in dry conditions.

The contact angle of PMMA synthesized by the ATRP method was measured as 95°. This contact angle presented the PMMA as a hydrophobic material. The contact angle was determined as 81° at 5 (wt.%) borax amount. Besides, the contact angle was determined as 71° at 10 (wt.%) borax addition. Borax has reduced the contact angle of PMMA in this study.

The surface of the PMMA/Borax composite indicated the increase of the hydrophilic properties with the rise of the borax addition to PMMA. In this context, the base PMMA synthesized by ATRP in this study is appropriate for the studies where being required the materials having low wettability properties. However, borax doping has improved wettability property in PMMA/Borax composite. Thus, the self-cleaning properties of the surface in the composite has increased due to borax reinforcement. This will be advantageous in many applications such as solar photovoltaics.

An external magnetic field in the range between -20.000 and +20.000 Oe was applied to measure the effect of the borax-doping to PMMA synthesized by the ATRP method. The magnetic properties of base PMMA presented diamagnetic properties (0,02 emu/g at -5.000 Oe) as the chemicals used in PMMA synthesized by the ATRP method have the diamagnetic properties. The result of the magnetic properties for base PMMA was similar with the industrial PMMA.

The magnetization of PMMA increased slightly with the reinforcement of borax and presented paramagnetic properties up to 5,000 Oe. The increase in the magnetization of PMMA/Borax composite samples was quite low (0,03 emu/g at 2.500 Oe for 10 (wt.%) borax amount.

In order to detect the functional groups formed in the samples, infrared rays with a wavelength of 4000-400 cm^{-1} were applied to the polymers. In FTIR spectroscopies of these polymers were detected the following peaks: the peaks formed at 2994 cm^{-1} and 2952 cm^{-1} belong to C-H stretching, 1772 cm^{-1} C = 0 stretching, 1484 cm^{-1} and 1435 cm^{-1} C-H bending or scissoring, 1271 cm^{-1} and 1240 cm^{-1} C-0 stretching, 1190 cm^{-1} C-O-C bending, 1144 cm-1 C-H$_2$ bending and finally, the peak formed at 1063 cm^{-1} belongs to the C-0 stretching. These bonds are structural characteristic properties of PMMA.

When the results of XRD analysis were evaluated, three humps (~ 10°–25°, 25-35°, 35-45°) formed in base PMMA (since the structure was amorphous, no peaks like in crystalline materials were found). On the other hand, the diffraction peaks at ~15°, 18°, 25°, and 30° were found in composite samples in this study. The intensity of the diffraction peaks was increased depending on the rise of borax addition.

One of the most important characteristics of PMMA is its high transmittance in the visible region. In order to determine these optical properties, PMMA/Borax composite samples were subjected to lights having a wavelength of 1100-300 nm in the UV-VIS spectrophotometer. However, the transmittance of base PMMA sample with 2 mm thickness could not be exceeding 60% in the visible region. On the other hand, borax addition of PMMA decreased the optical transmittance and resulted with the rise of opaque properties in PMMA.

Thermogravimetric analysis was examined to measure the thermal stability of PMMA/Borax composites. The weight loss at 5 % occurred in base PMMA at 208 °C. The weight loss at 5 % occurred in PMMA with 5 (wt. %) borax amount at 203 °C. Besides, the weight loss at 5 % occurred in PMMA with 10 (wt. %) borax amount at 192 °C. The borax reinforcement of PMMA decreased thermal stability. It was detected in TGA that as the amount of borax additive increases, the mass loss of the composite increases around 200 °C. This is because the borax contains a high amount of moisture. In high-temperature applications, borax doping in composite should be limited as much as possible in these applications as this will increase mass loss and reduce the thermal stability of the composite.

REFERENCES

[1] **Trends 2018**. In Photovoltaic applications survey report of selected IEA Countries between 1992 and 2017. Adress: http://www.iea-pvps. org/fileadmin/dam/intranet/task1/IEA_PVPS_Trends_2018_in_Photo voltaic_Applications.pdf. Date retrieved: 20.09.2019.

[2] **Url-1** *<Https://Yearbook.Enerdata.Net/Renewables/Wind-Solar-ShareElectricity -PrOduction.Html>*, date retrieved: 20.09.2019.

[3] **REN21 members, renewables** (2019). *Global status report, from <https://www.ren21.net/wp-content/uploads/2019/05/gsr_2019_full_ report_en.pdf>*, date retrieved: 20.09.2019.

[4] **BP Statistical review of world energy** 2018. from*<www.bp.com › dam › bp › global › corporate › pdfs › energy-economics>*, date retrieved: 20.09.2019.

[5] **Wang**, **B.**, **Lin**, **Q.**, **Shen, C.**, **Han, Y.**, **Tang, J.** , **Chen H.** (2014). Synthesis of MA POSS–PMMA as an intraocular lens material with high light transmittance and good cytocompatibility, *RSC Adv., 2014, 4,* 52959.

[6] **Poomalai**, **P., Siddaramaiah** (2005) 'Studies on Poly(Methyl Methacrylate) (PMMA) and thermoplastic Polyurethane (TPU) Blends', *Journal of Macromolecular Science, Part A, **42**:10, 1399 — 1407.

[7] **Kumar, M.** (2015). Properties of PMMA/clay nanocomposites prepared using various compatibilizers *Macromolecular Research, **April 2009**,Volume 17,* Issue4, pp 240–244.

[8] **Vian, V. D.**, **Denton, N. L**. (2018). Hardness comparison of polymers pecimens produced with different processes, Purdue University Purdue e-Pubs, *ASEE IL-IN Section Conference. 3.*

[9] **Haitham, R.**, **Raheem**, **A.** , **Abdullah, H. A.**, **S. S. Ahmed**. (2017). Mechanical properties of composites materials reinforced in ceramic particles " *International Journal of Mechanical and Production Engineering (IJMPE)*, **Volume: 5,** Issue-6.

[10] **Thomas, P.**, **Dakshayini, B. S.**, **Kushwaha**, **H. S.**, **Vaish R.** (2015). Effect of Sr2TiMnO6 fillers on mechanical, dielectric and thermal behavior of PMMA polymer , *Journal of Advanced Dielectrics **Vol. 05**,* No. 03,1550018, doi:10.1142/S2010135X15500186.

[11] **Url-2** *<https://www.makeitfrom.com/materialproperties/Polymethylmethacrylate-P MMA-Acrylic>*, date retrieved: 20.09.2019

[12] **Schenck, J. F.** (1993). "The role of magnetic susceptibility in magnetic resonance imaging: MRI magnetic compatibility of the first and second kinds". *Medical Physics, **23*** (6): 815–850(23), doi: 10.1118/1.597854.

[13] **Bel, T.**, **Yahya, N**, **Cimenoglu H.**, **Arslan, C.**, **Baydogan, N.** (2018). The Examination of the changes in the magnetic properties of the Poly(methyl methacrylate) *Journal of Physics: Conference Series 1123 (1),* 012005.

[14] **Ma, Y.**, **Cao, X.**, **Feng, X.**, **Ma, Y.,** **Zou, H.** (2007). Fabrication of super-hydrophobic film from PMMA with intrinsic water contact angle below 90, *Polymer*, *48* (26):7455-7460, doi: 10.1016/j.polymer.2007.10.038.

[15] **Thukkaram, M.**, **Sitaram, S.**, **Kannaiyan, S. K**, **Subbiahdoss, G.** (2014). Antibacterial efficacy of iron-oxide nanoparticles against biofilms on different biomaterial surfaces*, International Journal of Biomaterials*, *Volume 2014,* Article ID 716080, 6 pages.

[16] **Ngai, J. H. L.**, **Ho, J. K**. **W.**, **Chan, R.**, **Cheung, S. H.**, **Leung, L M.**, **So, S. K.** Growth, characterization, and thin film transistor application of CH3NH3PbI3 perovskite on polymeric gate dielectric layers *RSC Advances, 7* (78):49353-49360, doi: 10.1039/C7RA08699G.

[17] **Park, H.**, **Kim, J. U.**, **Park, S.** (2012). High-throughput preparation of complex multi-scale patterns from block copolymer/homopolymer blend films *Nanoscale*, *4*, Issue 4, 2012, doi: 10.1039/c2nr11792d

[18] **Url-3** *<https://www.sigmaaldrich.com/catalog/product/aldrich/182230?lang= en&region=TR>,* date retrieved: 20.09.2019.

[19] **Wu, G., Tao, Y., Zhang, H.** (2008). Influence of molecular weight of poly (methyl methacrylate) on its miscibility with poly (vinyl chloride) in the solution, *Polymer Bulletin 60*, 363–370 (2008). doi 10.1007/s00289-007-0853-y

[20] **Mohammad, S. A.**, **Shingdilwar, S.**, **Banerjee, S.** (2020). Recoverable and recyclable nickel–cobalt magnetic alloy nanoparticle catalyzed reversible deactivation radical polymerization of methyl methacrylate at 25 °C, *Polymer Chemistry*, *Issue 2*, 2020, doi:10.1039/C9PY00942F

[21] **Jeon, H. J.** , **Youk, J. H**, **Ahn, S. H.**, **Choi, J. H.**, **Cho, K. S.** (2009). Synthesis of high molecular weight 3-arm star PMMA by ARGET ATRP. *Macromolecular Research, Volume 17*, pages 240–244(2009).

[22] **Bellan, C. S., Sugumaran, S., Sengoden, R.** (2013). Spin coated nano scale PMMA films for organic thin film transistors, *Physics Procedia 49*:145–157, doi: 10.1016/j.phpro.2013.10.021.

[23] **Stojanović**, **D. B.** , **Brajovic, L.**, **Orlović, A.**, **Dramlic, D.**, **Radmilović, Uskokovic, Aleksic, V.,P., R.** (2019). Transparent PMMA/silica nanocomposites containing silica nanoparticles coating under supercritical conditions, *Progress in Organic Coatings, 76*, (4):626–631, doi: 10.1016/j.porgcoat.2012.12.002.

[24] **Ferk, G.**, **Krajnc, P.**, **Hamler, A.**, **Mertelj, A.**, **Cebollada, F.**, **Drofenik, M., Monolithic, D L.** (2015). Magneto-Optical Nanocomposites of Barium Hexaferrite Platelets in PMMA, *Scientific Reports*, *Volume 5*, Article number: 11395, doi: 10.1038/srep11395

[25] **Matyjaszewski, K.** *Comparison and classification of controlled/living radical polymerizations* Krzysztof Matyjaszewski, Chapter 1, doi 10.1021/bk-2000-0768.ch001

[26] **Mishra, V. and Kumar, R. (2012).** Living radical polymerızatıon a revıew, *Journal of Scientific Research Banaras Hindu University, Varanasi, Vol. 56*, 2012 141-176 ISSN : 0447-9483, doi: 10.1002/anie.200604473.

[27] **Çankaya, G.** (2011). *Yeni bir yaşayan kontrollü radikal başlatma sistemi: çinko alkil halojenür*, Thesis (M.Sc.). İstanbul Technical University, Intitute of Science and Technology.

[28] **Sigma Aldrich** ,Controlled Radical Materials Science Polymerization Guide, ATRP | RAFT | NMP, from *<https://www.sigmaaldrich.com/technical-documents/articles/crp-guide.html>*. date retrieved: 20.09.2019.

[29] **Bel, T., Arslan, C., Baydoğan, N.** (2018) PMMA / mikroküre/montmorillonite nanokompozit ve PMMA /mikroküre/halloysite nanokompozitin atom transfer radikal polimerizasyon tekniği ile üretilmesi ve mekanik özelliklerinin karşılaştırmalı olarak incelenmesi *Article in Journal of the Faculty of Engineering and Architecture of Gazi University. April 2018*, doi: 10.17341/gazimmfd.416525.

[30] **Maimaitituersun, M.** 2017 *Properties of Poly(Methyl Methacrylate/Graphene nanoplatelets nanocomposite*. M.Sc. Thesis. İstanbul Technical University, Institute of Science and Technology.

[31] **Ulag, S.** (2017). *The Investıgatıon of the irradiation effect on PMMA /MWCNTS polymer nanocomposıtes* Thesis (M.Sc.) İstanbul Technical University, Institute of Science and Technology.

[32] **Bel, T.**, **Arslan, C.**, **Baydogan, N.** (2019). Radiation shielding properties of Poly(methyl methacrylate)/colemanite composite for the use in mixed irradiation fields of neutrons and gamma rays. *Materials Chemistry and Physics Volume 221*, 1 January 2019, Pages 58-67.

[33] **Çelik, M. S.** (1996). Bor Minerallerinin Flatasyonunda Şlamın Etki Mekanizması.

[34] **Url-4** *<http://www.etimaden.gov.tr/bor-elementi>,* date retrieved: 20.09.2019.

[35] **Lide, D. R.** (1998-1999). *CRC Handbook of Chemistry and Physics,*79. Edition The elements 4-6.

[36] **Safety Data Sheet of Sodium tetraborate decahydrate** in Sigma-Aldrich, Version 6.1, Revision Date 14.01.2019.

[37] **The product data sheet for Borax**. In Etimaden *<www.etimaden.gov.tr › chemical-products>*. date retrieved: 20.09.2019.

[38] **Coleman, J. N.**, **Khan, U.**, **Blau, W. J.**, **Gun, Y. K.** (2006). Small but strong: A review of the mechanical properties of carbon nanotube–polymer composites, *Article in Carbon, Volume 44*, Issue 9, August 2006, Pages 1624-1652, doi: 10.1016/j.carbon.2006.02.038.

[39] **Url-5** *<https://polyfill.com.vn/polymer-implies-numerous-monomers-the-charac terization-accumulation>*, date retrieved: 20.09.2019.

[40] **Rudin, A., Choi, P.** (2013*). The Elements of Polymer Science &Engineering, Alfred Rudin and Philip Choi,* 3rd Edition, pp.16.

[41] **Brandrup, J.** *Poylmer Handbook 4th Edition*, p.p 4, I-3.

[42] **Url-6** <*https://www.toppr.com/guides/chemistry/polymers/classification-of-poly mers*>, date retrieved: 20.09.2019.

[43] **Chauvel-Lebret, D. J.**, **Auroy, P.**, **Bonnaure-Mallet, M.** (2002). *Polymeric biomaterials: Biocompatibility of Elastomers* (2.Edition*)*. New York, NY: Marcel Dekker AG.

[44] **Mallick, P. K.** (2010) Thermoplastics and thermoplastic–matrix composites for lightweight automotive, In book: *Materials, Design and Manufacturing for Lightweight Vehicles*, p.p 174, doi: 10.1533/9781845697822.1.174.

[45] **Url-7** <*http://www.materials.unsw.edu.au/tutorials/online-tutorials/8 polymer-ty pes*>, date retrieved: 20.09.2019.

[46] **Abbas, A. S. , Mohamed, F. A.** (2015). Production and evaluation of liquid hydrocarbon fuel from thermal pyrolysis of virgin Polyethylene Plastic, *Iraqi Journal of Chemical and Petroleum Engineering* ,***Vol.16*** No.1 21- 33 ISSN: 1997-4884.

[47] **Url-8** <*http://ossarchive.adm.ntu.edu.sg/2016-17/cm8001-group6/index.html%3 Fp=46.html*>, date retrieved: 20.09.2019.

[48] **Shrivastava, A.** (2018). *Introduction to Plastics Engineering, first edition*

[49] **Url-9** <*https://kids.britannica.com/students/assembly/view/267*>, date retrieved: 20.09.2019.

[50] **Url-10** <*https://www.slideshare.net/kalender13/ayse-kalemtas-malzemebilimigi ris*>, Polimer Malzemeler Ders Notları, Yrd. Doç. Dr. Ayşe KALEMTAŞ, date retrieved: 20.09.2019.

[51] **Gokel, G. W.** (2004). *Dean's Handbook of Organic Chemistry, 2. Edition*, p 10-2.

[52] **Url-11** <*https://www.e-education.psu.edu/matse81/node/2210*>, date retrieved: 20.09.2019.

[53] **Demirbay, B.** (2017). *Film formation, morphological, optical and electrical percolation behaviors of PS/MWCNT and PS/GO nanocomposite films*, Thesis for: Master's Degree doi: 10.13140/RG.2.2.12577.35682.

[54] **Url-12** <*https://www.cmu.edu/gelfand/education/k12-teachers/polymers/polym er-architecture/index.html*>, date retrieved: 20.09.2019.

[55] **Gokel, G. E**, **Gokel ,G. W., John A**. (2004). *Dean Dean's Handbook of Organic Chemistry* second Edition, p.p 10-2.

[56] **Koltzenburg, S., Maskos, M., Nuyken O.** (2017) *Polymer Chemistry* First edition, p.p:4-5.

[57] **Url-13**<*https://sciencing.com/calculate-degree-polymerization-8762591.html*> date retrieved: 20.09.2019.

[58] **Saçak, M.** *Polimer Kimyası,* 6. Edition. p6-8.

[59] **Url14** < https://polymerdatabase.com/polymer%20chemistry/Stepgrowth%20 Polymerization.html*>, date retrieved: 20.09.2019.

[60] **Koltzenburg, S., Maskos, M., Nuyken, O.** (2017). *Polymer Chemistry,* first edition, p.p.166.

[61] **Url-15** <*http://www.passmyexams.co.uk/GCSE/chemistry/condensation-polymer isation.html* >*,* date retrieved: 20.09.2019.

[62] **Url16** <*https://chem.libretexts.org/Bookshelves/Organic_Chemistry/Map%3A_ Organic_Chemistry_(Smith)/Chapter_31%3A_Synthetic_Polymers/31.2 %3A_ChainGrowth_Polymers%E2%80%94Addition_Polymers>,* date retrieved: 20.09.2019.

[63] **Url17** <*https://polymerdatabase.com/polymer%20chemistry/radical%20mech anüsm.html>,* date retrieved: 20.09.2019.

[64] **Url18** <*http://taner.balikesir.edu.tr/dersler/polimer_kimyasi/polimerizasyon/ra dikal_zincir_polimerizasyon.html>,* date retrieved: 20.09.2019.

[65] **Rudin, A.**, **Choi, P.** (2013). *The Elements of Polymer Science & Engineering* (Third Edition).

[66] **Grajales, S.**, Ph.D. Aldrich, Materials Science Milwaukee, *Sigma-Aldrich, Materials-Science Material-Matters, Polymers for Advanced Architectures* **Volume 6**, Number 3.

[67] **Url19** <*yunus.hacettepe.edu.tr/~damlacetin/kmu407/index.../radikalpolimerizas yonu.pdf>,* date retrieved: 20.09.2019.

[68] **Wei Q.** (2009). Emerging approaches to the surface modification of textiles *Woodhead Publishing Series in Textiles, 2009*, Pages 318-323, doi: 10.1533/9781845696689.318.

[69] **Johnson, J. A.** (2012). Construction of stimuli-responsive polymers and polymer networks using controlled, living polymerizations and highly efficient organic reactions, *Acromolecules, 2012, 45*, 18, 7317-7328, Publication Date: August 10, 2012, doi: 10.1021/ma300817v.

[70] **Url20** <*https://www.sigmaaldrich.com/catalog/product/aldrich/m55909?lang= en&region=TR&gclid=Cj0KCQjwkK_qBRD8ARIsAOteukDWTLVIRb7 z6sxdRgyWGeRP0FcYsoVgT8a1TN4n9U20VA5kVQASJ8aAj0rEALw_ wcB>* , date retrieved: 20.09.2019.

[71] **Matyjaszewski, K., Xia, J.** (2001). *Chem. Rev. 2001*, 101, 9, 2921-2990. Publication Date: September 12, 2001, doi: 10.1021/cr940534g.

[72] **Url-21** <*https://scientificpolymer.com/density-of-polymers-by-density>,*

date retrieved: 20.09.2019.

[73] **Url-22** <*https://www.magmaweld.com.tr/metallerin-temelozellikleri/i/223>* date retrieved: 20.09.2019.

[74] **Franck, V. A.**, **Biederbick, K. H.** (1984). *Kunststoff-Kompendium,* Vogel-Buchverlag, Wurzburg.

[75] **Url-23** <*https://www.steelforge.com/literature/metal-melting-ranges>,* date retrieved: 20.09.2019.

[76] **Url-24** <https://www.futureocean.org/ozeanwissen/topics/plastic.php>, date retrieved: 20.09.2019.

[77] **Url-25** <*https://theconversation.com/the-world-of-plastics-in-numbers-100291*> accessed at 29.09.2019.

[78] **Brandrup, J.**, **Immergut, E. H., Grulke, E. A.** (2003). *Polymer Handbook*, Fourth Edition ,p.p I2-6.

[79] **Wiley, J. and Sons.** (2013). Wiley Properties and Behavior of Polymers, p.p 870.

[80] **Aygün, B.** (2015). *Nükleer uygulamalarda radyasyon güvenliği amacıyla yeni kalkan malzemelerin deneysel ve monte carlo simülasyon kodları (cern-fluka ve geant4) ile belirlenmesi ve fabrikasyonu*, Master thesis.Ataturk University.

[81] **Michler, G. H., Calleja, F. J. B.** (2012). *Nano and Micromechanics of Polymers*, p196.

[82] **Url-26** <*https://www.makeitfrom.com/material-properties/Polymethylmethacrylate-PMMA-Acrylic*>, date retrieved: 20.09.2019.

[83] **Brandrup, J.**, **Immergut, E. H., Grulke, E. A.** *Polymer Handbook,* fourth Edition , p.p: V87.

[84] **Barandiaran, I.** (2016). Nanocomposites based on nanostructured PI-b-PMMA copolymer and selectively placed PMMA-modified magnetic nanoparticles: Morphological and magnetic characterization, *European Polymer Journal* **, Volume 75**, February 2016, Pages 514-524, doi: 10.1016/j.eurpolymj.2016.01.005

[85] **Qin, S. J.**, **Fornara, A., Toprak, M., Muhammed, M., Kim, K. D.** (2009). Synthesis and magnetic properties of bulk transparent PMMA/Fe-oxide nanocomposites, *Nanotechnology ,20* (2009) 185607 (6pp).

[86] **Url-27** <*https://cdn.britannica.com/76/276-050-7BFF196F/position-light-electromagnetic-spectrum-range-right.jpg*>, date retrieved: 20.09.2019.

[87] **Glick, R. E.** (1961). "On the Diamagnetic Susceptibility of Gases". J. *Phy Chem. 65* (9): 1552–1555(22).

[88] **Wapler, M. C., Leupold, J.**; **Dragonu, I, Elverfeldt, D.**, **Zaitsev, M.**, **Wallrabe, U**. (2014). "Magnetic properties of materials for MR engineering, micro-MR and beyond" *JMR. 242: 233–242(24). doi: 10.1016/j.jmr.2014.02.005*

[89] **Arrighini, G. P.**, **Maestro, M., Moccia, R.** (1968). "Magnetic Properties of Polyatomic Molecules: Magnetic Susceptibility of H2O, NH3, CH4, H2O2". *J. Chem. Phys. 49* (2): 882–889(25).

[90] **Nave and Carl, L**. (2008). Magnetic Properties of Solids. *HyperPhysics*. retrieved 2008-11-09. (26).

[91] **Carmen** and **Stefanita, G.** (2012). *Magnetism, Basic and Applications*, p.p 4-5.

[92] **Url-28**<*https://www.makeitfrom.com/materialproperties/Polymethylmethacrylate-PMMA-Acrylic* >, date retrieved: 20.09.2019.

[93] **Url-29** <*https://nptel.ac.in/courses/113104005/76*>, date retrieved: 20.09.2019.

[94] **Url-30**< *https://www.physics-and-radio-electronics.com/physics/magnetism/paramagnetism.html*>, date retrieved: 20.09.2019.

[95] **Elías, M. I. F.**, **Gustavo, C. G.**, **Héctor, P. M.**, **Alberto, A. G. E., L. L. P., David D. I.** (2013). Análisis de Ruido de Barkhausen en probetas a tensıón, Memorıas *Del XVIII Congreso Internacional Anual De La Somim,21 al 23 De Septiembre, 2013* Pachuca, México.

[96] **Url-31** *<https://studylibtr.com/doc/4552394/b%C3%B6l%C3%BCm-9>,* N.B Teşneli, Bölüm 8 malzemelerin manyetik özellikleri, date retrieved: 20.09.2019.

[97] **Gürda, O.** Elektromanyetik *Dalga Teorisi, second Edition 2017* Bursa, p.p:6.

[98] **Url-32** *<https://science.nasa.gov/ems/02_anatomy>,* date retrieved: 20.09.2019.

[99] **Griffits, D.J.** Introduction to Electrodynamics,4. Edition, p.p:385.

[100] **Daud, H.**, **Sagayan,V., Yahya, N., Najwati W.** (2009). Modeling of electromagnetic waves using statistical and numerical techniques, *First International Visual Informatics Conference, IVIC 2009* Kuala Lumpur, Malaysia, November 11-13, 2009 Proceedings.

[101] **Walker, J.** Fundamentals of Physics,8th Edition, p.p:1094.

[102] **Daneshga, S.** (2015*). Remote sensing observations for monitoring coastal zones: Volturno River mouth case study* Thesis for: Master of Science, doi: 10.13140/RG.2.1.3806.9209.

[103] **Orhun, Ö., Tanişli, M.** Elektromanyetik Dalgalar, Anadolu Üniversitesi Açık Öğretim Fakültesi Chapter 11, P179-181.

[104] **Walker, J.** Fundamentals of Physics,8th Edition, p.p :1093-95.

[105] **Url-32** <https://science.nasa.gov/ems>, date retrieved: 20.09.2019.

[106] **Url-33** <https://www.cyberphysics.co.uk/topics/light/color.html>, date retrieved: 20.09.2019.

[107] **Antic, Ž., Krsmanovic, R.**, **Marinovic-Cincovic, M., Dramicanin, M.D.** (2010). Gd2O3:Eu3+/PMMA Composite: Thermal and Luminescence Properties. *Acta Physica Polonica A.* ***Vol. 117*** (2010)

[108] **Zhang, H. J**, **Fan, R. Q.**, **Wang, X.-M., Wang, P., Wang, Y. L**, **Yang, Y. L.** Preparation, characterization, and properties of PMMA-doped polymer film materials: a study on the effect of terbium *44,2871. Dalton Transactions,* ***Issue 6***, 2015

[109] **Abomostafa, H.**, **Gad, S. A.**, **Khalaf, A**. **I.** (2018). Improving the Optical, Mechanical and Dielectric Properties of PMMA: Mg1−x Cu_xO Based Polymer Nanocomposites, Journal of Inorganic and Organometallic Polymers and Materials (2018). *Journal of Inorganic and Organometallic Polymers and Materials,* **28**:2759–2769, *1-8*, May 2019, doi: 10.1007/s10904-019-01205-0

[110] **Taa'y, W. A. A.**, **Oboudi, S. F.**, **Yousif, E.**, **Nabi, M. A., Yusop, R. M.**, **Derawi, D.** (2015). Fabrication and characterization of Nickel Chloride doped PMMA Films, Hindawi *Publishing Corporation Advances in Materials Science and Engineering*, *Volume 2015*, Article ID 913260, 5 pages, doi: 10.1155/2015/913260.

[111] **Kaur, R. and Samra K. S.** (2018). Electrical and mechanical behavior of polymethymethacrylate/cadmium sulphide composites, *Physica B: Condensed Matter 538* (2018) 29–34, doi:10.1016/j.physb.2018.03.019.

[112] **Su, P.G**, **Sunb, Y.L**, **Lin, C. C**. (2006). Humidity sensor based on PMMA simultaneously doped with two different salts, sensors and actuators, *B 113* (2006) 883–886, doi: 10.1016/j.snb.2005.03.052.

[113] **Zhang**, **Y.**, **Chen, Huang**, **Y. Y. L.**, **Chai**, **Z. G.**, **Shen, L. J. Xiao, Y.-H.** (2017). The antifungal effects and mechanical properties of silver bromide/cationic polymer nanocomposite-modified Poly-methylmethacrylate-based dental resin, *Scientific Reports*, doi:10.1038/s41598-017-01686-4.

[114] **Kiran, M. S. R. N.**, **Raidongia, K., Ramamurty, U.**, **Rao, C. N. R**. (2011).

Improved mechanical properties of polymer nanocomposites incorporating graphene-like BN: Dependence on the number of BN layers. *Scripta Materialia, 64* (6), 592-595. doi: 10.1016/j.scriptamat.2010.12.007.

[115] **Turan, P.**, **Alkan, M.**, **Turhan, Y.**, **Gündüz, Z.**, **Dogan, M.** (2015). Synthesis, Characterization and Rheological Properties of Boronoxide, *Polymer Nanocomposites*. Retrieved April 11, 2016, from: http://waset.org/pdf/books/?id=21154&pageNumber=535.

[116] **Yifei, Y.**, **Lin, Z.**, **Lijie, H.**, **Wei, W.**, **Guanhui, M.** (2011). Size effect of added LaB6 particles on optical properties of LaB6 /polymer composites. *Journal of Solid State Chemistry, 184* (12), 3364-3367.

[117] **Url-33** *<http://www.etimaden.gov.tr/en/chemical-products>,* date retrieved: 20.09.2019.

[118], **Ipekoglu, U. and Polat, M.** (1987). *Bor Enstitüsüne Genel Bakış Madenilik Dergisi Sayı* **1**, s 5-16,1987.

[119] *The Economics of Boron*.(1993).7th.Edtion, Roskill Information Services, London.

[120] **Url-34** *<http://www.etimaden.gov.tr/en/boron-element>,* date retrieved: 20.09.2019.

[121] **Atalay, Ö.** (2012). *Magnezyum borat sentezi ve alev geciktirici pigment olarak kullanılabilirliği*, Yüksek Lisans Tezi, Gazi Üniversitesi Fen Bilimleri Enstitüsü, Ankara.

[122] **Aydın, D. Y.**, **Gürü, Ayar, M., B, Çakanyıldırım, Ç.** (2016). Bor bileşiklerinin alev geciktirici ve yüksek sıcaklığa dayanıklı pigment olarak uygulanabilirliği. *Journal of Boron*, *Yıl 2016*, **Cilt 1** , Sayı 1, Sayfalar 33-39.

[123] **Url-35***<https://study.com/academy/lesson/what-is-boron-facts-uses-propert ies-benefits.html>,* date retrieved: 20.09.2019.

[124] **Çelik, Ç**. (2010). *Nano boyutta titanyum diborür katkılı sıcak preslenmiş hegzagonal bor nitrür–titanyum diborür kompozitlerinin özelliklerinin incelenmesi.* Thesis (M.Sc.), Istanbul Technical University, Institute of Science and Technology.

[125] **Spohn, M. T.** (1994). *Boron Carbide Minerals* p.p: 113-115.

[126] **Lide, D.R.** (2003). *CRC Handbook of Chemistry and Physics*, p.p: 4-144.

[127] **Tombal, T.D.**, **Özkan, Ş.G.**, **Ünver, İ.K, Osmanlıoğlu, A. E**. (2016). Bor bileşiklerinin özellikleri, üretimi, kullanımı ve nükleer reaktör teknolojisinde önemi, *Boron Dergisi*, *Yıl 2016*, **Cilt 1** , Sayı 2, Sayfalar 86-95.

[128] **Acarkan, N.** Boron Products and Their Uses, İTÜ. Maden Fakültesi, Cevher ve Kömür Hazırlama Anabilim Dalı., *from <https://docplayer.biz.tr/ 4621438-Bor-urun-cesitleri-ve-kullanim-alanlari-boron-products-and-their-uses.html>*.

[129] **Url-36** <http://www.taek.gov.tr/tr/sik-sorulan-sorular/148-malzeme-teknolojisi -sss/952-xrd-nedir-x-isini-kirinimi-nedir.html>, date retrieved: 20.09.2019.

[130] **Url-37** <https://merlab.metu.edu.tr/tr/x-isini-difraktometresi>, date retrieved: 20.09.2019.

[131] **Misture, S. T.**, **Snyder**, **R. L.** (2001). In Encyclopedia of Materials Science and Technology*, Reference Work, 2001.*

[132] **Url38** <h*ttps://serc.carleton.edu/research_education/geochemsheets/tech niques/XRD.html>*, accessed at 20.09.2019.

[133] **Url-39** <*https://arum.ogu.edu.tr/Sayfa/Index/19/x-isinlari-xrd-ve-xrf-analiz biri mi>*, date retrieved: 20.09.2019.

[134] **Wuhrer, R. and Moran K** .(2018). A new life for the wavelength-dispersive X-ray spectrometer (WDS): incorporation of a silicon drift detector into the WDS for improved quantification and X-ray mapping, *IOP Conference Series: Materials Science and Engineering, Volume 304, conference 1,* doi: 10.1088/1757-899X/304/1/012021.

[135] **Rudin, A.** (1999). Mechanical properties of polymer solids and liquids, in: A. Rudin (Ed.), *Elements of Polymer Science and Engineering*, second ed Academic Press, San Diego, 1999, pp. 377_443.

[136] **Chanda, M.** (2013). *Introduction to Polymer Science and Chemistry: A Problem Solving Approach*, second ed., CRC Press, Boca Raton, FL, 2013, p. 29.

[137] **McKeen, L.W.** (2012) *Permeability Properties of Plastics and Elastomers*, third ed.William Andrew Publishing, Oxford, 2012. pp. 21_37.

[138] **Schultz, J. L. and Wilks, E. S.** (2000). Nomenclature of Polymers, *Encyclopedia of Polymer Science and Technology*, Wiley, Hoboken, NJ.

[139] **McKeen, W.** (2009). *The Effect of Creep and Other Time Related Factors on Plastics and Elastomers* (Second Edition).

[140] **Url-40** <*https://www.laboratorynetwork.com/doc/analysis-method-ensures better-polymer-qualit-0001>,* date retrieved: 20.09.2019.

[141] **Url-41** <*https://www.chegg.com/homework-help/questions-and-answers/def ine-molecular-weight-degree-polymerization-graphical-relationship molecular-weight-poly-q12052059>,* date retrieved: 20.09.2019.

[142] **Rees, O. J.** (2011). *Fourier Transform Infrared Spectroscopy: Developments, Techniques and Applications*, p.p:1.

[143] **Kılıç, G. B. and Karahan, A. G.** (2010). Fourıer Transform Infrared (FTIR) Spectroscopy and its usage in identıfıcatıon of lactic acıd bacteria, *Gıda Dergisi Yıl 2010, Cilt 35*, Sayı 6, Sayfalar 445 – 452.

[144] **Url-42** *<https://potkam.arel.edu.tr/cihazlar/fouirer-transform-infrared-spektro fotometre-ftir>,* date retrieved: 20.09.2019.

[145] **Url-43** *<https://knowbeetutoring.files.wordpress.com/2017/11/22-infrared-spe ctroscopy.pdf>,* date retrieved: 20.09.2019.

[146] **Ojeda, J. J. and Dittrich, M.** (2012). Fourier Transform Infrared Spectroscopy for Molecular Analysis of Microbial Cells, *Methods Mol Biol. 2012*; **881:**187-211,doi: 10.1007/978-1-61779-827-6_8.

[147] **CHE2202, Chapter 15, Learn 19**, Infrared Spectroscopy and Mass Spectrometry,*from<https://webcache.googleusercontent.com/search? q=cache:9UhNIiK_yoIJ:https://classdat.appstate.edu/AAS/CHE/learn ks/Organic%2520(archive)/Organic%2520II%2520-%2520Klein/Cha*

pter%252015/Lecture%2520-%2520Ch%252015.ppt+&cd=1&hl=

tr&ctclnk&gl=tr>, date retrieved: 20.09.2019.

[148] **Salem Press.** (2018). *Encyclopedia of Science*, 2018, 5p.

[149] **Url44** *<https://www.selcuk.edu.tr/ileri_arge/birim/web/sayfa/ayrinti/5874/tr>* date retrieved: 20.09.2019.

[150] **KAPAKİN K. A. T.** (2016). Scanning- Elektron Mikroskobu, *YYÜ Vet Fak Derg, 2006*, *17* (1-2):55-58.

[151] **Bozzola, J. J and Russell, L. D.** (1998). *Electron Microscopy Principles and Techniques for Biologist,* 2. Edition. Jones and Bartlett Publishing, Inc. London.

[152] **Ji, Z.** (2016). Use of composition a land combinatorial nanomaterial libraries for biological studies *Science Bulletin, Volume 61*, Issue 10, May 2016, Pages 755-771.

[153] **Url-45** *<https://blog.phenom-world.com/what-is-sem>,* date retrieved:

20.09.2019.

[154] **Warlock, M.** (2012). *nitrogen and nanocarbon systems, Thesis for: Doctorat (A&Paris Tech); PhD. Autre. Ecole nationalesupérieure d'arts et métiers* ENSAM, 2012. Français: 2012ENAM0037ff. ffpastel-00843104f

[155] **Alam, A.U.** (2014*). Surface Analysis of Materials for Direct Wafer Bonding,* Thesis for: MASc, doi: 10.13140/RG.2.2.31167.82080.

[156] **Url-46** *<http://www.ramehart.com/newsletters/2011-11_news.htm>,* date retrieved: 20.09.2019.

[157] **Toboonsung, B.** (2019). Surface morphologies and durability on water contact angle of Titanium Dioxide Nanoparticle Thin Films *Key Engineering Materials* ***798***:158-162, doi: 10.13140/RG.2.2.31167.82080.

[158] **Fraunhofer**, **J.A.** (2012). Review article adhesion and Cohesion, *International Journal of Dentistry **2012 (3):***951324, doi: 10.1155/2012/951324.

[159] **Url-47***<http://info.alchemy-spetec.com/blog/hydrophobic-vs-hydrophilic poly urethanes>,* date retrieved: 20.09.2019.

[160] **Nishino, Meguro, T., Nakamae, M., Matsushita, K. M., Ueda, Langmuir, Y.** *1999,* 15, 432.

[161] **Masashi, M., Nakajima, A., Fujishima, A., Hashimoto, K., Watanabe, T.** (2010). Effects of the surface roughness on sliding angles of water droplets on super hydrophobic surfaces, *Langmuir 2000*, **16**, 13, 5754-5760, doi: 10.1021/la991660o.

[162] **Yuan, Y. and Lee, T. R.** (2013). *Contact angle and wetting properties, Surface Science Techniques*, pp 3-34|.

[163] **Url-48** *<https://www.must.edu.eg/publications/2846>,* date retrieved: 20.09.2019.

[164] **Spectroscopic Analysis Part 4** – *Molecular energy levels and IR Spectroscopy* Chulalongkorn University, Bangkok, Thailand January 2012 Dr Ron Beckett Water.

[165] **Kim, S. J.**, **Kim, D. K., Kang, D. H.** (2015).Using UVC Light emitting diodes at wavelengths of 266 to 279 nanometers to inactivate foodborne pathogens and pasteurize sliced cheese. Appl Environ *Microbiol. 2015* Sep **18**;82(1):11-7. doi: 10.1128/AEM.02092-15. Print 2016 Jan 1.

[166] **Url-49** *<https://textilelearner.blogspot.com/2013/05/an-overview-of-colour-and textile-dyes.htm >,* date retrieved: 20.09.2019.

[167] **Ayetenew**. Addis Ababa University ,principle, application and instrumentation of UV- visible Spectrophotometer from *<https://www.slideshare.net/ AyetenewAbitaDesa/principle-application-and-instrumentation-of-uv-visible-spectrophotometer>.* date retrieved: 20.09.2019.

[168] **Chen, C W.** (2013) Magnetism and metallurgy of soft magnetic materials. *Courier Corporation, 2013*. Release Date: 2013-02-19.

[169] **Derek, J. and Craik,** "Magnetism: principles and applications." Magnetism Principles and Applications, by Derek J. Craik, pp. 468. ISBN 0-471-95417-9. *Wiley-VCH*, September 2003. (2003): 468.

[170] **White, R. L., Wickersheim, K. A.** (2013). *Magnetism and Magnetic Materials*: 1965 Digest. Elsevier, 2013, eBook ISBN: 9781483269115.

[171] **David, J.** (2015). *Introduction to magnetism and magnetic materials. CRC press*, (third edition).

[172] **Url50** *<https://www.purdue.edu/discoverypark/birck/files/PPMS%20overview %20and%20gallery.pdf>,* date retrieved: 20.09.2019.

[173] **Url-51** *<https://cumerlab.cu.edu.tr/cu/laboratuvarlar/cihazlar-listesi/ppms-fiziksel-ozellikler-olcum-sistemi>*, date retrieved: 20.09.2019.

[174] **Url-52** *<https://www.sigmaaldrich.com/catalog/search?term=108-88-3&interface=CAS%20No.&N=0+&mode=partialmax&lang=en&region=TR&focus=product>*, date retrieved: 20.09.2019.

[175] **Url53** *<https://vlab.amrita.edu/?sub=2&brch=190&sim=603&cnt=1>*, date retrieved: 20.09.2019.

[176] **Chuah, H. H., Lin-Vien, D., Soni, U.** (2001). Poly(trimethyleneterephthalate) molecular weight and Mark–Houwink equation *Polymer, 42*, (16), 7137-7139, doi: 10.1016/S0032-3861(01)00043-X.

[177] **Behrouzian, F., Razavi, S. M., Karazhiyan, H.**, (2014). Intrinsic viscosity of cress (Lepidium sativum) seed gum: effect of salts and sugars. *Food Hydrocolloid. 35* (2014) 100-105, doi: 10.1016/j.foodhyd.2013.04.019.

[178] **Razavi, S. M., Moghaddam, T. M., Emadzadeh, B., Salehi, F.** (2012). Dilute solution properties of wild sage (Salvia macrosiphon) seed gum. *Food Hydrocoll. 29*, (1) (2012) 205-210.

[179] **Pamies, R.**, **Cifre, J. G. H., Martínez, M. D. C. L., Torre, J. G.** (2018). Determination of intrinsic viscosities of macromolecules and nanoparticles. Comparison of single-point and dilution procedures, *Colloid Polym. Sci. 286* (11) (2008) 1223-1231.

[180**]** **Safety Data Sheet of MMA from Merck**, Yeni düzenleme tarihi 28.02.2017 **<**_http://www.merckmillipore.com/INTERSHOP/web/WFS/ Merck-TR-Site/tr_TR/-/USD/ProcessMSDS-Start?PlainSKU=MDA_ CHEM-800590_ **>**, Kaçıncı Düzenleme Olduğu 2.8.

[181] **Url-54** *<http://www.handbookofmineralogy.org/pdfs/borax.pdf>*, date retrieved: 20.09.2019. Borax 2001-2005 Mineral Data Publishing, version 1.

[182] **Url-55** *<http://www.ox.ac.uk/news/2016-06-09-lighting-colour-affects-sleep-and-wakefulnessl>*, date retrieved: 20.09.2019.

[183] **Thakur, V. K.**, **Vennerberg, D., Madboulybcand, S. A., Kessler, M. R.** (2014). Bio-inspired green surface functionalization of PMMA for multifunctional capacitors, , *RSC Advances*, *Issue 13*, 2014 doi: 10.1039/c3ra46592f.

[184] **Arul, K. T.**, **Mannam, R., Ramachandra Ra, M. S.** (2019). ,Energy harvesting of PZT/PMMA composite flexible films *CrystEngComm*, *Issue 22*, 2019, doi: 10.1016/j.cap.2019.01.003.

[185] **Xie, W.**, **Zou, C.**, **Tang, Z.**, **H. Fu**, **Zhu, X.**, **Kuanga, J., Denga, Y.** (2017) Well-crystallized borax prepared from boron bearing tailings by sodium roasting and pressure leaching, *RSC Advances 2017, 7,* 31042.

[186] **Ramesh, S.** (2007). FTIR studies of PVC/PMMA blend based polymerelectrolyte, *SPECTROCHIMACTA* a mol biomol spectrosc. 2007 Apr;**66v** (4-5):1237-42. Epub 2006 Jun 23., doi: 10.1016/j.saa.2006.06.012.

[187] **Arulsankar, A., Kulasekarapandian, K., Jeya, S., Jayanthi S., Sundaresan, B.** (2013), Investigation of the structural, electrical and morphological properties of Mg2+ ion conducting Nanocomposite SolidPolymer Electrolytes based on PMMA, *Materials Science , published 2013*, doi: 10.1007/s11581-019-03104-3.

[188] **Awazu, K.** and **Onuki H.** (1997). Photo-induced synthesis of amorphous SiO 2 film from tetramethoxy-silane on polymethylmethacrylate at room temperature, *Journal of Non-Crystalline Solids*: *Volume 215*, Issues 2–3, 2 July 1997, Pages 176-181.

[189] **Wang, X. , Qu, W., Chen, G.**(2011), Fabrication of graphene/poly(methyl methacrylate) composite electrode for capillary electrophoretic determination of bioactive constituents in Herba Geranii *Journal of Chromatography A, 1218*, (**32***):*5542-8 doi: 10.1016/j.chroma. 2011.06.034.

[190] **Baydoğan, N.**, **Koken, N.**, **Bel, T.**, **Urper, O.** (2018). Multi-Scale self-healing Nanocomposite Shıelding materıal for aerospace, *Polymer and nanocomposites: Symposium*, 21-22 February 2018, Abstract book.

[191] **Chang, K. C.**; **Ji, W. F., Li, C. W., Chang, C. H., Peng, Y. Y., Yeh, J. M., Liu, W. R.** (2014). The effect of varying carboxylic-group content in reduced graphene oxides on the anticorrosive properties of PMMA/reduced graphene oxide composites, *Express Polymer Letters, 8* (12):908-919 doi: 10.3144/expresspolymlett.2014.92.

[192] **Shih, T-T, Hsu, I-H., Wu, J. F., Lin, C.H., Chang, Y.**, (2013). Sun Development of chip-based photo catalyst-assisted reduction device to couple high performance liquid chromatography and inductively coupled plasma-mass spectrometry for determination of inorganic selenium species, *Journal of Chromatography A 1304,* (**21**)**:**101–108, doi: 10.1016/j.chroma.2013.06.067.

[193] **Monsores, K. G. C.**, **Silva, A. O., Oliveira S. S., J. G Passos, R. R.P. Weber.** (2019) Influence of ultraviolet radiation on poly methylmethacrylate (PMMA), Karollyne Monsores, Influence of ultraviolet radiation on polymethyl methacrylate (PMMA). *Journal of Materials Research and Technology, Volume 8*, Issue 5, September–October 2019, Pages 3713-3718.

[194] **Al‑Emam, E., Motawea, A. G., Janssens, K., Cae, J.** (2019). Evaluation of polyvinyl alcohol–borax/ agarose (PVA–B/AG) blend hydrogels for removal of deteriorated consolidants from ancient Egyptian wall paintings, *Heritage Science, 7*: 22, Springer, 2019.

[195] **Yilmaz, E. A**. **and Kuntman, A.** (2008). *Polimerik yalıtkanlarda yüzey özelliklerinin Temas açısı ile incelenmesi, Elektrik–Elektronik–Bilgisayar Mühendisliği Sempozyumu (ELECO2008)*, Bursa, Türkiye, Kasim 2008, ss.107-111.

[196] **Ayrilmis, N.**, **Dundar, T.**, **Candan, Z.**, **Akbulut, T.** (2009). Wettability of fire retardant treated laminated veneer lumber (LVL) manufactured from veneers dried at different temperatures, *BioResources 4:*4, 1536-1544, 2009.

[197] **Bel, T., Yahya, N, Cimenoglu, H, Arslan, C, Baydogan N**. (2018) The Examination of the Changes in the Magnetic Properties of the Poly(methyl methacrylate) *Journal of Physics: Conference Series 1123* (1), 012005.

[198] **Li, S.**, **Qin, J., Fornara, A., Toprak, M., Muhammed, M., Kim, D. K.** (2009). Synthesis and magnetic properties of bulk transparent PMMA/Fe-oxide nanocomposites. *Nanotechnology, 20* (18):185607, doi: 10.1088/0957-4484/20/18/185607.

[199] **Yiğit, Y.**, **Kilislioglu, A.**, **Karakus, S.**, **Baydogan, N.** (2019). Determination of the Intrinsic Viscosity and Molecular Weight of Poly(methyl methacrylate) Blends. *Journal of Investigations on Engineering and Technology, Year 2019, Volume 2 ,* Issue 2, Pages 34-39.

[200] **Url56** *<https://www.sigmaaldrich.com/catalog/product/aldrich/182230?lang= en&region=TR>,* date retrieved: 20.09.2019.

[201] **Tamboli, M.S.**, **Palei, P.**, **Patil, S. S, Kulkarni, M. V, Maldar, N. N, Kale, B.** (2014). Polymethyl methacrylate (PMMA)–bismuth ferrite (BFO) nanocomposite: low loss and high dielectric constant materials with perceptible magnetic properties, *Dalton Transactions 43* ,(35), doi: 10.1039/c4dt00947a.

CURRICULUM VITAE

Name Surname: Yusuf YİĞİT

Place and Date of Birth: Beşiktaş- 15/09/1989

E-Mail: yigit18@itu.edu.tr

EDUCATION:

B.Sc.: 2013, Uludağ University , Faculty of Engineering and Architecture,
Mechanical Engineer.

PUBLICATIONS :

- **Y. Yiğit,** A. Kilislioglu, S. Karakus, N. Baydogan. *Determination of the Intrinsic Viscosity and Molecular Weight of Poly(methyl methacrylate) Blends.* Journal of Investigations on Engineering and Technology, Year 2019, Volume 2 , Issue 2, Pages 34-39.

PRESENTATIONS :

- **Y. Yiğit**, A. Kilislioglu, S. Karakus, N. Baydogan. Determination of the intrinsic viscosity and molecular weight of Poly(methyl methacrylate) blends, *Çukurova Üniversitesi International Conference on Condensed Matter and Material Sciences, 14-19 October 2019.* Adana, Turkey.